HELLENIC REPUBLIC
UNIVERSITY OF WESTERN MACEDONIA
FACULTY OF ENGINEERING
DEPARTMENT OF CHEMICAL ENGINEERING

DIPLOMA THESIS

Space materials characterization and development of standoff bonding process

Orfeas Batzilis
155

Supervisor: Adamos Stimoniaris

Co-supervisors:

a) Konstantinos Tsanaktsidis

b) Vaios Karagiannis

Kozani, 29/09/2022

HELLENIC REPUBLIC
UNIVERSITY OF WESTERN MACEDONIA
FACULTY OF ENGINEERING
DEPARTMENT OF CHEMICAL ENGINEERING

ΔΙΠΛΩΜΑΤΙΚΗ ΕΡΓΑΣΙΑ

Χαρακτηρισμός υλικών για διαστημικές εφαρμογές και ανάπτυξη μεθόδου κόλλησης αποστατών

Μπατζιλής Ορφέας
155

Επιβλέπων: Στημονιάρης Αδάμος

Επόπτες:

α) Τσανακτσίδης Κωνσταντίνος

β) Καραγιάννης Βάϊος

Κοζάνη, 29/09/2022

A portion of this thesis has been presented, as a poster, at the International Symposium on Materials in the Space Environment 15 (ISMSE15).

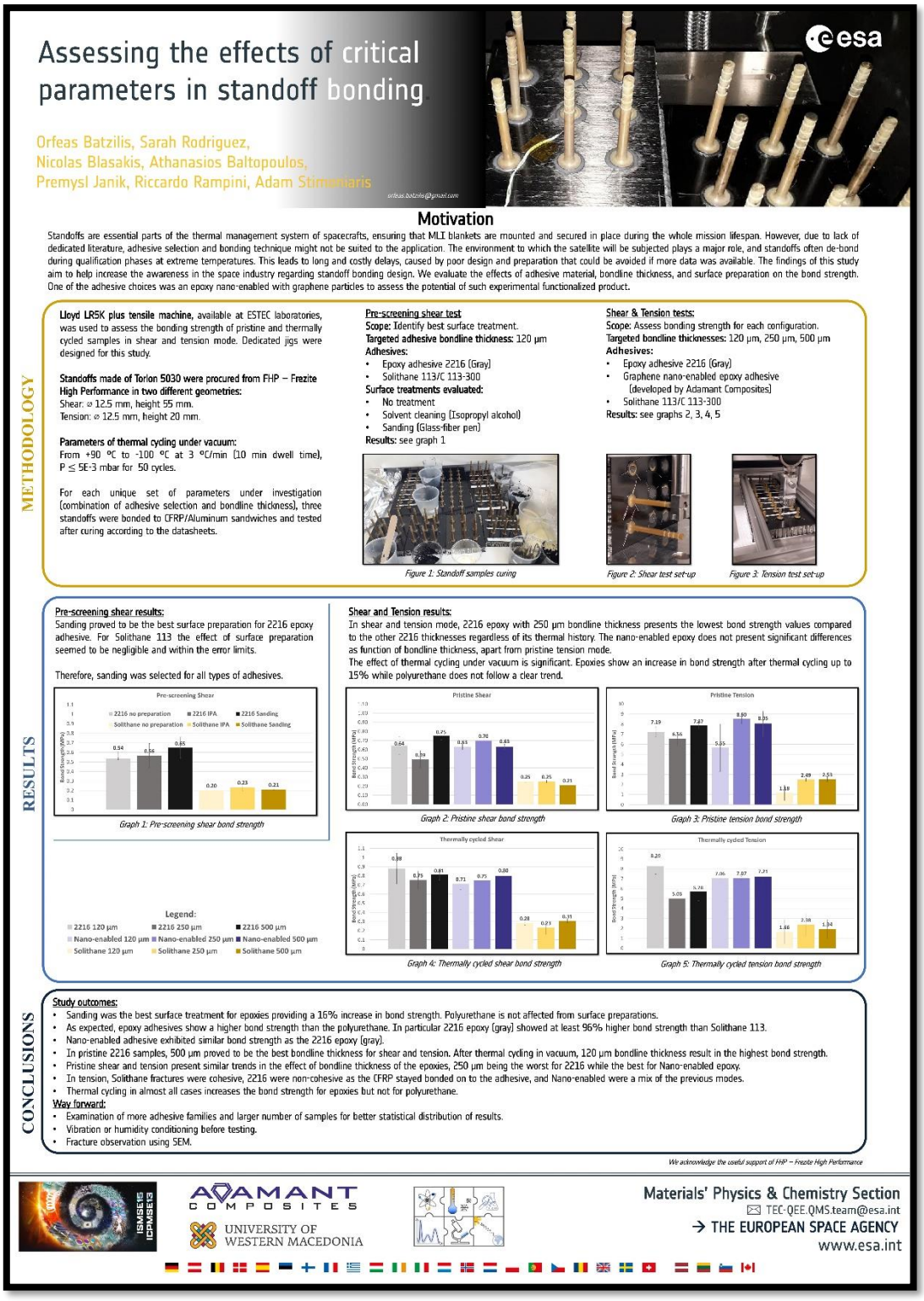

Acknowledgements

The work included in this thesis could not have been performed in such an extent and quality without the help of many people. I am more than grateful not only for the great technical knowledge and insights that I got, but most importantly, for the full support, love, and unreserved trust that they showed me.

Abstract

In this thesis, chemical and physical characterization of polymeric and composite materials suitable for space applications is presented. In addition, the effect of several critical parameters in standoff bonding is assessed and analyzed.

Space materials and processes must withstand harsh environmental conditions such as extreme thermal cycling, radiation effects, plasma, debris and more. In particular, large temperature gradients can impact how structures and related materials behave due to changes in properties such as the glass transition temperature, the coefficient of thermal expansion, the storage and loss moduli etc. These properties must be considered when designing a spacecraft since unexpected values can cause the deformation or even breakage of materials, undermining their structural stability. However, the data provided by the manufacturer is often not precise or complete enough, so dedicated testing is needed.

To investigate the properties of some of these materials, thermal analysis was performed. Nano-enabled materials were included in order to evaluate the effect of added fillers on the basic properties. Results show that a trade-off must be considered between such properties and the benefit of having additional functionalities such as thermal and electrical conductivity.

To assess the effects of critical parameters in standoff bonding process, tensile tests were performed for pristine and thermally cycled samples. For the latter, the aim was to simulate the approximate temperature cycles a spacecraft will encounter between -100°C and 90°C sustained during several orbits in Low Earth Orbit (LEO). Despite the fact that standoff bonding is an integral part of the thermal management system of space missions – by ensuring that the Multi-Layer Insulation (MLI) blankets stay in place – there is a lack of dedicated literature and the bonding is often poorly designed. This results in failures during qualification phases as the standoffs de-bond, causing long and costly delays that could have been avoided if more data was available. The aim of this standoff bonding assessment is to study how different adhesives, surface treatments and bondline

affect the resulting bonding strength. The adhesives considered were epoxy, graphene nano-enabled epoxy and polyurethane; the surface treatments under study were no treatment, isopropyl alcohol (IPA) cleaning and fiber glass pen sanding and the bondline thicknesses selected were 120 μm, 250 μm, 500 μm. Results confirm the expected higher strength of epoxies vs polyurethane. Further, thermal cycling tended to improve the bonding strength of most epoxy and nano-enabled epoxy samples, while polyurethane seemed to not be so affected by temperature excursions.

Keywords: Adhesives, Composites, Standoff Bonding, Thermal Characterization, Nano-enabled.

Περίληψη

Στην παρούσα διπλωματική εργασία παρουσιάζεται ο χημικός και φυσικός χαρακτηρισμός πολυμερών και σύνθετων υλικών κατάλληλων για χρήση σε διαστημικές εφαρμογές. Επιπλέον, αξιολογείται η επίδραση κρίσιμων παραμέτρων στην κόλληση αποστατών.

Τα υλικά για διαστημικές εφαρμογές πρέπει να αντέχουν στις αντίξοες περιβαλλοντικές συνθήκες, όπως ακραίες θερμοκρασιακές διαφορές, ακτινοβολία, πλάσμα, διαστημικά θραύσματα κ.α. Ειδικότερα, οι μεγάλες διαβαθμίσεις στην θερμοκρασία μπορούν να επηρεάσουν τον τρόπο συμπεριφοράς κατασκευών και των υλικών που τα αποτελούν λόγω αλλαγών στην δομή τους και τις ιδιότητές τους όπως η θερμοκρασία υαλώδους μετάπτωσης (Tg), ο συντελεστής θερμικής διαστολής (CTE), τα μέτρα απώλειας και αποθήκευσης (storage and loss moduli) κτλπ. Οι συγκεκριμένες ιδιότητες πρέπει να ληφθούν υπόψη κατά το σχεδιασμό ενός διαστημικού σκάφους καθώς απροσδόκητες τιμές των ιδιοτήτων μπορούν να προκαλέσουν παραμόρφωση ή ακόμα και θραύση των υλικών, υπονομεύοντας τη δομική τους σταθερότητα. Ωστόσο, συχνά τα δεδομένα που παρέχονται από τον κατασκευαστή των υλικών δεν είναι αρκετά ακριβή ή πλήρη, επομένως απαιτούνται περαιτέρω εξειδικευμένες αναλύσεις.

Προκειμένου να διερευνηθούν οι ιδιότητες των υλικών, πραγματοποιήθηκε θερμική ανάλυση. Υλικά στα οποία έχουν προστεθεί νανοσωματίδια συμπεριλήφθηκαν προκειμένου να αξιολογηθεί η επίδραση των πληρωτικών νανοσωματιδίων στις βασικές ιδιότητες του αρχικού υλικού. Τα αποτελέσματα δείχνουν πως πρέπει να εξεταστεί η αντιστάθμιση των αλλαγών σε βασικές ιδιότητες με τα πλεονεκτήματα που προσφέρουν τα πληρωτικά όπως η θερμική και η ηλεκτρική αγωγιμότητα.

Για να αξιολογηθούν οι επιδράσεις σημαντικών παραμέτρων στης διαδικασία κόλλησης αποστατών, πραγματοποιήθηκαν δοκιμές εφελκυσμού στα αρχικά αλλά και στα δείγματα τα οποία υποβλήθηκαν σε θερμικούς κύκλους. Οι θερμικοί κύκλοι παργματοποιήθηκαν προκειμένου να προσομοιώθούν οι συνθήκες που θα συναντήσει ένας δορυφόρος μεταξύ -100°C και 90°C κατά την διάρκεια πολλών τροχιών στην Χαμηλή Γήινη Τροχία (LEO). Παρά το γεγονός ότι η κόλληση αποστατών είναι αναπόσπαστο μέρος του συστήματος θερμικής διαχείρισης των διαστημικών

αποστολών, μιας και διασφαλίζει ότι τα καλύμματα μόνωσης πολλαπλών στρωμάτων (MLI) παραμένουν στην θέση τους, υπάρχει έλλειψη εξειδικευμένης βιβλιογραφίας και έτσι συχνά η κόλληση είναι σχεδιασμένη λάθος. Αυτό έχει ως αποτέλεσμα την αστοχία των κολλήσεων και επομένως την αποκόλλησή τους κατά την διάρκεια ελέγχων προκαλώντας μεγάλες και δαπανηρές καθυστερήσεις που θα μπορούσαν να είχαν αποφευχθεί αν υπήρχαν περισσότερα δεδομένα εξαρχής. Στόχος της αξιολόγησης των κρίσιμων παραμέτρων της κόλλησης αποστατών είναι να μελετηθεί πως οι διαφορετικές κόλλες, επιφανειακές επεξεργασίες και το πάχος της κόλλησης επηρεάζει την αντοχή της κόλλησης. Οι κόλλες που εξετάστηκαν ήταν εποξειδικές, εποξειδικές με νανοσωματίδια γραφενίου, και πολυουρεθάνης. Οι επιφανειακές επεξεργασίες που εξετάστηκαν ήταν, επιφάνεια χωρίς επεξεργασία, επιφάνεια καθαρισμένη με ισοπροπυλική αλκοόλη (IPA) και επιφάνεια τριμμένη με χρήση στυλού από ίνες γυαλιού (fiber-glass). Τα πάχη κόλλησης που επιλέχθηκαν ήταν 120 μm, 250 μm και 500 μm. Τα αποτελέσματα επιβεβαιώνουν την αναμενόμενα υψηλότερη αντοχή κόλλησης των εποξειδικών κολλών έναντι αυτού της πολυουρεθάνης. Περαιτέρω, οι θερμικοί κύκλοι βελτίωσαν την αντοχή των κολλήσεων και των δύο εποξειδικών κολλών, ενώ η κόλλα πολυουρεθάνης φάνηκε να μην επηρεάζεται από τις διακυμάνσεις της θερμοκρασίας.

Λέξεις κλειδιά: Κόλλες, Σύνθετα, Κόλληση Αποστατών, Θερμικός Χαρακτηρισμός, Νάνο-ενισχυμένα.

Contents

1. INTRODUCTION

Material selection and process design are crucial across all industries. They are even more critical regarding space industry when they are subject to unique environmental conditions. Case in point, BEPICOLOMBO spacecraft will orbit around Mercury, the planet closest to the Sun, thus encountering mainly high temperatures (up to 450°C (1)) and radiation doses as well as a significant amount of charged particles . Contrastingly, JUICE spacecraft will orbit Jupiter and its three large moons, Ganymede, Callisto and Europa (2). As they are relatively far from the Sun, the spacecraft will be subjected mainly to extreme cold temperatures (down to -180°C) and harsh radiation (3) filled with charged particles due to a strong magnetic field (4). The specific and unique environmental conditions that each mission faces, are even more important as it is an extreme engineering challenge to repair a spacecraft while in orbit, and most importantly does not make much economic sense yet. Spacecrafts are not designed to be repairable, but to be resilient with multiple back-up systems.

Figure 1. Left: Bepicolombo spacecraft. Right: JUICE spacecraft

In this study, polymeric and composite materials, such as adhesives carbon fiber reinforced polymers are analyzed to ensure their adequacy to space mission requirements. For example, determining the glass transition temperature (Tg) of an structural adhesive can help us understand that it must not be used in a mission if it will reach a higher temperature than the Tg, as it will compromise the structural integrity of the joint. An assessment of standoff bonding critical parameters is also investigated, with

the goal to provide openly available data regarding the bond strength of different parameter configurations in a domain that lacks dedicated literature.

In both studies nano-enabled materials were also used. Nano-enabling materials with silver, graphene etc. enhances one or more target properties. For example, graphene transforms an insulating adhesive into a thermally and electrically conductive glue. However, the effect of these additives on the physical properties of the final product must be studied. While thermal conductivity would increase, the coefficient of thermal expansion (CTE) could vary from the pristine material, and if not measured it can lead to stresses and failures due to CTE mismatch. For this reason, it is crucial to characterize the main properties of enhanced materials such as Tg, CTE, viscoelastic properties etc.

Standoffs are used in spacecrafts to mount in place Multi-layer Insulation (MLI) blankets. MLI is used as an insulator in vacuum environments, either for space missions or cryogenics. Common insulation materials, such as the ones used in home construction function by reducing heat transfer mainly by means of conduction and convection. In a vacuum environment, for example between the spacecraft and the space environment, conduction and convection mechanisms are not present and only radiation occurs. Therefore, to reduce radiation heat loss to or from space, a radiative material such as MLI must be used. If MLI was directly wrapped in contact with the structure of the satellite, it would create significant heat transfer paths in which conduction would play a leading role. To avoid these heat transfer channels, standoffs are used to mount MLI in place eliminating the points of contact between MLI and the spacecraft.

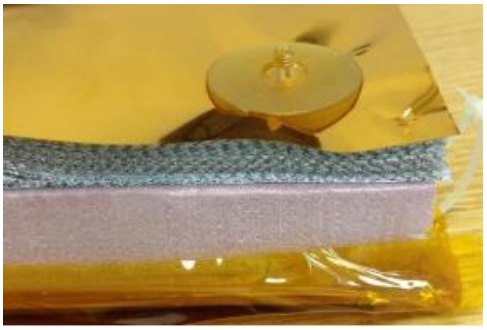

Figure 2. An MLI standoff holding the MLI blanket to the substrate (5)

European standards such as the European Cooperation for Space Standardization (ECSS) require all new materials and processes to be verified, validated and qualified, ensuring their suitability for the intended applications. Standoff bonding, currently is a common cause of non-conformances (NC) occurring often as a result of poor design and preparation. In such NCs issues with adhesive selection, curing or application procedures emerge during the qualification campaign. Further investigations are required, often considering different materials or processes, which imply additional delta-qualifications and therefore costly delays. These unexpected issues could be avoided if more data were openly available. Current open-source research, while adequate, only examines epoxies and specifically in cryogenic temperatures .

The scope of this thesis is to characterize space-relevant materials and determine basic properties, which would then be beneficial for the European Space community. The material characterization was performed using thermal analysis techniques such as Differential Scanning Calorimetry (DSC), Thermogravimetric analysis (TGA), Dynamic Mechanical Analysis (DMA), Thermomechanical analysis (TMA) and Dilatometry. Further, we focused on the bonding method and selection of adhesives in a very common process in space industry: standoff bonding. In this case, the bonding strength was measured using a tensile machine, pulling in shear and tension modes. The effects of different adhesives, bondline thickness and surface preparation were assessed and evaluated. We have also considered the effects of temperature cycling to conclude how and when critical parameters affect the bonding strength. Residual stresses in the adhesives are expected to have an effect on the bonding strength of pristine versus thermally cycled samples. The effect of these stresses can be magnified by the bondline thickness, and therefore the amount of adhesive material. Epoxy adhesive is expected to show bigger strength than polyurethane and enabled epoxy. About surface preparations, sanding is expected to work better than cleaning with isopropyl alcohol (IPA), and cleaning with IPA is expected to perform better than no surface preparation.

In the next chapters, there will be a discussion about the types of materials tested in this study, which techniques were used and what were the methods followed. Then a

presentation of the results will follow and finally the conclusions. Datasheets of materials and characterization results can be found in the appendixes.

2. MATERIALS

In this chapter we present the materials that were characterized and used for the standoff bonding assessment. We also discuss about the different types of these materials such as sandwich panels, Carbon-Fiber-Reinforced-Polymers (CFRPs) and adhesives as well as their typical uses and their importance in the space industry.

2.1. Adhesives

An adhesive is any non-metallic substance, used to bind two items together chemically or physically . It can be applied either to one or to both surfaces, offering multiple advantages in comparison to other binding techniques (such as welding, mechanical fastenings etc). Some of the advantages include resistance to flex and vibration, superior chemical and heat resistance, equal stress distribution, cost effective while also offering a significant mass reduction.

The main disadvantage of adhesives is that they are organic substances that react to the environment in space. Charged particles, Atomic Oxygen (ATOX) and UV radiation usually degrade organic materials, decreasing their performance. For example, UV radiation impinging over the adhesive can result in a change of color which, in turn, could impact the absorptivity or emissivity. This effect, for an adhesive used in solar-cell cover glass, can introduce substantial reduction in the solar array efficiency, decreasing the power generated to the satellite instruments and components (6).Another example is the effect of vacuum, which makes adhesives outgas and release unbound molecules which can then stick to contamination-sensitive items – such as mirrors or glasses – and can end up affecting the measurements. Curing is the cross-linking reaction of the adhesive.

As part of structural applications, adhesives are used very often. In particular, relevant to this study, they are used to bond CFRP plates with aluminum honeycomb creating a CFRP/Aluminum sandwich panel which is used as a main structural element of most of the satellites (7). In sandwich structures the adhesives used are often in film

form, as this implies a constant thickness throughout the whole structure and therefore similar and expected properties.

They are also commonly used for bonding wires all over the spacecraft, and also in all sorts of secondary structural applications (8). For example: optical lenses bonded to the telescope structure, beam splitter geometries created by bonding glasses in different orientations, or standoff bonding to CFRP.

Figure 3. Examples of cured film adhesives for material characterization

Figure 4. Cured adhesives for material characterization

Figure 5. Standoff bonding cured adhesives for DSC test

2.1.1. Epoxy resin adhesives

Epoxy resin adhesives, part of thermosetting class of plastics, are usually two-part adhesives with a reactive prepolymer and a polymer that contain oxiranes (IUPAC for epoxide groups, see Figure 6) (9). In order to cure, these adhesives react with a catalyst present either by themselves or with other co-reactants referred as hardeners or curatives. They have good mechanical properties, high bonding strength and are resistant to chemicals. An important feature of epoxy resin adhesives is that they do not shrink excessively during curing and most of them do not absorb moisture. Also, they have a long shelf life and electrical and thermal insulating properties.

Figure 6. Epoxide group

2.1.2. Polyurethane adhesives

Polyurethane is a thermosetting polymer composed of organic parts connected by urethane (–NH–(C=O)–O–) links (10). They can be manufactured from a variety of

different materials resulting in different properties and therefore applications. To produce it, diisocyanates react with polyols with a catalyst or UV light. The polyurethane adhesives are either one- or two-part adhesives that offer good toughness under low temperatures but they do not perform as good for long-term high temperature exposure. Because of their low viscosity they are easy to process. Once cured they are flexible to adapt to different complex geometries due to their softness and therefore are often used in potting applications (11). Figure 7 shows the chemical reaction of a polyol, diol, with diisocyanate to produce polyurethane.

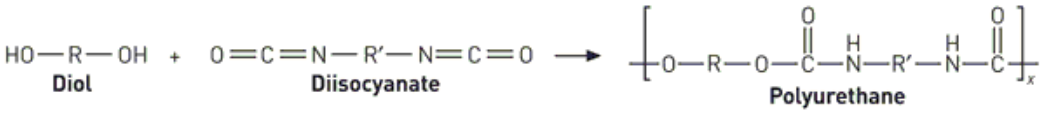

Figure 7. Polyurethane synthesis reaction example

2.1.3. Silicone adhesives

Silicone adhesives are thermosetting polymers made up of siloxane, their basic component is the silicon-oxygen chain (⋯–Si–O–Si–O–Si–O–⋯) where two organic groups, such as methyl, attach to the silicon center. Silicones, compared to other adhesives, stand out for their flexibility and resistance to high temperatures chemicals (12). In Figure 8 we can see the silicon-oxygen chain connected with methyl groups.

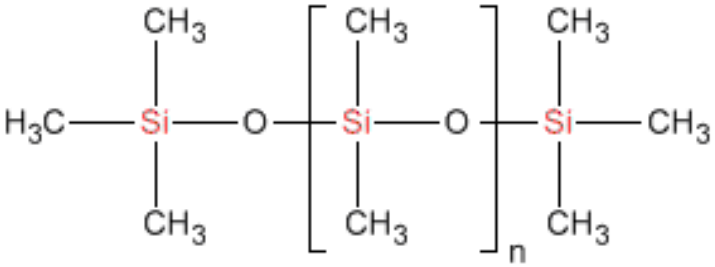

Figure 8. Chemical structure of siloxane (silicon-oxygen chain connected with methyl groups)

2.1.4. Adhesives used for standoff bonding study

For the standoff bonding study, 3 different adhesives were used:

- 3M™ Scotch-Weld™ Epoxy Adhesive 2216
- Graphene nano-enabled epoxy adhesive
- Solithane 113/C 113-300

2.1.4.1. 3M™ Scotch-Weld™ Epoxy Adhesive 2216 (Gray)

Scotch-Weld™ 2216 epoxy adhesive from 3M™ (Figure 9), commonly known as '2216', is a two-part epoxy adhesive that is considered appropriate for applications in which vibrations – such as the ones during launch – and thermal expansion and contraction are present. It is also good for very low temperatures as it does not become too brittle. These features, along with its high bonding strength make it a great choice for standoff bonding.

The two parts consist of the accelerator (A) which is a modified amine, and the base (B) which is a modified epoxy and they are mixed in a A:B=7:5 ratio by weight. After mixing it has a work life of 90 minutes. According to the datasheet, several curing profiles can be applied. In this study, we followed the recommendation to cure the mixed result for 7 days at room temperature. The technical datasheet can be found in the Appendix A (page 71).

Figure 9. 2216 adhesive used for standoff bonding

2.1.4.2. Graphene nano-enabled epoxy adhesive

Graphene nano-enabled epoxy adhesive was developed and supplied by Adamant Composites LTD. In addition to the common advantages of an epoxy, it also has enhanced functionalities such as high thermal and electrical conductivity (13). These properties can make it a great candidate for innovative applications where it is not just a structural component, but it also plays role in thermal management, electrical discharge etc. As mentioned previously, before being applied to spacecrafts, it must be validated for use to confirm its suitability. We present here some basic characterization, as a humble step towards qualification of this nano-enabling process.

Figure 10. Graphene nano-enabled adhesive used for standoff bonding

2.1.4.3. Solithane 113/C 113-300

Solithane 113/C 113-300 is a two-part polyurethane adhesive that is often used in potting. It is not a common adhesive for structural applications as it has lower bonding strength, and it is not UV resistant, so it often needs to be coated if it will be exposed to the space environment. Solithane 113 has excellent resistance to ultra-high vacuum environments. Also, it has been proven that it can be conductive when filled with silver powder, and it is used extensively with an excellent manufacturing reproducibility and a

low cost (14). Even though is not used in standoff bonding, its easy processing, low cost, and relative easy procurement make it a possible candidate for future missions to use it either pristine or filled with particles improving its stiffness. The two parts are the accelerator and base and they are mixed in a ratio of A:B=73:100 by weight. Curing occurs after 7 days in room temperature or in multiple temperatures and times that can be found in its datasheet in Appendix B at page 74.

Figure 11. Solithane 113 adhesive used for standoff bonding

2.2. CFRP panels

Carbon Fiber Reinforced Polymers (CFRPs) are composite materials that are made of resin matrix with carbon fiber reinforcement. They are an integral part of many industries like automotive, marine, energy and aerospace where a material with high strength to weight ratio is required.

As with all composite materials, the material properties of CFRPs depend on the composition and ratio of matrix and reinforcement elements. In particular, the alignment of the carbon fibers and the fiber-to-polymer ratio will dictate the final behavior of the composite material.In general, there are two common ways in which the carbon fibers can be orientated (15): Quasi-isotropically or anisotropically. The former orientation is achieved by laying down carbon fiber plies in $0^o/90^o$ degrees and $-45^o/45^o$ degrees, and therefore results in the material having strength and stiffness equal in all directions in-

plane. The later is achieved by laying the carbon fibers plies only in $0^o/90^o$ degrees (16), which means that the CFRP plate will have different strength and stiffness in different directions. The anisotropic orientation results in a material which is weaker against its grains but stronger along the grains in comparison to its quasi-isotropic counterpart.

CFRP panels can also be enabled by doping with small quantities of materials that introduce improved properties and functionalities. The new properties can be electrical conductivity, thermal conductivity, or even increased toughness.

Figure 12. CFRP plates used for material characterization

2.3. CFRP/Aluminum sandwich structure

CFRP/Aluminum sandwich structures consist of CFRP plates that are adhered, often by using film adhesives, to an aluminum honeycomb structure. This material falls under the category of sandwich-structured composites. The core consists of a honeycomb structure made of aluminum that, by itself, presents a low resistance against deformations. When sandwiched between two plates of high strength material, the final product presents very high stiffness, in particular to bending, with low overall density (17). This low density is one of the core properties of this material composition. In space applications, weight and precision are two paramount factors. On the one hand, the cost of launching a spacecraft, can range up to 55000€ per kilogram. On the other hand, it is

critical to maintain the desired geometry of the structure, which usually holds telescopes and highly sensitive instrumentation.

In the figure below, the drawing *A* represents the whole sandwich structure, *B* is the skin (CFRP plates) and C the core (aluminum honeycomb structure).

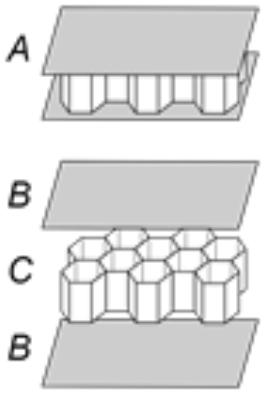

Figure 13. Composite sandwich structure diagram

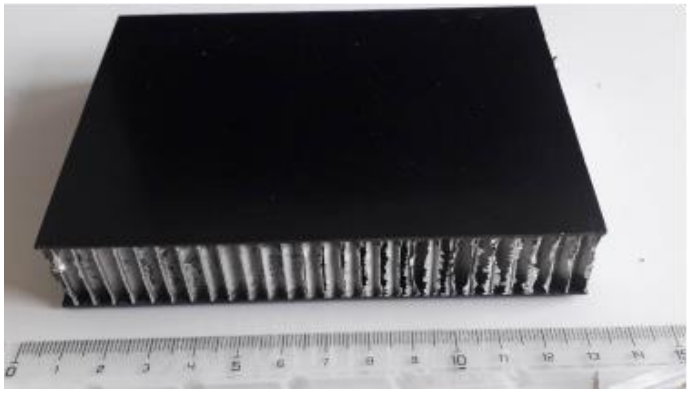

Figure 14. CFRP/Aluminum sandwich used in standoff bonding shear test

2.4. Standoffs

Standoffs are used as spacers to ensure that Multi-layer insulation (MLI) blankets stay fixed in place. MLI is the thermal insulation used in spacecrafts and it consists of multiple layers of thin sheets. These sheets commonly include polyimide (e.g. Kapton), dacron, or silver aluminized mylar. As explained in chapter 1, the function of the MLI is to reduce the thermal loss due to radiation, which is the predominant way of heat transfer

in vacuum. If the MLI was in contact with the satellite, then there would be heat transfer by means of conduction. Standoffs reduce the points of contact between the satellite and the MLI.

Typically, standoffs are made out of plastics and in some cases even metal. In this study the standoffs used were made from Torlon® 5030 HF, a thermoplastic that is often used for these types of applications. Torlon is resistant to chemicals and mechanical stresses, and it has a low coefficient of thermal expansion as well as dimensional stability (18).

Two geometries of standoffs made of Torlon® 5030 HF were procured from FHP:

- Long standoffs for shear testing (12.5 mm diameter base, 55mm height)
- Short standoffs for tensile testing (12.5 mm diameter base, 20mm height)

Figure 15. Left: Standoff used for shear testing. Right: Standoff used for tension testing

2.5. Materials tested

In Table 1 the reader can find the samples tested in the frame of this thesis using thermal analysis techniques. First, we have CFRP plates that underwent TGA, DSC and DMA (3-point bending) analysis. All of the CFRP plates were made from the same fibers and epoxy. Then, there are the film adhesives, filled with nano-particles, that were tested in TGA, DSC and TMA. In particular, for TMA, the film adhesives were sandwiched between aluminum plates in order to be able to measure with the current set-up. Measuring film adhesives is complicated and requires a specific instrument sample set

up. TGA and DSC tests were also performed for some other adhesives comprising common ones used in space industry (epoxies like 2216, AV138, Redux 312L or silicones like 93-500 or RTV-S 691) and nano-enabled ones. The two silicone adhesives were tested in DMA and in Dilatometer only with main scope to identify the glass transition temperature and compare it with the value obtained from DSC.

Table 1. Material characterization test table

Material	Sample ID	Description	Tests				
			TGA	DSC	DMA	TMA	DIL
CFRP	P36-CM-012-04	CFRP plates (epoxy polymer)	✓	✓	✓		
	P36-CM-013-02		✓	✓	✓		
	P36-CM-014-04		✓	✓	✓		
	P36-CM-031-01A		✓	✓	✓		
	P36-CM-025-02	Nano-enabled CFRP plates (epoxy polymer)	✓	✓	✓		
	P36-CM-026-02		✓	✓	✓		
	P36-CM-027-02		✓	✓	✓		
	P36-CM-032-01A		✓	✓	✓		
Film adhesive	S120	Epoxy adhesive with fillers	✓	✓		✓	
	S121	Epoxy adhesive with fillers	✓	✓		✓	
	S122	Epoxy adhesive with fillers	✓	✓		✓	
	S129	Epoxy adhesive with fillers and supported	✓	✓		✓	
	S133	Epoxy adhesive with fillers	✓	✓		✓	
	S134/S135	Epoxy adhesive with fillers				✓	
	S137	Epoxy adhesive with fillers and supported	✓	✓		✓	
	S138/S139	Epoxy adhesive with fillers and supported				✓	
	P32-Ref	Epoxy adhesive with fillers and supported				✓	
Other adhesives	P36-DC 47 / 48 / 51	Nano-enabled epoxy adhesive	✓	✓			
	P36-Redux312L	Redux 312L	✓	✓			
	P36-2216Grey	3M 2216 Grey	✓	✓			
	P32-Araldite	Araldite adhesive	✓	✓			
	P36-AV138M-1/HV998	AV138M-1/HV998 adhesive	✓	✓			
	P36-DC-9-Th26	Epoxy adhesive	✓	✓			
	P36-M21-Th77	Epoxy adhesive with fillers	✓	✓			
	DOWSIL 93-500	Silicone adhesive		✓	✓		✓
	RTV-S691	Silicone adhesive		✓	✓		✓

Regarding the standoff bonding applications, two main test types were carried out. Initially, a pre-screening test was performed in pristine samples in shear mode. This pre-screening was performed using 2216 and Solithane adhesives and a 120 μm spacer to achieve a specific bondline thickness (Table 2). The purpose of pre-screening was to identify which surface preparation was better, for which 3 standoffs were bonded for each adhesive. The surface preparation methods considered were: (i) no treatment, (ii) cleaning with just Isopropyl alcohol solvent (IPA) and (iii) sanding and then cleaning with solvent.

Table 2. Standoff bonding surface treatment test

Pre-screening shear test (Pristine)			
Adhesive	Surface preparation		
	No treatment	Solvent (IPA)	Sanding
3M™ Scotch-Weld™ Epoxy Adhesive 2216 (Gray)	3	3	3
Solithane 113/C 113-300	3	3	3

After the pre-screening test, the best surface treatment was selected and tests in shear and tension were performed, both for pristine and thermally cycled samples. For these tests, in addition to 2216 and Solithane, a graphene nano-enabled epoxy was tested. For each adhesive, three different bondline thicknesses were selected, 120 μm, 250 μm and 500 μm. For each set of parameters, three standoffs were bonded and tested (see Table 3).

Table 3. Test table: Number of standoffs bonded to each adhesive, in Tension & Shear

Shear test (Pristine)			
Adhesive	Bonding thickness (um)		
	120	250	500
3M™ Scotch-Weld™ Epoxy Adhesive 2216 (Gray)	3	3	3
Solithane 113/C 113-300	3	3	3
Graphene nano-enabled epoxy	3	3	3

Shear test (Thermally cycled)			
Adhesive	Bonding thickness (um)		
	120	250	500
3M™ Scotch-Weld™ Epoxy Adhesive 2216 (Gray)	3	3	3
Solithane 113/C 113-300	3	3	3
Graphene nano-enabled epoxy	3	3	3

Tensile test (Pristine)			
Adhesive	Bonding thickness (um)		
	120	250	500
3M™ Scotch-Weld™ Epoxy Adhesive 2216 (Gray)	3	3	3
Solithane 113/C 113-300	3	3	3
Graphene nano-enabled epoxy	3	3	3

Tensile test (Thermally cycled)			
Adhesive	Bonding thickness (um)		
	120	250	500
3M™ Scotch-Weld™ Epoxy Adhesive 2216 (Gray)	3	3	3
Solithane 113/C 113-300	3	3	3
Graphene nano-enabled epoxy	3	3	3

3. METHODOLOGY: INSTRUMENTS AND PROCEDURES

In chapter 3 we introduce the instruments used to perform thermal analysis, thermal cycling and tensile testing. All the testing presented in this thesis was performed in the *TEC-Q Materials and Electrical Components laboratory* in ESA/ESTEC. In addition to referring to the method principles of the instruments, we also analyze the specific procedures that were followed for the material list discussed in the previous section.

In summary, the basic characterization of CFRP plates and adhesives was conducted using thermal analysis (3.1). The goal was to assess physical or chemical stability of the materials under heating and/or cooling. Thermal analysis can show the presence of thermal or mechanical history in polymers, which makes it an excellent tool for characterizing and designing manufacturing processes as well as to estimate the life expectancy in various environments (19). This chapter presents the techniques applied: Thermogravimetric Analysis (3.1.1), Differential scanning calorimetry (3.1.2), Thermomechanical analysis and Dilatometry (3.1.3), and Dynamic mechanical analysis (3.1.4).

Further, a bonding procedure was developed in this work for preparing the surface, mixing and applying the adhesive and bonding the standoffs to the substrates to ensure proper curing. This is presented in 3.2.

In section 3.3 the thermal vacuum chamber (TVAC) is presented. TVAC was used to thermally cycle the standoff samples to identify changes in the bonding strength.

Finally, in section 3.4, the mechanical testing in tensile and shear mode is discussed as to how it was used to determine the bonding strength.

3.1. Thermal analysis

3.1.1. Thermogravimetric analysis (TGA)

In a TGA experiment, the mass of a sample is measured while undergoing a temperature program. The program can be isothermal or a temperature scan, resulting in mass loss versus time or temperature. Typically, the atmosphere is purged with inert, dry-nitrogen gas, but if oxidation needs to be examined an air or oxygen purge is available. Temperature scans can be performed from room temperature up to 1600°C at controlled heating rates. Typical sample size is around 25 mg.

This technique is used as a screening test to investigate the thermal endurance of a material. Mass loss at low temperature may be attributed to offgassing of water or volatile additives. Distinct mass loss steps well above 100°C are likely to be the result of (partial) decomposition. This can be a concern for materials that need to withstand an elevated service temperature, such as thermal control materials for inner solar system planetary missions. Reaction mechanisms of oxidation and kinetics of pyrolysis and combustion processes can also be identified. Finally, TGA can also help to identify the maximum temperature target for DSC.

The used instrument, that can be seen in the Figure 16, is a calibrated TGA/DSC 3+ of Mettler-Toledo available in ESTEC laboratories. The temperature program to which the samples were subjected was the same for all the samples, starting at room temperature up to 900°C with a heating rate of 10 K/min and N_2 as inert gas with a flow of 70 ml/min. Clean alumina sample holders with 150 μL capacity were used. This crucible material was chosen at it is resistant to high temperatures, and its volume was sufficient to hold a sample mass range of approximately 25-30 mg, which is high enough to show a notable mass change, but low enough to minimize temperature gradient inside the sample. Blank (empty) crucibles were also measured in order to remove the buoyancy effect that is many times apparent in this type of analysis under gas atmosphere (19).

Figure 16. TGA/DSC 3+ instrument

The table below (Table 4) shows the parameters that were selected for the TGA tests, shown also pictorially in Graph 1.

Table 4. TGA method parameters

Segment	Heating
Starting temperature	25.00 °C
Ending temperature	900.00 °C
Heating rate	10.00 K/min
Gas	N_2, 70 ml/min

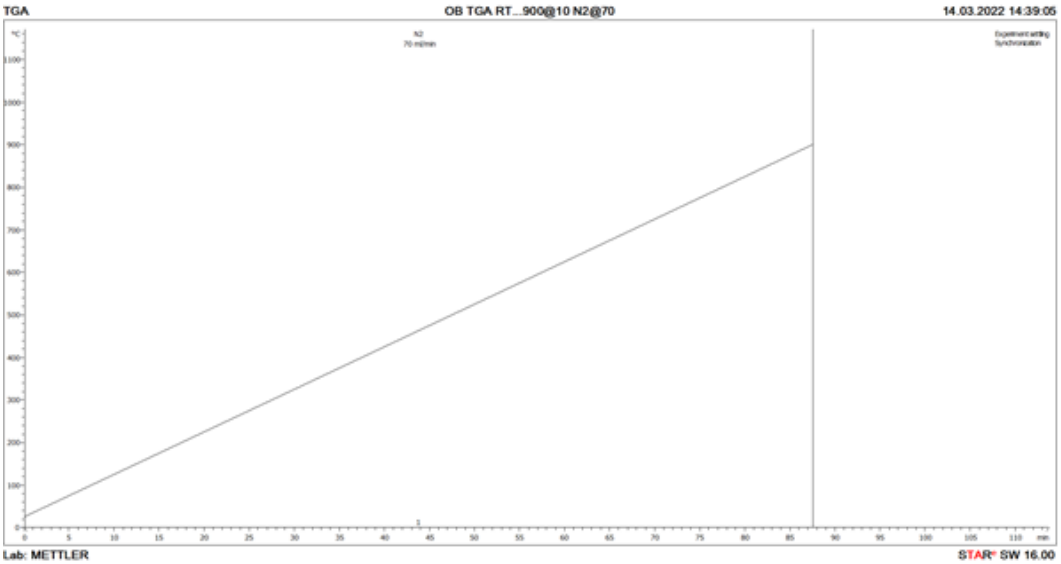

Graph 1. TGA temperature method, from RT to 900 °C at 10 K/min under N_2 atmosphere

3.1.2. Differential scanning calorimetry (DSC)

In a DSC experiment the temperature of a sample within an inert crucible is compared to an empty reference crucible while undergoing a temperature program. When the sample goes through a transition its temperature differs from the reference crucible as heat is absorbed or released to undergo such transition. The apparatus keeps the reference temperature synchronous to the programmed method, allowing the heat flow to or from the sample material to be calculated. This technique reveals material transitions that influence the specific heat as well as endo- or exothermal effects, such as phase transitions, glass transitions or curing. Typically, the furnace, see Figure 19, is purged with dry nitrogen gas to prevent oxidation. A distinction between reversible (e.g., glass transition, melting) and irreversible (e.g., curing) transitions can be made by heat-cool-heat methods. Typical areas of interest are the cure verification of adhesives and the transition temperatures of polymers.

Calibrated DSC 822 instrument of Mettler-Toledo available at ESTEC laboratories, that can be seen in the Figure 17, was used in this study to identify if polymeric materials were fully cured and to find the glass transition temperature (Tg). Tg is one of the key

parameters in polymers; below Tg, they become glassy (stiff and brittle)(20), and above Tg the polymer becomes rubbery and soft (21).

The temperature method for DSC was the same for each sample, except for the maximum temperature limit which was selected depending on the material. The starting temperature was 25°C and a heating rate of ± 10 K/min was used. First the material is cooled down to -50°C, and then heated up to the maximum temperature (see example for CFRP in Table 5). The whole method consisted of 3 cooling/heating cycles (Graph 2). The cycling method is really important as it can help identify in the first heating if there are any pre-stresses in the material or any post curing effects. That way we can be more certain of the actual glass transition temperature or other phase transitions that are apparent to the material and method. N_2 was used as inert gas with a flow of 50 ml/min. The maximum temperature used was calculated by having the temperature that the material loses 1% of its total mass in the TGA minus 50 °C. For example, CFRP plates had a 1% mass loss temperature at least above 250 °C. Therefore, the maximum temperature at DSC was selected as 200 °C. Finally, the sample mass was around 10-20 mg to minimize gradient temperature in the sample. In DSC the sample pan was aluminum with a volume of 40 μl and a hermetically sealed lid that was punctured in order of the volatiles to be able to be released. The lid also allows the sample to remain in contact with the bottom of the pan, which is important since the thermocouple is located in the bottom of the sample and the reference pan.

Figure 17. DSC 822 instrument

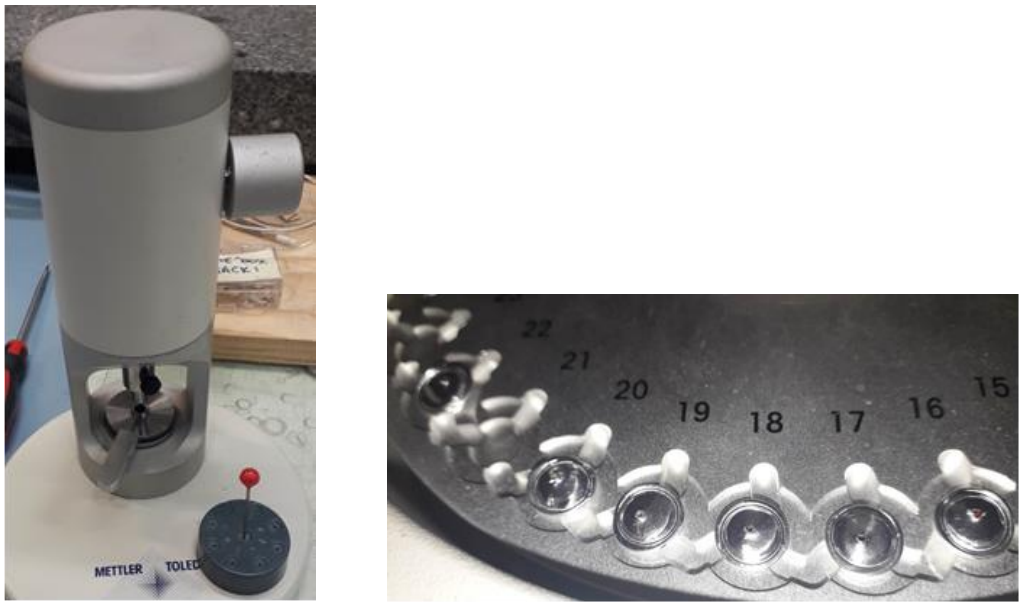

Figure 18. Left: Clamping device for DSC pans. Right: DSC sample tray

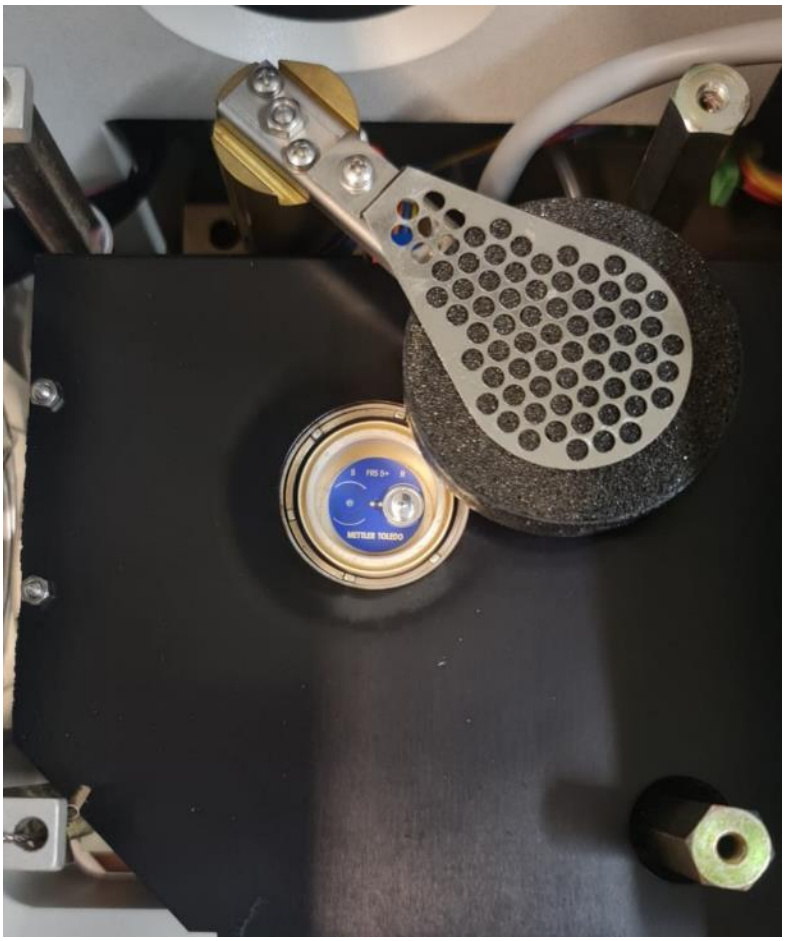

Figure 19. DSC 822 open furnace

Table 5. DSC method parameters CFRP example

CFRP Method	**Segments**						
	Cooling	**Heating**	**Cooling**	**Heating**	**Cooling**	**Heating**	**Cooling**
Starting Temperature	25.00 °C	-50.00 °C	200.00 °C	-50.00 °C	200.00 °C	-50.00 °C	200.00 °C
Ending Temperature	-50.00 °C	200.00 °C	-50.00 °C	200.00 °C	-50.00 °C	200.00 °C	25.00 °C
Heating rate	-10.00 K/min	+10.00 K/min	-10.00 K/min	+10.00 K/min	-10.00 K/min	+10.00 K/min	-10.00 K/min
Gas	N2, 50 ml/min						

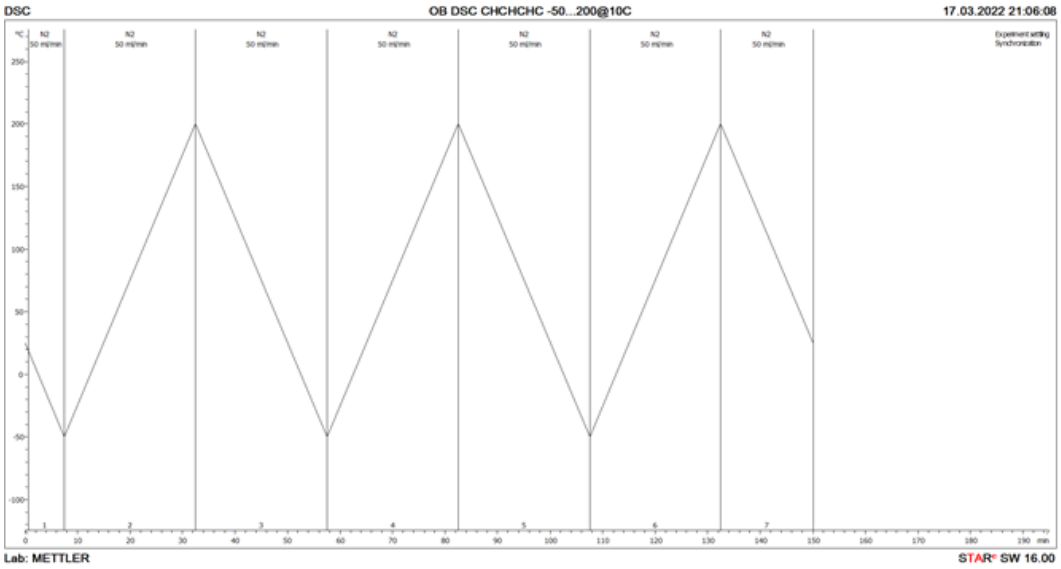

Graph 2. DSC method showing three heat-cool cycles between -50 And 200 °C at 10 K/min

3.1.3. Thermomechanical analysis (TMA) and Dilatometry (DIL)

To calculate the coefficient of thermal expansion (CTE) of adhesives, TMA and Dilatometer were used. These two techniques share some similarities. They are used to measure the uni-dimensional change as a function of time/temperature. This dimensional change is driven by the temperature range selected by the user in the program. Is important to have a relatively low heating/cooling rate to ensure that dimensional changes - due to expansion/contraction of atomic or molecular structure- are allowed to take place. The sample is placed into the furnace of the instrument where a probe applies a negligible force to ensure good contact. Then, while heating/cooling, the dimensional change of the sample causes movement of the probe, which is used by the instrument to determine the change of sample length (22).

CTE is an important value as spacecrafts often undergo extreme thermal cycles during their missions. These extreme cycles, along with the fact that the spacecraft is made out of many different materials, can introduce thermally induced stresses resulting in structural issues. For example, a joint between a metal and a composite that have a

significant CTE mismatch, will face thermally induced stresses after being subject to a temperature difference, as the composite will work against the contraction of the metal. Therefore for fastening and bonding applications it is necessary that the substrate and adherend materials have a CTE as similar as possible to avoid such incidents.

The calibrated TMA and dilatometer apparatus used in this study, as they can be seen in Figure 20 and Figure 21 respectively, were TMA 841 from Mettler Toledo and DIL402C from Netzsch, available at ESTEC laboratories. TMA specimens must have two flat and parallel surfaces in the measurement direction and the maximum dimensions should not exceed 10 x 10 x 10 mm^3. Dilatometer specimens must also have two flat and parallel surfaces, with a length between 10 mm and 30 mm and a diameter up to 8 mm. In the figures below (Figure 22 and Figure 23) we can see the sample set up in the TMA and Dilatometry instruments respectively.

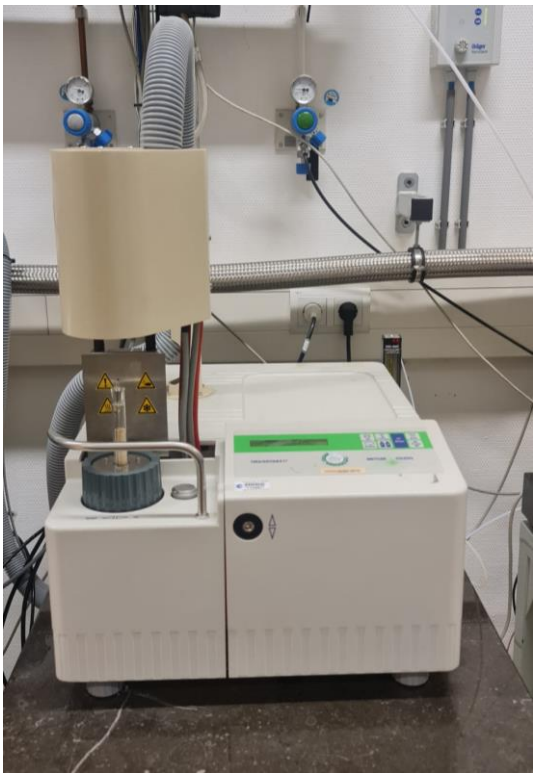

Figure 20. TMA 841 instrument

Figure 21. DIL 402C instrument

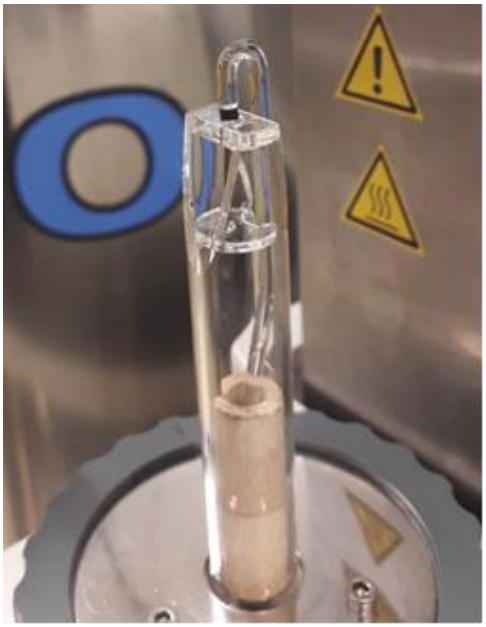

Figure 22. TMA sample set up

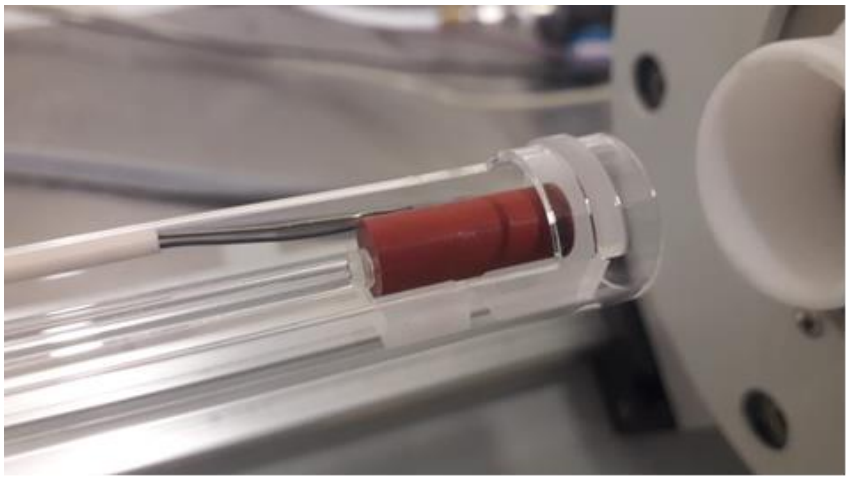

Figure 23. Dilatometer sample set up

The methods for both types of measurements we identical. As it can be shown in Graph 3, two cooling/heating cycles were performed between -150°C to 150 °C with a rate of 3 K/min. The sample environment was purged with N_2 at a rate of 50 ml/min and the force that the probe was applying to the sample was 0.020 N.

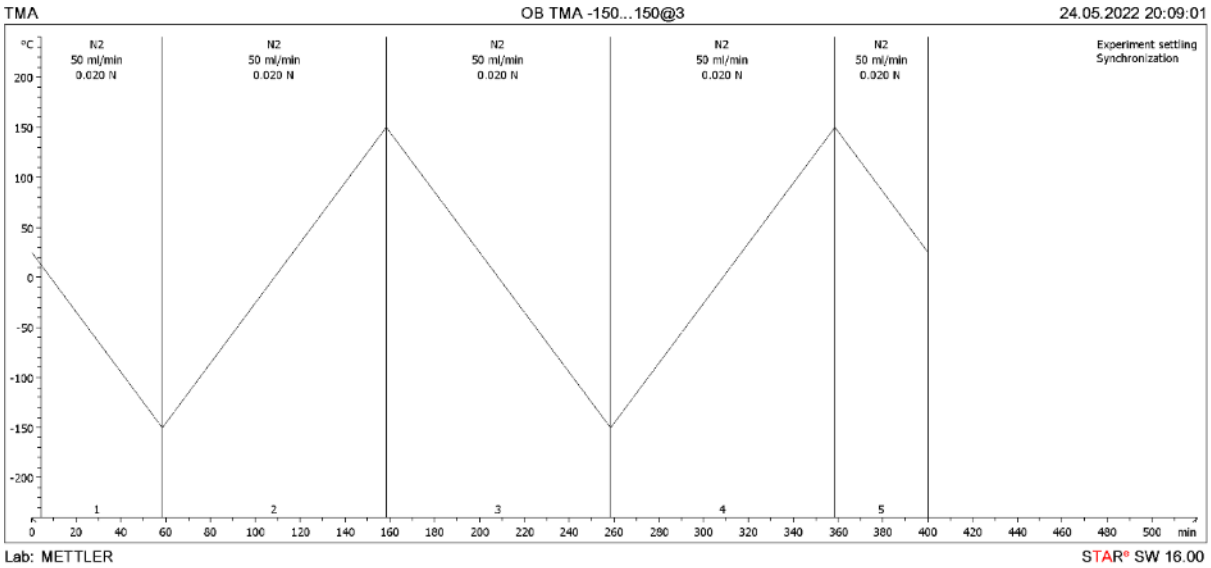

Graph 3. TMA method applied to the samples to measure CTE

3.1.4. Dynamic mechanical analysis (DMA)

In a DMA experiment visco-elastic properties of a sample material subjected to a temperature program are determined. An oscillating load with a fixed frequency is applied onto the sample and the response amplitude of the sample provides information about the visco-elasticity and the modulus. This technique reveals any transitions that influence these mechanical properties and it is especially sensitive to more subtle secondary and tertiary (γ) transitions at low temperature, besides the glass transition.

The storage modulus (M', E' or G' in 3-point bending, tension or shear respectively) is proportional to the energy stored elastically and reversibly. The loss modulus (M'', E'', G'') is proportional to the energy transformed in heat and irreversibly dissipated. The loss factor (tan δ) is the tangent of the phase shift (δ) between the force amplitude and the displacement amplitude. This loss factor, calculated by dividing the loss modulus with the storage modulus. describes the damping behaviour: ideally elastic materials show no phase shift, corresponding to a loss factor of zero, and ideally viscous materials show a 90° shift, corresponding to an infinitely high loss factor.

Specimens are scanned from –150°C up to 500°C under slow heating rates under dry nitrogen atmosphere. The instrument can be equipped with different probes to accommodate various sample shapes and a wide modulus range. Specimens can be tested in shear, tension, compression, cantilever, three-point bending and creep-relaxation modes. The instruments used in this thesis, see Figure 24 and Figure 25 respectively, are the DMA 1 and the DMA 861 of Mettler-Toledo available at ESTEC laboratories. CFRP plates were measured under 3-point bending tests using DMA1 and adhesives were tested in shear mode using DMA 861.

The CFRP samples underwent a single temperature ramp up from room temperature to 250°C. The parameters chosen were frequency of 1Hz, force of 5 N or displacement of 30 μm as well as an offset force of 2N. The offset force is usually necessary for 3-point bending tests as it prevents buckling. It should be noted that pre-tests were done in order to find the most suitable parameters. This means that the final parameters

were chosen due to the sample showing linear behavior for the specific method. For some samples, a force of 2 N and a displacement of 10 μm was also tested, as the higher force and displacement would permanently bend the sample. In Figure 26 we can see the 3-point bending set up from top and side view.

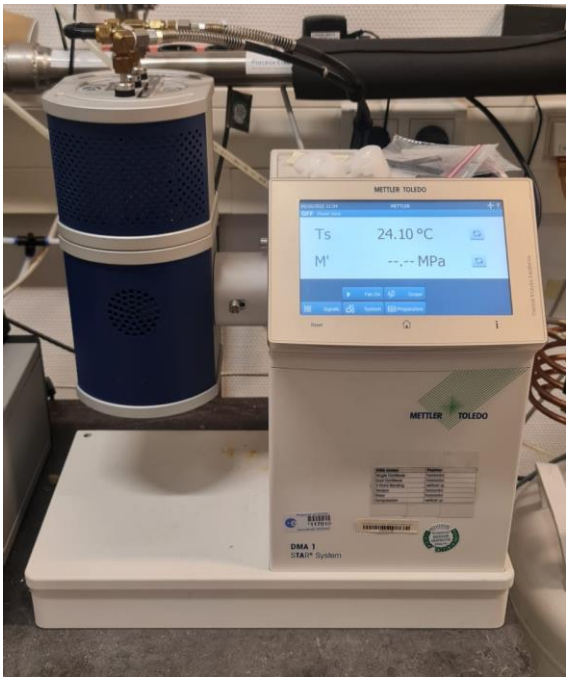

Figure 24. DMA1 instrument

Figure 25. DMA 861 instrument

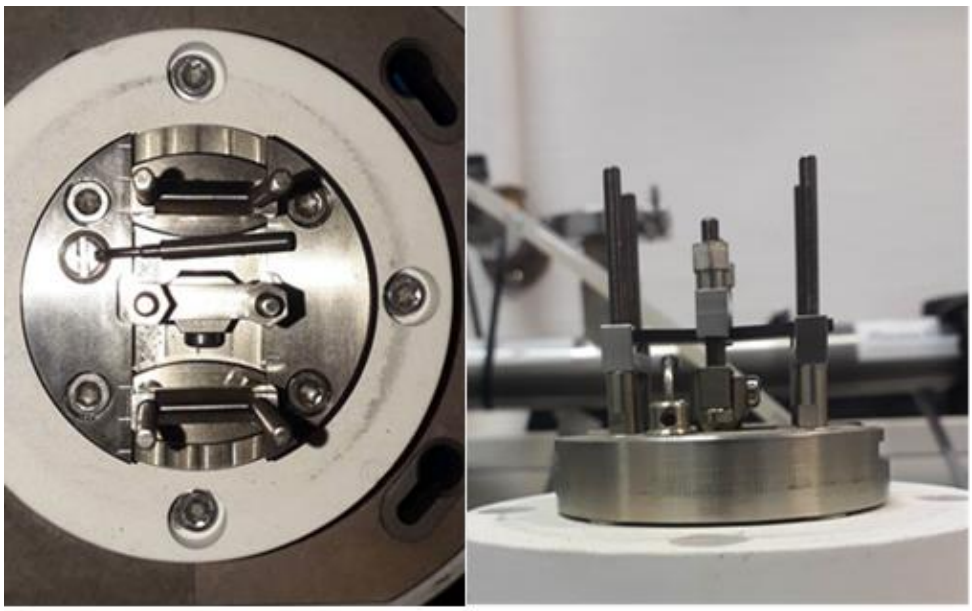

Figure 26. DMA1 3-point bending sample set up. Left: top view .Right: side view

Adhesives were tested from -150°C to 100°C with a frequency of 1 Hz, displacement of 20 μm and force of 2 N to identify their Tg. In Figure 27 we present the method parameters selected for shear testing, while Figure 28 shows the preparation of shear sample as well as way it is set up in the DMA 861 instrument.

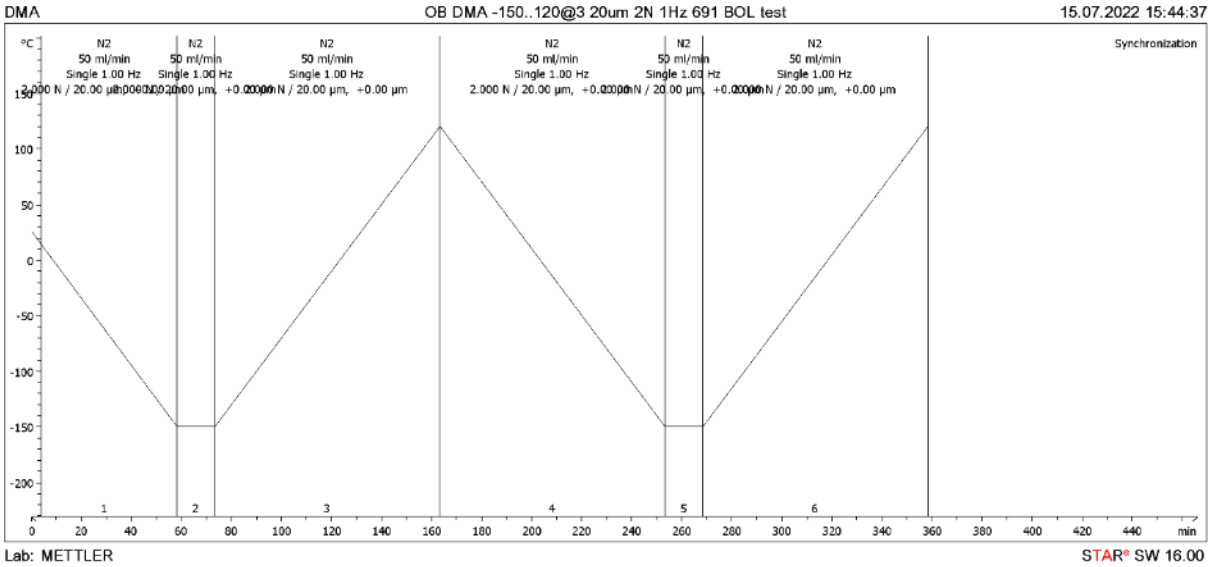

Figure 27. DMA method to which the shear samples were subjected

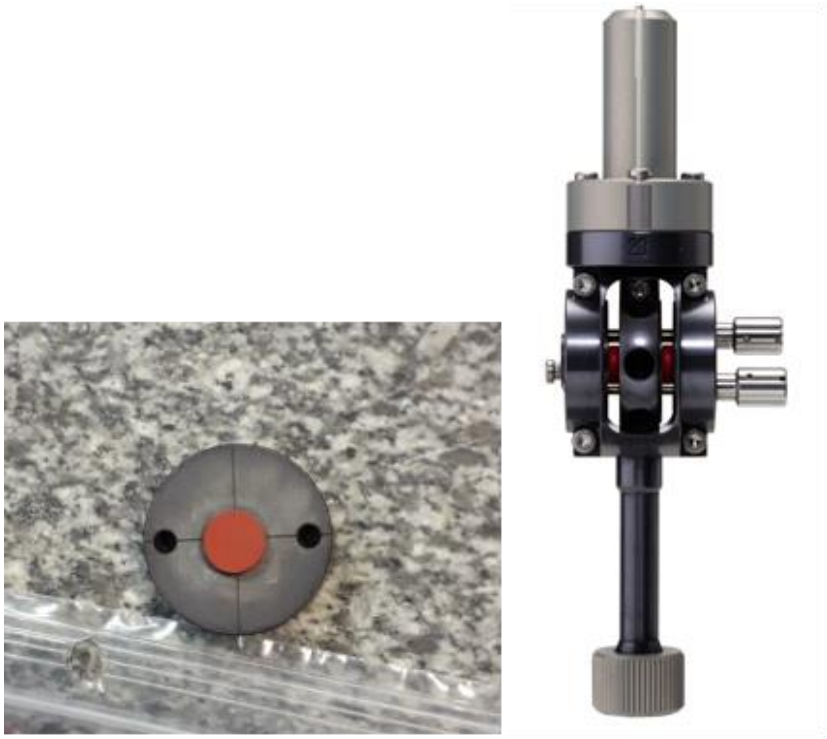

Figure 28. Left: DMA sample preparation in shear. Right: DMA Shear mode set up

3.2. Standoff bonding

The first step in the adhesive bonding process was to study the effect of surface preparation of sandwich panels and standoffs. All standoffs were cleaned with isopropyl alcohol (IPA). For the sandwich panels the CFRP had 3 different preparations: (i) no treatment, (ii) IPA cleaning and (iii) sanding using fiber glass pen and then IPA cleaning to remove any sanding debris. Figure 29 below shows the sanding process of the CFRP, after this step IPA cleaning was performed. Figure 30 shows the fiber-glass pen used to sand the CFRP surface.

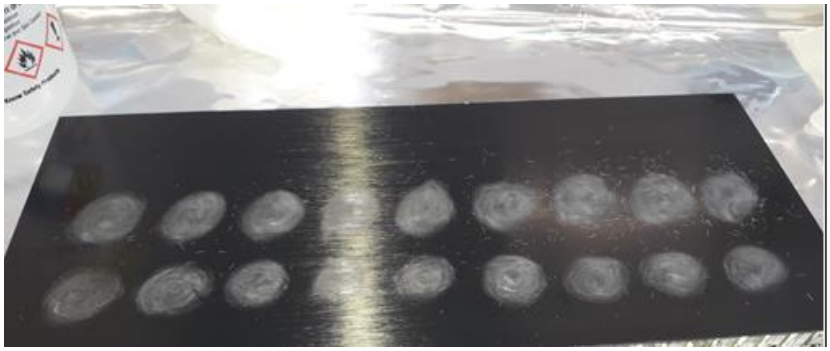

Figure 29. Sanding surface preparation

Figure 30. Fiber-glass pen used for sanding

The screening test showed that the best surface treatment consisted of sanding and cleaning with IPA. This method was then applied to the CFRP substrates to which standoffs were bonded with different thicknesses.

After the surfaces were prepared, they were laid on top of clean poly-wipe. Then the mixing of the adhesives took place. An empty plastic cup container was weighed, and

then parts A and B were poured in accordance with the weight ratio suggested by the manufacturer. They were then carefully mixed with a clean wooden spatula, aiming to minimize entrapped air bubbles. After the adhesive was thoroughly mixed for at least 30 s, the cup was placed inside a vacuum chamber, and it was cycled 3 times between atmospheric pressure and vacuum to remove any air pockets were introduced during the mixing. Then, it was carefully inserted in syringes to help the adhesive application. Figure 31 shows the mixed nano-enabled adhesive after vacuuming, prior to inserting in the syringe and Figure 32 depicts the nano-enabled adhesive in the syringe, right before the application.

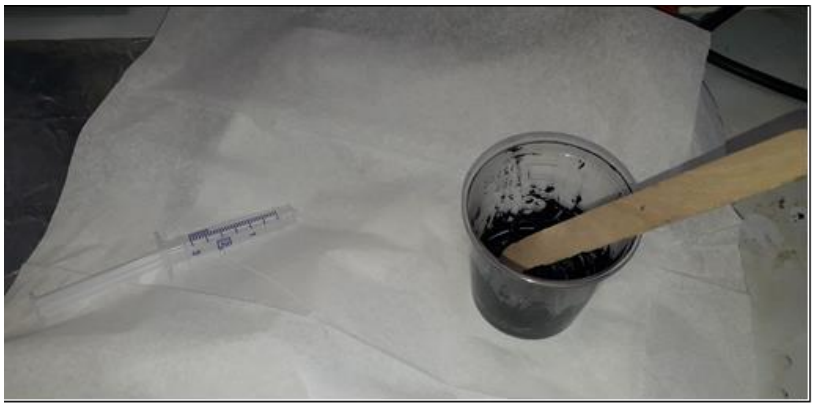

Figure 31. Mixed nano-enabled adhesive and empty syringe for standoff bonding

Figure 32. Syringe filled with nano-enabled adhesive

With the adhesive and surfaces ready, the bonding procedure started. At first, a small amount of adhesive in form of a blob was laid in the sandwich panel. Then the 3 spacers that would secure the bondline thickness were laid as evenly as possible separated 120 degrees from one another. After the spacers were in place, a small amount of adhesive was applied to the bottom of the base of the standoff and, using tweezers, it was pressed firmly to the bonding area for a couple of seconds. While placing the standoff onto the CFRP it was important to pay attention to the spacer wires as they would often move resulting in a not ideal placement or even being removed completely. To avoid this, it was important to try to keep them in place by holding them while also pressing down the standoff. After this procedure was performed for one adhesive, the procedure was repeated for the other ones, then the samples were left to cure for at least 7 days.

Before testing the samples, DSC tests were performed in the cured adhesives to ensure that it had fully cured and that they were properly prepared and mixed. Results are presented in 4.1.2.

Figure 33 depicts the standoff samples while curing, as well as the cups with the remaining adhesive (allowed to cure in the same conditions prior to DSC testing).

Figure 33. Standoffs and extra adhesive curing in room temperature

3.3. Thermal cycling vacuum chamber

To compare pristine samples with thermally cycled samples, a thermal cycling vacuum (TVAC) chamber was used. The samples were kept for a about a day just in vacuum, to reach high vacuum, as representative as possible for space applications. This was the aimed temperature range, at sample level, in the TVAC chamber.

It is worth noting that the maximum temperature of 90°C was also selected to ensure the stability of the sandwich panel, as the CFRP was bonded to the Aluminum honeycomb with a film adhesive that has a Tg of 90°C. We wanted to ensure that the standoffs would not get displaced after the thermal vacuum exposure.

In total, the samples were exposed to 50 heat-cool cycles. We opted for 50 cycles because they are enough to showcase differences with respect to pristine samples while allowing for testing within a reasonable schedule. The heating rate was 3 K/min and a dwell time after heating and cooling of 10 minutes, to reduce any thermal lag and allow the extreme temperatures to be reached. To identify the correct method parameters, a pre-test was performed using just sandwich panels without any samples. This was needed because the sandwich panel, which is sitting directly in contact with the heating/cooling plate (Figure 34) acts as an insulator for the top surface in which the glued samples would be. Finally, a thermocouple was attached to the top surface of each panel to have a good reading of the actual temperature that was present in each sample.

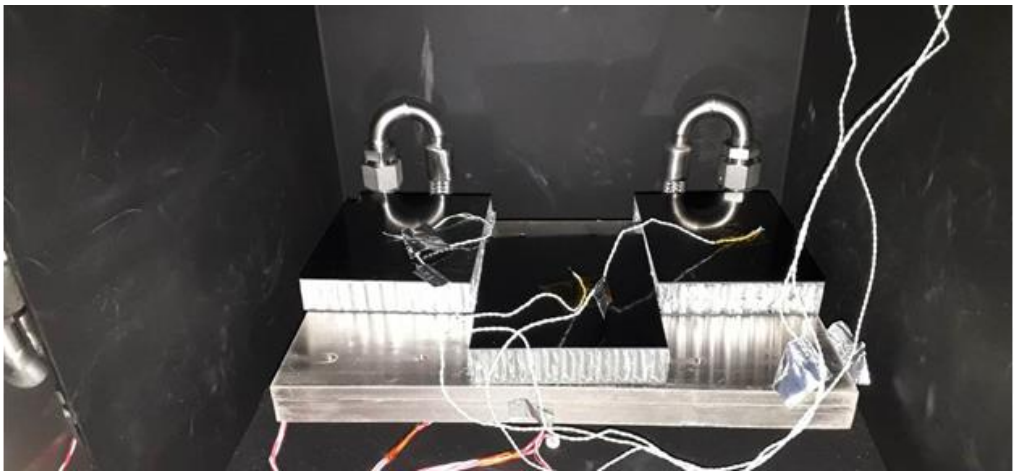

Figure 34. Thermal cycling vacuum chamber with dummy samples for fit check

3.4. Tensile & Shear testing

To measure the strength of the bonding the LR5K Plus tensile instrument by AMETEK, as it can be seen in the Figure 35 , was used. The following parameters were chosen: pulling rate of 5 mm/min and 0.5 N pre-force. If the instrument sensed a drop of more than 10% it would stop. This limit was sufficient to detect when the standoffs had debonded.

Figure 35. Lloyd LR5K Plus tensile instrument

As the sample geometry was not the standard lap-shar samples used in this instrument, the available jigs were not able to clamp the samples correctly. For this reason, it was necessary to design and manufacture dedicated custom jigs for the tension and shear tests. The initial jig concept design was done in Fusion360 CAD software (see Figure 36). After some iterations the final jigs were manufactured in collaboration with the workshop at ESA. The jigs were made out of stainless steel, with some parts made out of aluminum.

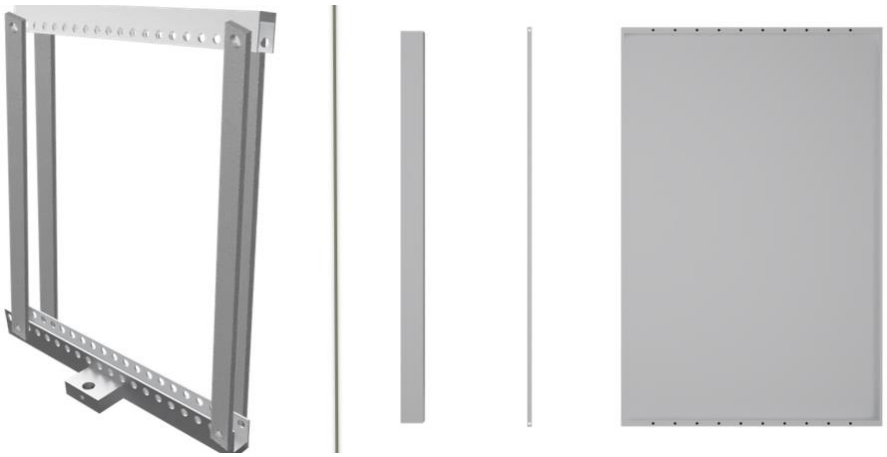

Figure 36. Initial jig concepts. Left: Shear jig. Right: Tension jig.

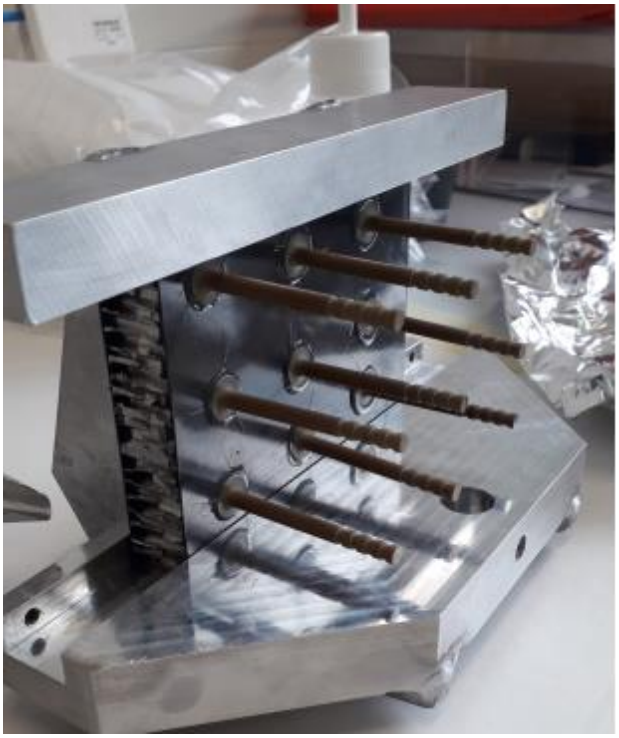

Figure 37. Shear mode jigs fit check

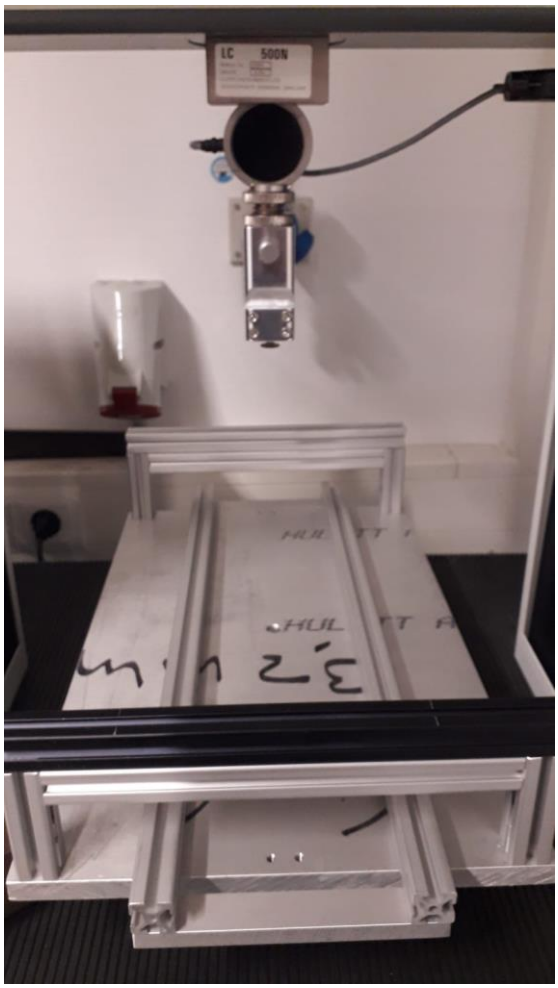

Figure 38. Custom tension jig set up

Figure 39. Left: Shear mode testing. Right: Tension mode testing

4. RESULTS

In this chapter the data obtained from thermal analysis (4.1) and the standoff bonding study (4.2) are presented. For each thermal analysis technique only a few graphs are displayed but the data for all sample are summarized in the corresponding tables. More graphs can be found in the appendixes.

4.1. Thermal characterization

4.1.1. TGA results

The evolution of mass loss was recorded for all the samples, normalized to the original mass of each specimen, and plotted as function of sample temperature. The 1st derivative (plotted on the top right) was also calculated in order to be able to discern the degradation steps responsible for the mass loss. The main parameters of interest were:

- The temperature at which it reached 1% mass loss
- The total mass loss in the whole temperature range
- The onset of the first degradation step
- The onset of the first derivative step
- The inflection point, where the mass loss rate peaks.

The graphs below present two examples of the TGA results obtained in this study. Graph 4 corresponds to a CFRP plate in which one degradation step can be observed, corresponding to the decomposition of the polymeric matrix. Since the fibers remain, the total mass loss is less than 25%. Graph 5 shows the mass loss of an adhesive sample, in which two degradation steps can be identified. Typically, a decrease of mass after 300 °C corresponds to pyrolysis of organic compounds. In the case of non-filled adhesives, the total mass loss is usually larger than the one of CFRP as they are made of mostly organic material. The TGA results for all specimens analyzed in this study (see Table 1) are summarized in Table 6. All the TGA graphs can be found in APPENDIX C: TGA graphs.

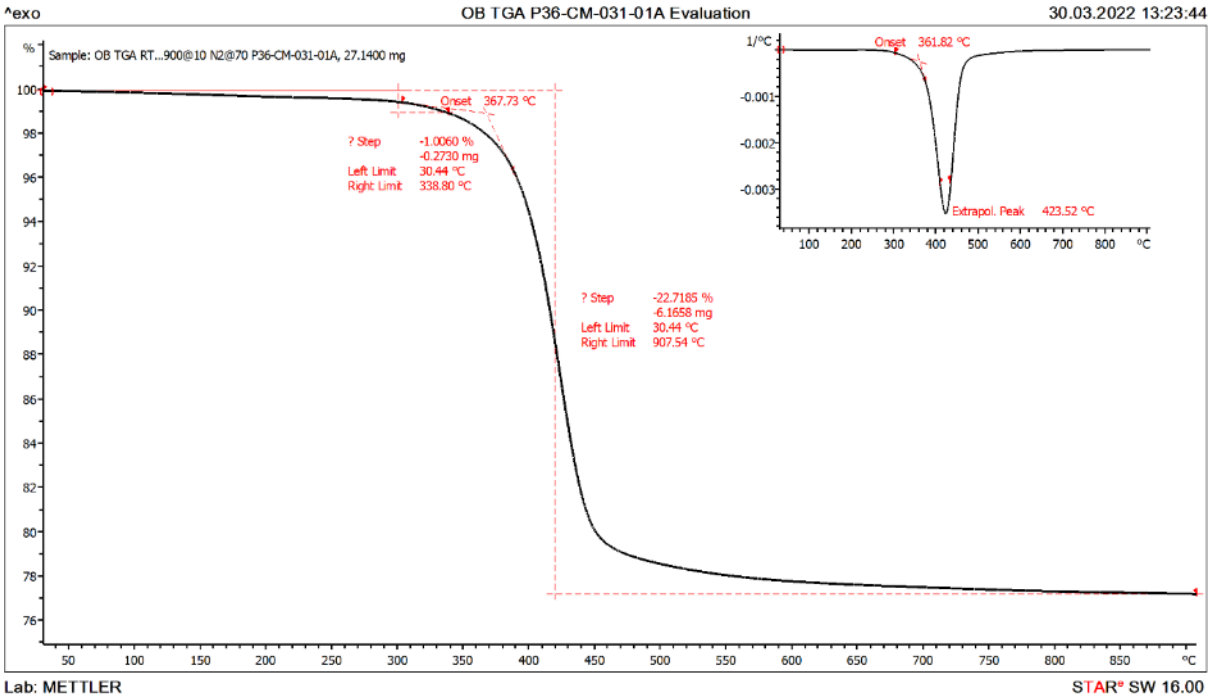

Graph 4. Normalized mass loss vs sample temperature of sample P36-CM-031-01A. Top right: calculated 1st derivative. Curves have been corrected for buoyancy.

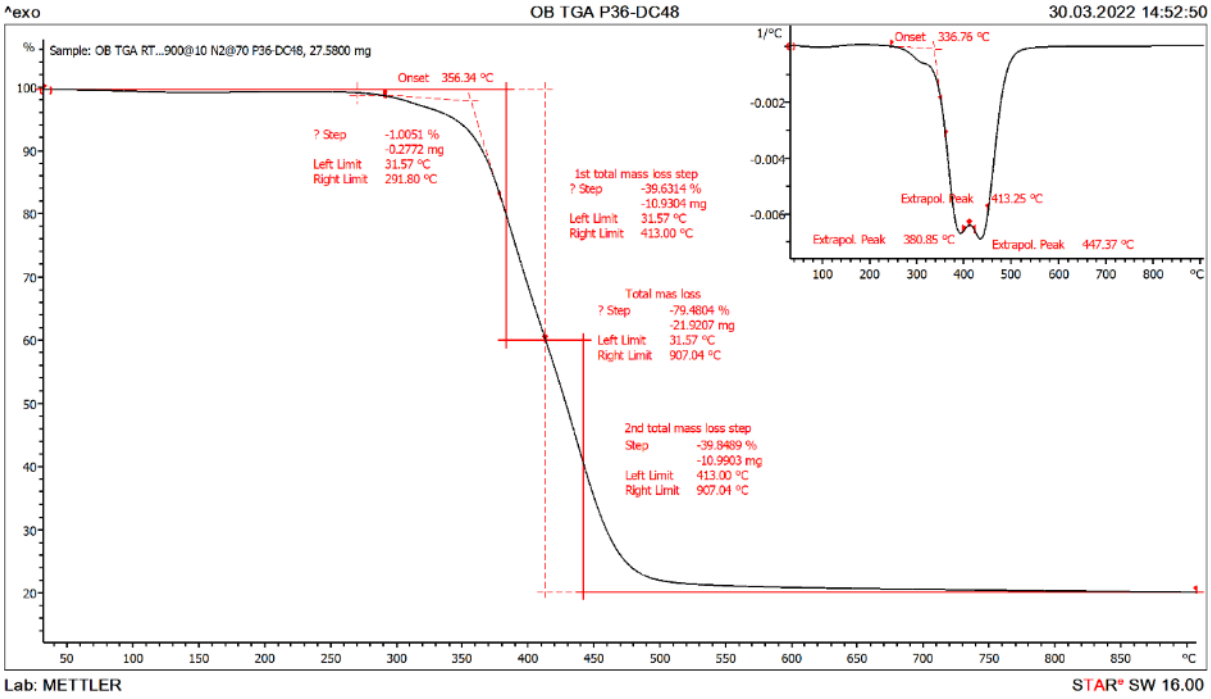

Graph 5. Normalized mass loss vs sample temperature of sample P36-DC48. Top right: calculated 1st derivative. Curves have been corrected for buoyancy.

From the curve showing normalized weight values vs sample temperature we derive data regarding the % of mass loss and the temperature, while from its 1st derivative we get information regarding the onset rate of the mass loss as well as its peak.

The amount of total mass loss between pristine CFRP and enabled CFRP plates did not seem to have significant differences. As expected, adhesives had greater mass losses than CFRPs. An interesting observation can be made regarding cured and uncured film adhesives. The cured film adhesives had slightly more mass loss than the uncured ones. This can be explained as uncured film adhesives used an amount of energy from the rising temperature to cure, while cured adhesives had all the energy used for the mass loss.

In summary:

Table 6. TGA results

Material		1% mass loss (°C)	Total mass loss (%)	Mass loss onset (°C)	mass loss rate onset (°C)	Peak mass loss rate (°C)
CFRP	**P36-CM-012-04**	340	25.7	377	365	406
	P36-CM-013-02	339	22.8	382	348	412
	P36-CM-014-04	340	23	365	343	406
	P36-CM-026-02	347	23.5	383	372	425
	P36-CM-027-02	342	25.2	377	364	423
	P36-CM-025-02	344	25.7	388	373	416
	P36-CM-031-01A	339	22.7	367	362	424
	P36-CM-032-01A	345	23.1	377	373	422
Film Adhesive	**P32-S120-C**	280	66.3	343	330	374
	P32-S121-C	330	20.8	355	336	380
	P32-S122-C	248	74.5	354	340	385
	P32-S129-C	267	74.2	354	329	407
	P32-S121-U	328	20.4	355	336	377
	P32-S122-U	110	73.9	353	338	386
	P32-S129-U	296	74	349	330	370
Other Adhesives	**P36-DC47**	268	80.4	355	327	370/(411)/449*
	P36-DC48	292	21.9	356	337	381/(413)/447*
	P36-DC51	285	79.8	351	339	379/(413)/452*
	P36-Redux312L	242	92.5	374	345	438
	P32-Araldite	313	26.8	351	337	376

	P36-2216Grey	329	68.2	360	343	378/(413)/441*
	P32-S133-ML	315	15.8	349	336	376
	P32-S137-ML	206	72.3	351	323	381
	P36-DC-9-Th26	188	96.5	369	356	402/(411)/432*
	P36-M21-Th77	166	81.5	360	338	382/(414)/445*

For the materials in which the mass loss was observed to occur in 2 steps., a dedicated Table 7 is presented.

Table 7. TGA additional results of samples with 2 step mass loss

Material	1st mass loss peak temperature (°C)	1st mass loss step (%)	Intermediate minimum peak temperature (°C)	2nd mass loss peak temperature (°C)	2nd mass loss step (%)
P36-DC47	370	41	411	449	39.4
P36-DC48	381	39.6	413	447	39.8
P36-DC51	379	39.5	413	452	40.3
P36-2216Grey	378	31.64	413	441	36.6
P36-DC-9-Th26	402	46.64	411	432	49.9
P36-M21-Th77	382	42.01	414	445	39.5

4.1.2. DSC results

As mentioned in chapter 3, DSC measurements were performed after TGA analysis. The maximum temperature was selected as 50°C less than the one at which 1% mass loss was observed. Table 8 below presents the Tg values calculated from the 3rd heating segment of each sample. The first heating ramp is applied in order to remove the residual volatiles, and post-cure if applicable. The second and third heatings then measure the polymer without a thermal history. The third segment is usually more stable, and therefore used here to present the results. As an example, in Figure 40 we present the normalized results of the three heating curves obtained for Araldite LY1556. The evolution of the Tg between the first and subsequent heating curves is clear. In addition, a small endothermic peak can be seen on the first heating curve (red) at around 65 °C. For all the materials three samples were tested for statistical purposes. However, for two

materials (P32-S133-ML and P32-S137-ML) there was enough material for only one sample to be analysed.

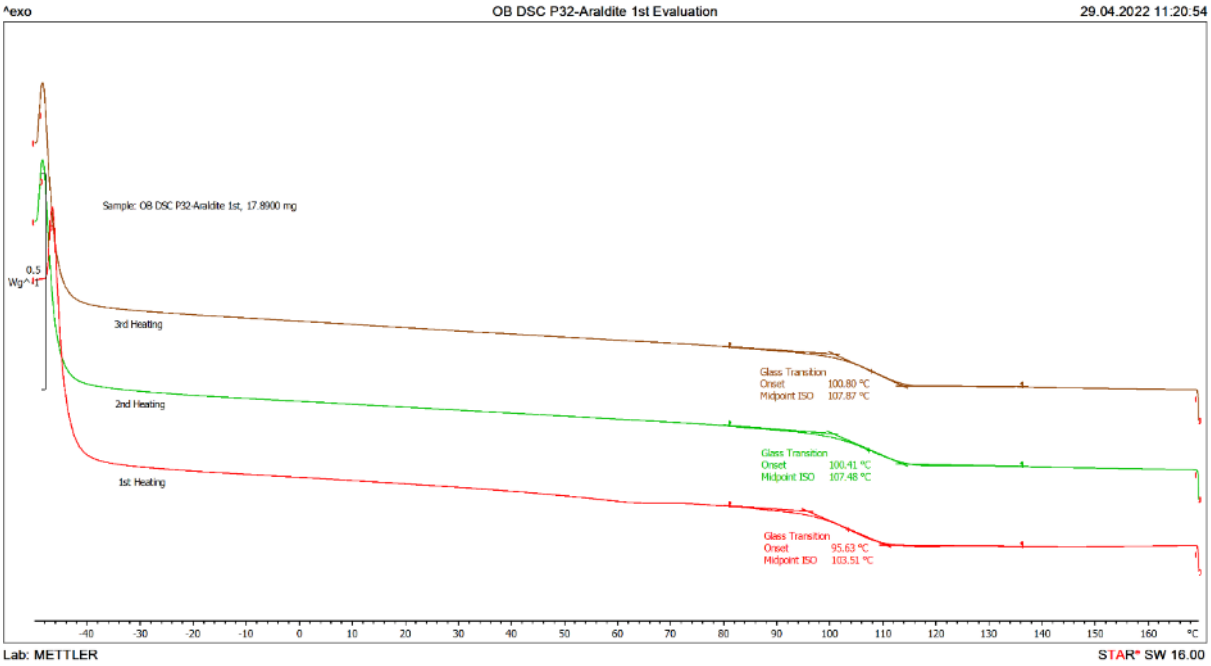

Figure 40. Example of DSC result, showing the normalized heat flow as function of sample temperature for Araldite. The calculated Tg are presented for each heating curve.

Table 8. Glass transition temperature of all specimens under study obtained via DSC.

Material		Tg (°C) obtained from 3rd heating				
		1st Sample	2nd Sample	3rd Sample	Average	StDev
CFRP	P36-CM-031-01A	164	166	163	164.3	1.2
	P36-CM-032-01A	175	174	174	174.3	0.5
	P36-CM-012-04	179	177	177	177.7	0.9
	P36-CM-013-02	176	174	176	175.3	0.9
	P36-CM-014-04	179	178	178	178.3	0.5
	P36-CM-025-02	180	179	180	179.7	0.5
	P36-CM-026-02	177	180	171	176.0	3.7
	P36-CM-027-02	179	182	181	180.7	1.2
Film Adhesives	P32-S120-C	111	113	110	111.3	1.2
	P32-S121-C	94	94	94	94.0	0.0
	P32-S122-C	89	89	89	89.0	0.0
	P32-S129-C	114	116	115	115.0	0.8
	P32-S121-U	89	82	85	85.3	2.9
	P32-S122-U	85	86	85	85.3	0.5

	P32-S129-U	100	100	100	100.0	0.0
Other Adhesive	**P36-DC47**	18	22	22	20.7	1.9
	P36-DC48	25	22	23	23.3	1.2
	P36-DC51	21	21	21	21.0	0.0
	P36-Redux312L	109	109	108	108.7	0.5
	P32-Araldite	108	108	108	108.0	0.0
	P36-2216Grey	27	26	26	26.3	0.5
	P32-S133-ML	76				
	P32-S137-ML	>90				
	RTV-S691	-115				
	DOWSIL 93-500	-122				
	P36-DC-9-Th26	18	16	8	14.0	4.3
	P36-M21-Th77	5	6	4	5.0	0.8

CFRP plates have higher glass transition temperature than adhesives and enabling CFRP plates seemed to not have any effect in Tg. Uncured film adhesives have slightly lower Tg than the cured ones. This could be due to the fact that cured adhesives have stronger forces between their molecules making it harder for them to overcome this higher energy and therefore to have an increase in molecular mobility.

It is worth mentioning that the Tg of P32-S137-ML was not identified in the DSC test, as this was only performed up to 100 °C. However, a glass transition can be intuited. Therefore, we assess that the P32-S137-ML Tg is above 90 °C.

Graph 6, Graph 7 and Graph 8 show the DSC curves of each adhesive used in standoff bonding for pristine shear, thermally cycled shear, pristine tension and thermally cycled tension. The graphs show that the adhesives were properly mixed and cured by the time the standoff bonding tests started. All the DSC graphs can be found in APPENDIX D: DSC Graphs.

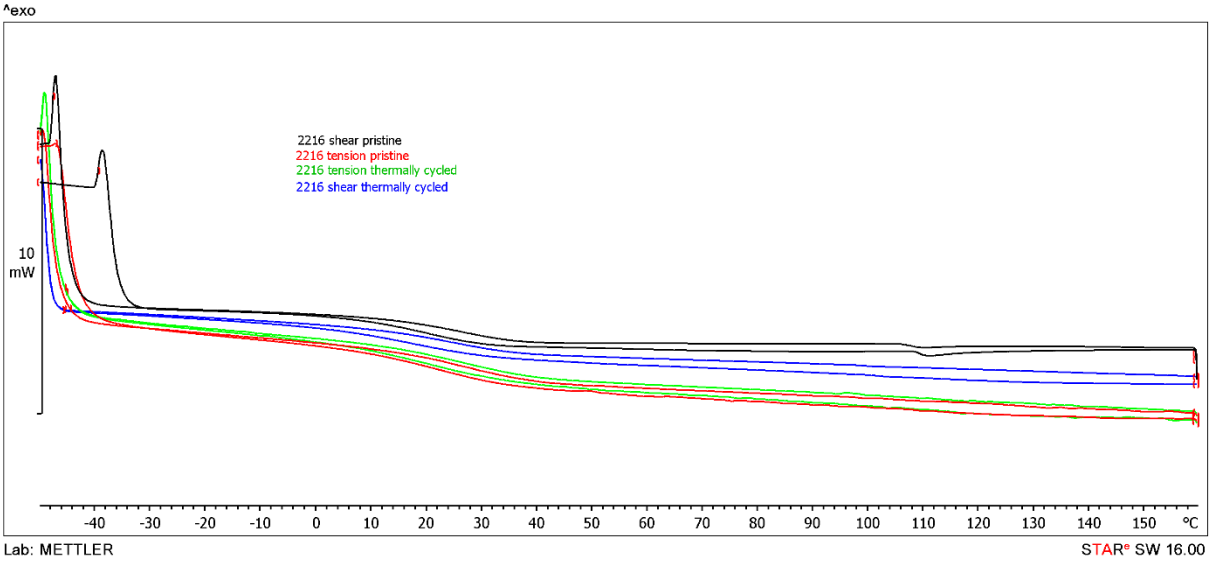

Graph 6. DSCs for 2216 adhesive used in standoff bonding

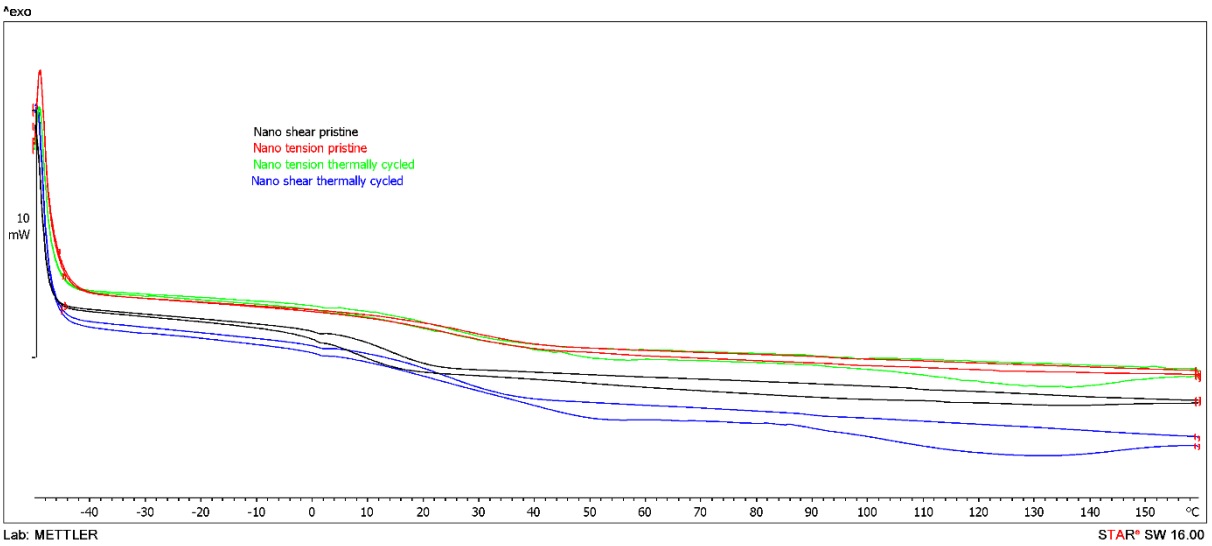

Graph 7. DSCs for nano-enabled adhesive used in standoff bonding

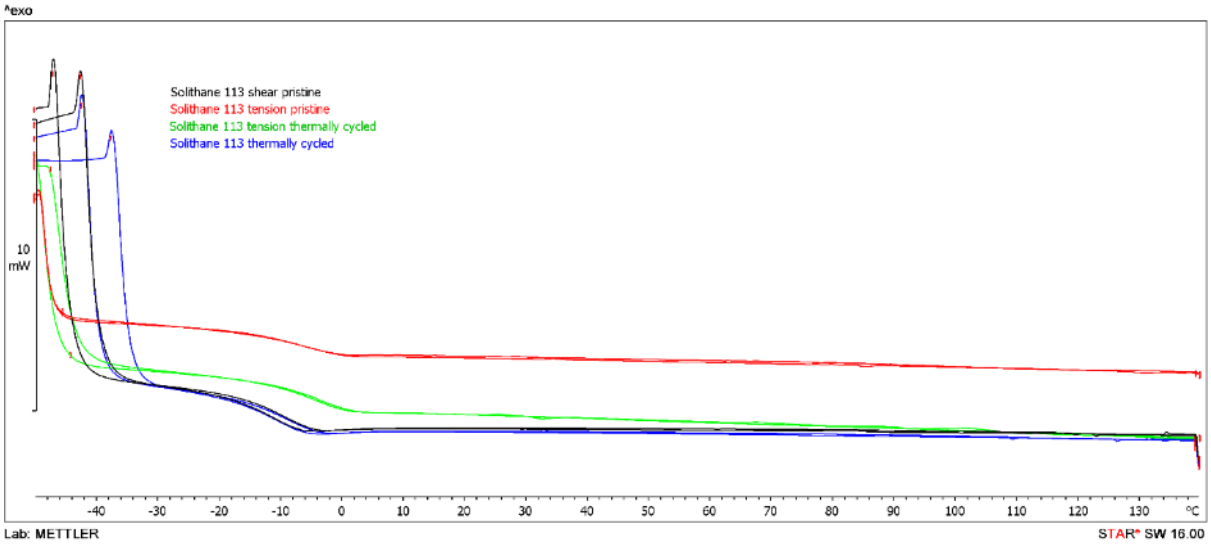

Graph 8. DSCs for Solithane113 used in standoff bonding

4.1.3. TMA and DIL results

The samples tested in TMA were consisting of two aluminum plates bonded with different adhesives. This was done to enable the testing of the adhesive film as films due to their thin nature are problematic when it comes to testing and they need a specific sample set up. An example of analyzed graph for the sample P32-S129-ML can be found in the Graph 9. All the TMA graphs can be found in APPENDIX E: TMA Graphs.

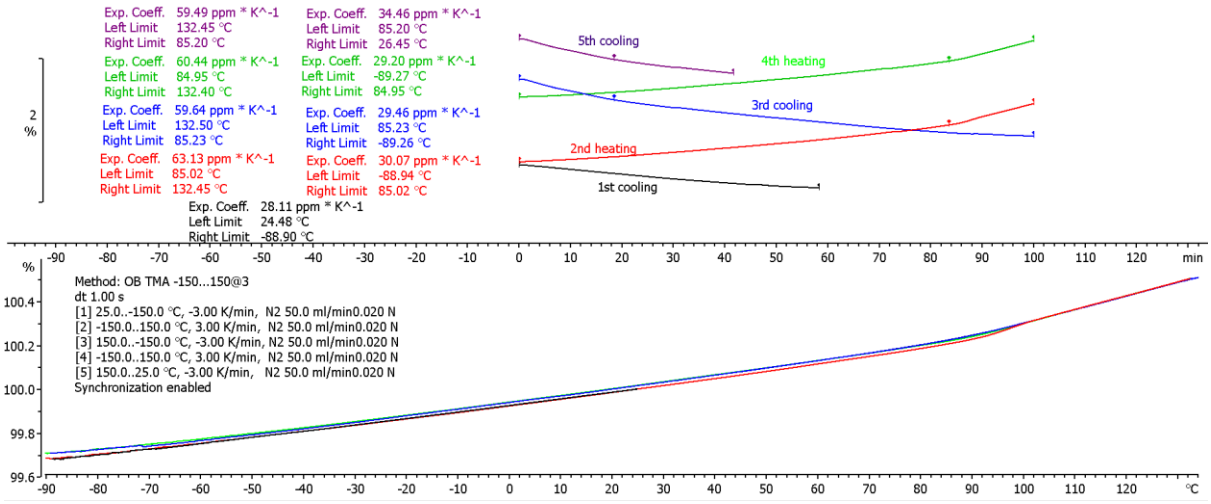

Graph 9. TMA P32-S129-ML. Top: Normalized length vs time. Down: Normalized length vs temperature

For TMA results the first table includes all the samples and the average coefficient of expansion for specific temperature ranges that were selected in order to calculate CTE in the linear regions. It should be noted that the temperature ranges are an approximation.

Table 9. TMA average results

Average CTE (ppm/K)						
Aluminum sandwich panel samples	Temperature range* (°C)					
	(-132,-90)**	(25,-90)	(-90,85)	(85,132)	(25,85)	(132,148)**
P32-S120-ML	-	23.6	26.7	40.4	29.8	-
P32-S121-ML	-	24.2	26.2	40.3	28.2	-
P32-S122-ML	-	25.2	27.1	37.3	29.9	-
P32-S129-ML	-	28.1	29.6	60.2	34.5	-
P32-S134-ML	-	25.5	27.1	33.3	29.7	-
P32-S135-ML	-	25.1	26.4	35.3	29.3	-
P32-S137-ML	-	25.9	28.1	44.0	30.6	-
P32-S138-ML	17.7	24.0	24.1	34.7	25.4	40.2
P32-S139-ML	17.7	23.9	24.3	37.2	26.6	38.8
P32-Ref	19.1	24.6	26.6	35.2	29.9	37.2

** The samples, P32-S138-ML, P32-S139-ML and P32-Ref reached a wider temperature range, even though there was no difference in the method, from the rest of the samples. The instrument for the rest of the samples did not manage to reach the whole temperature range that was specified.

It must be noted that these values correspond to the whole sample setup and not just the adhesive itself.

Two different silicone adhesives were tested in the dilatometer. One was the RTV-S691 and the other was the DOWSIL 93-500. Both samples were tested at the beginning of life (BOL) meaning without having any thermal history, and the other were tested AGED meaning they have been cycled 10 times between -150 °C and 150 °C. Below, in the Graph 10, Graph 11, Graph 12 and Graph 13 the normalized sample length versus temperature can be seen. These graphs were used to derive the CTE and the Tg.

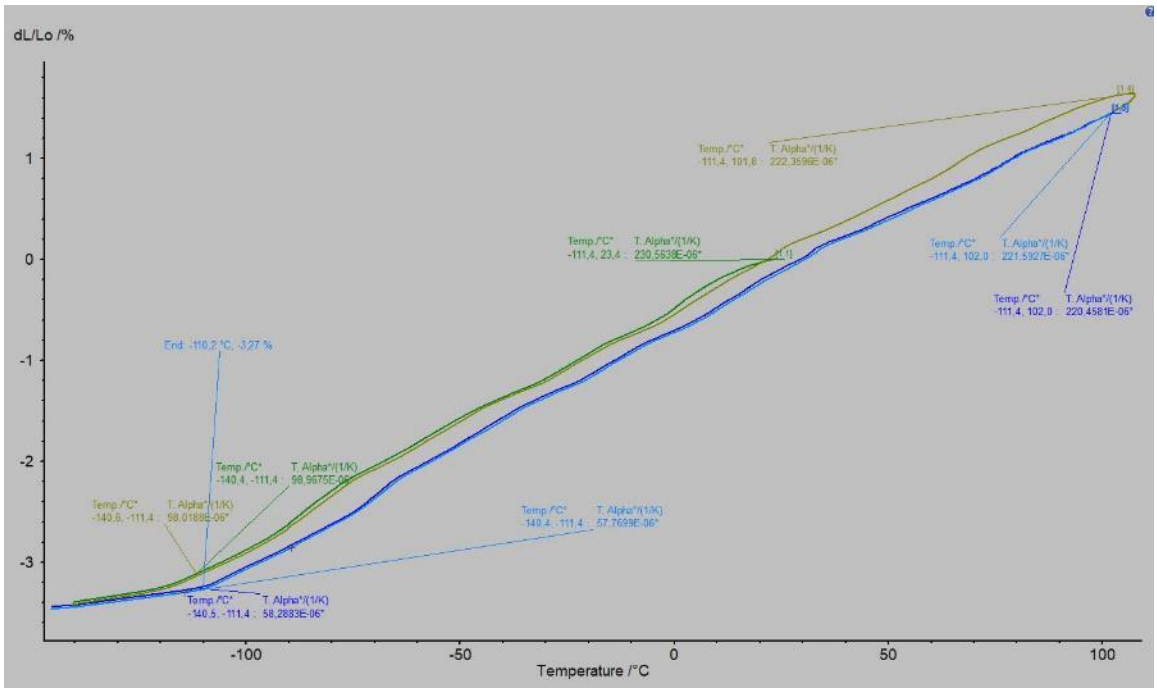

Graph 10. DIL RTV-S691 BOL

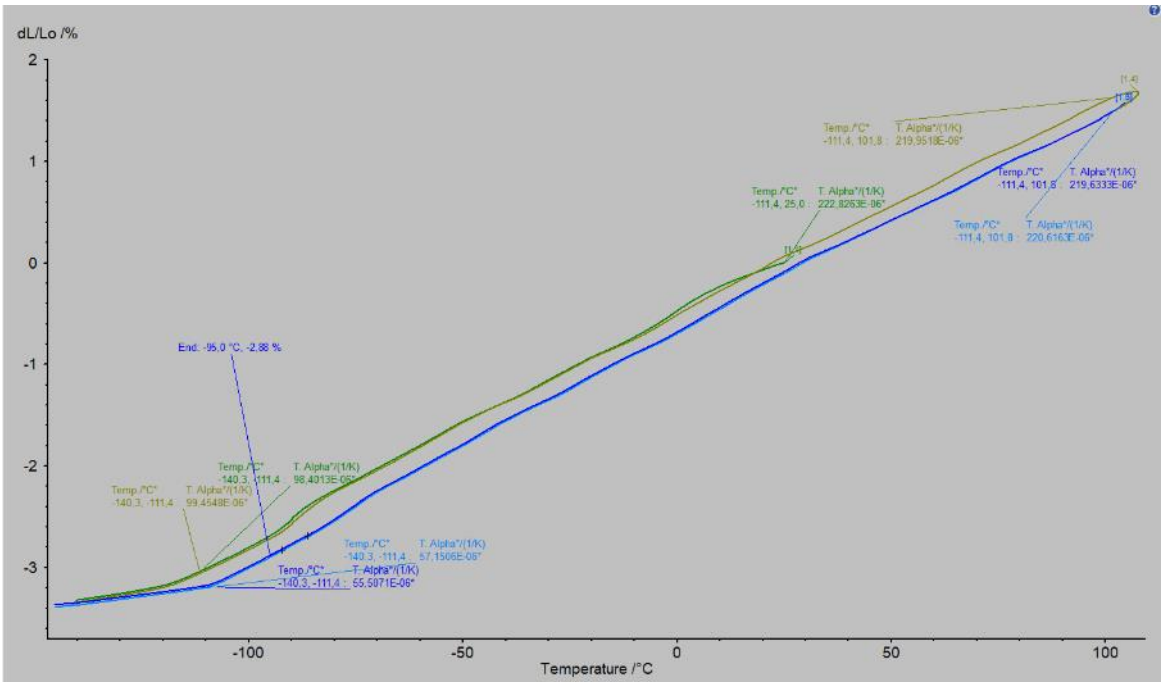

Graph 11. DIL RTV-S691 AGED

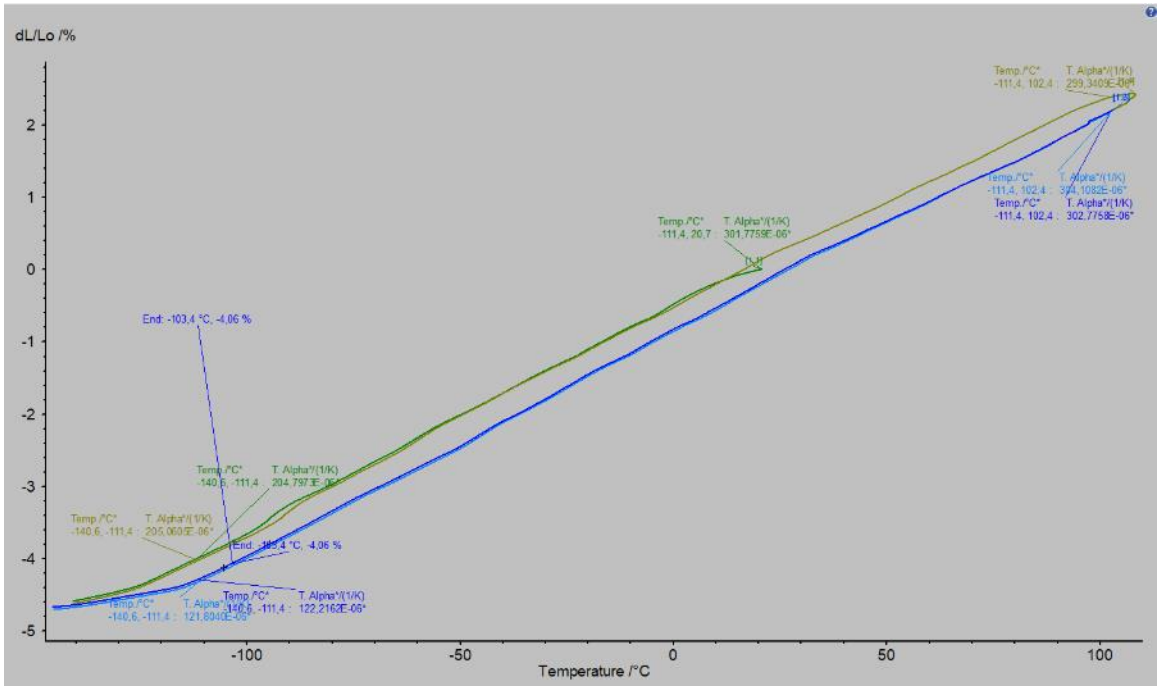

Graph 12. DIL DOWSIL 93-500 BOL

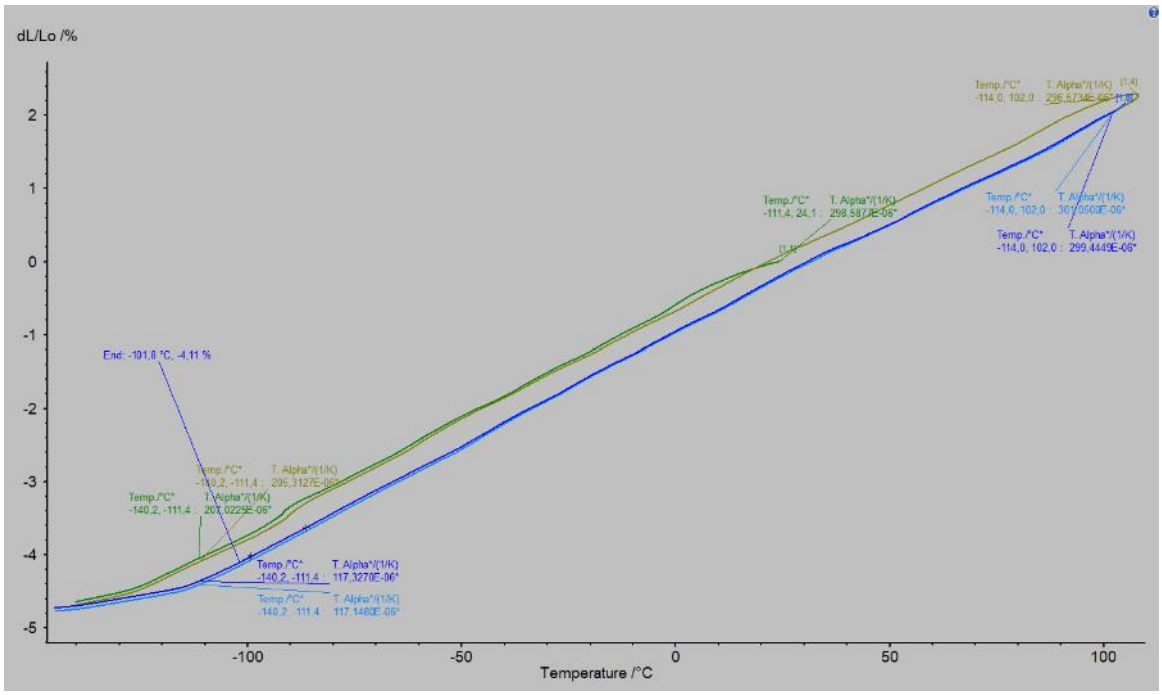

Graph 13. DIL DOWSIL 93-500 AGED

The Dilatometer derived CTE results can be found in the tables below. Again, the temperature ranges were selected to calculate CTE in linear parts of the graph. The Tg of RTV-S691 BOL was -110 ^{o}C, RTV-S691 AGED was -95 ^{o}C, DOWSIL 93-500 BOL was -103 ^{o}C and finally DOWSIL 93-500 AGED was -102 ^{o}C.

As it can be seen in the Table 10 and Table 11, both silicones seem to not be affected by the aging as their CTE values are almost identical.

Table 10. DIL RTV-S691 results. Left: BOL. Right: AGED

CTE (ppm/K)				CTE (ppm/K)			
BOL RTV-S691	Temperature range* (°C)			AGED RTV-S691	Temperature range* (°C)		
Segment	-140..-111	-111..102	-111..25	Segment	-140..-111	-111..102	-111..25
1st cooling	99	-	231*	1st cooling	98	-	223
2nd heating	58	220	-	2nd heating	55	220	-
3rd cooling	98	222	-	3rd cooling	99	220	-
4th heating	58	222	-	4th heating	57	221	-

Table 11. DIL DOWSIL 93-500 results. Left: BOL. Right: AGED

CTE (ppm/K)				CTE (ppm/K)			
BOL DC93-500	Temperature range* (°C)			AGED DC93-500	Temperature range* (°C)		
Segment	-140..-111	-111..102	-111..25	Segment	-140..-111	-111..102	-111..25
1st cooling	205	-	302	1st cooling	207	-	299
2nd heating	122	303	-	2nd heating	117	299	-
3rd cooling	205	299	-	3rd cooling	205	297	-
4th heating	122	304	-	4th heating	117	301	-

4.1.4. DMA results

In Graph 14 we see the storage modulus and the tan delta values starting at room temperature. We can see that the ability of the CFRP plate to store energy elastically is reduced as the temperature is getting higher. Finally, as it is well known, we can also see in the peak of tan delta that the Tg can be derived also from DMA giving us similar results with the DSC analysis.

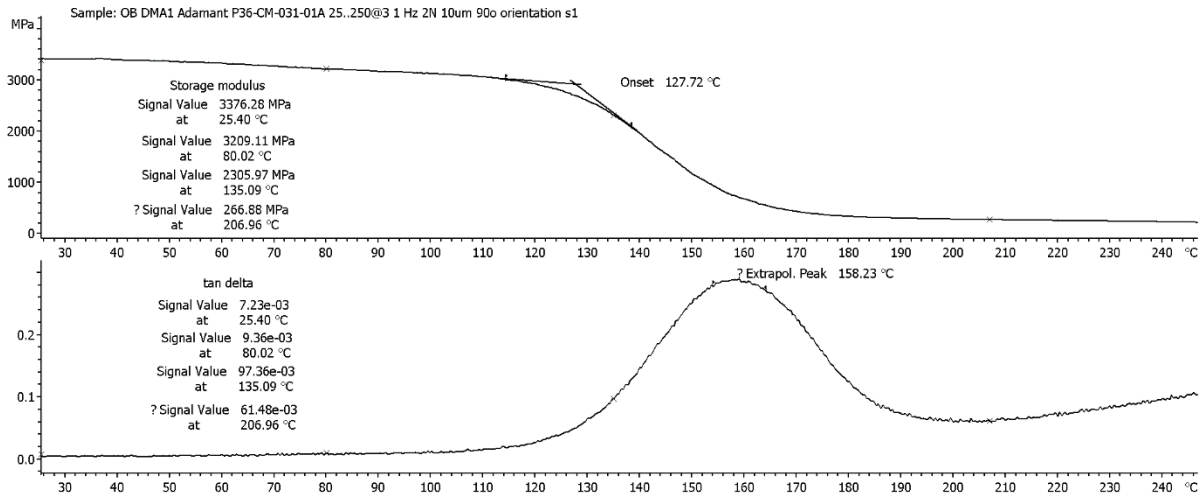

Graph 14. DMA curve of P36-CM-031-01A. Top: Storage modulus (M') vs temperature. Down: Tan delta vs temperature

The DMA results are in the Graph 15 below. The Graph 15 shows the storage and loss moduli as well as the tan delta of the 90° and 0° orientation of unidirectional CFRP plates as well as the quasi-isotropical CFRP plates.

As 0° orientation we have set the orientation that the force is parallel to the fibers also known as the strong orientation. As 90° orientation of the unidirectional plates we have set the weak orientation as the force is vertical to the fiber alignment. For some materials, three different samples were tested depending on the material availability. All the data values are referring to a temperature of 25°C. All the DMA graphs can be found in APPENDIX F: DMA Graphs.

In the Graph 15 below there are the average storage and loss moduli values of samples. There we can see that enabling CFRPs have a significant effect on loss and storage moduli.

- Red marks = enabled CFRP
- Black marks = pristine CFRP
- Hollow marks = weak orientation 90 °
- Full marks = strong orientation 0 ° or quasi-isotropic plate

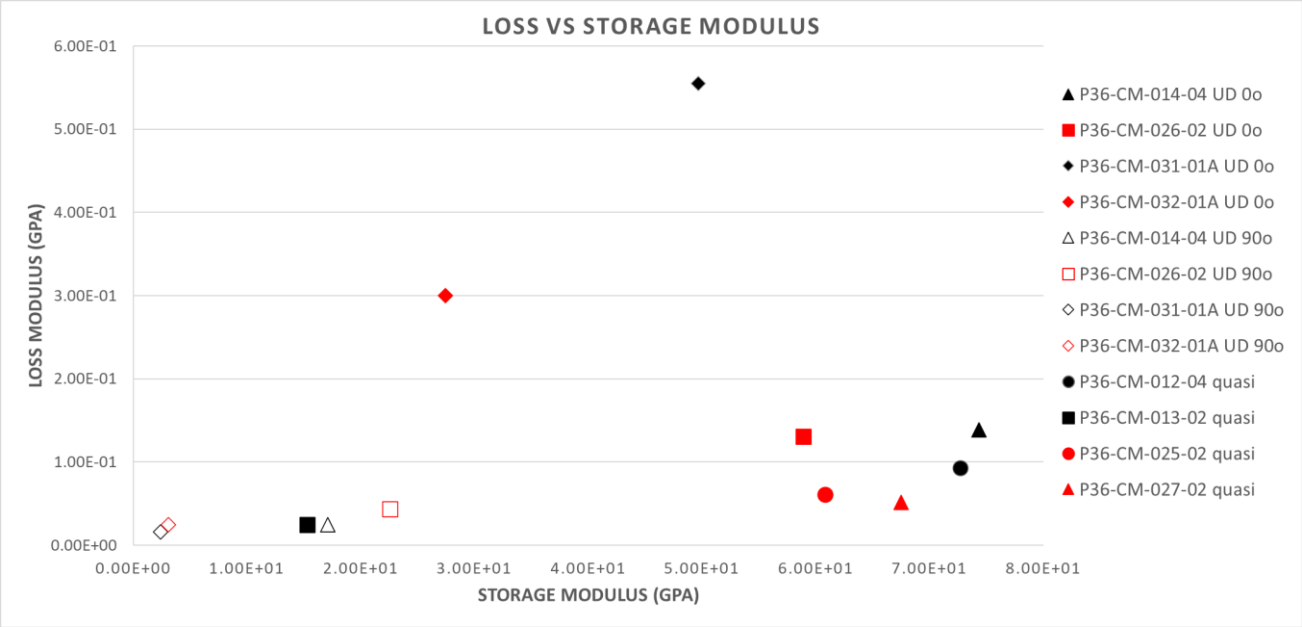

Graph 15. DMA Loss vs Storage modulus average results

From the Graph 16 and Graph 17 the Tg values are derived from the onset of tan delta.

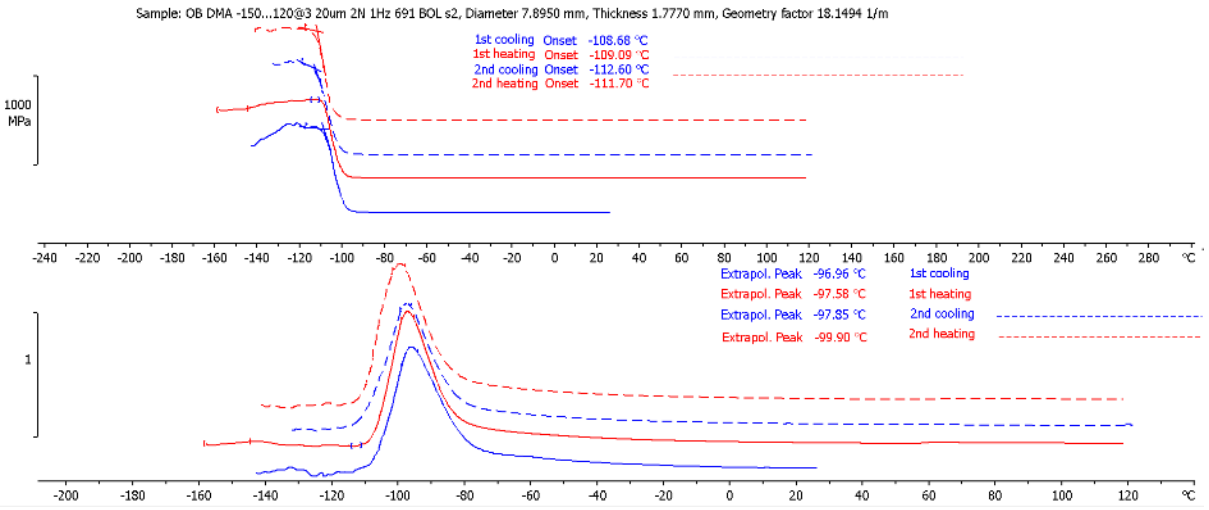

Graph 16. DMA shear RTV-S691. Top: storage modulus (G'). Down: Tan delta

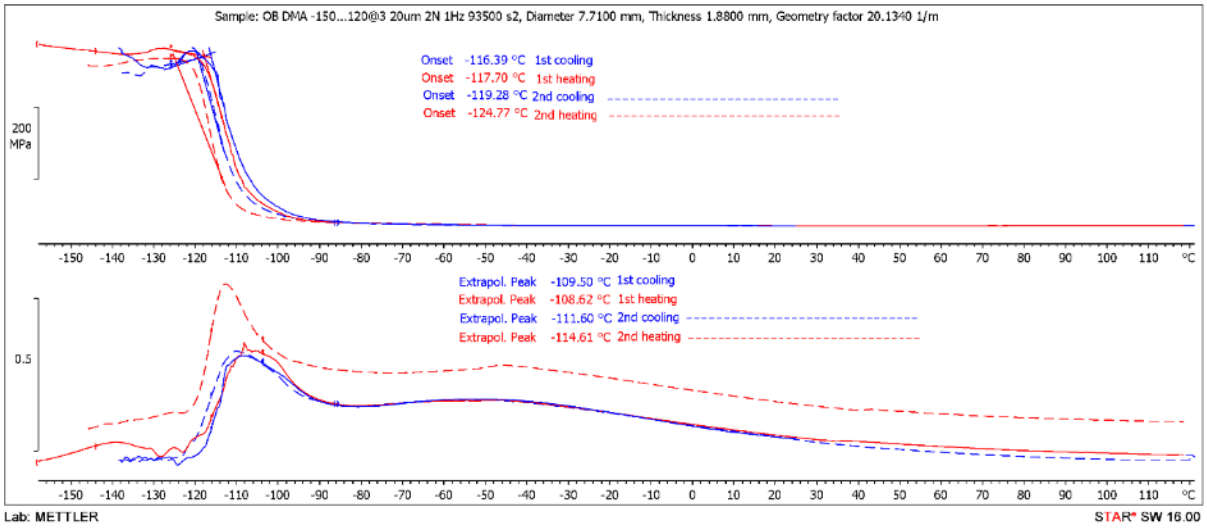

Graph 17. DMA shear DOWSIL 93-50.0 Top: storage modulus (G'). Down: Tan delta

Derived from DMA method, RTV-S691 has a Tg around -97 °C while DOWSIL 93-500 has around -111 °C. The difference in the Tg of both samples compared to the Tg derived from DSC, where RTV-S691 had a Tg around -155 °C and DOWSIL 93-500 had a Tg of around -122 °C, is due to the different technique, as well as the lower heating rate of TMA (3 K/min) compared to the heating rate of DSC (10 K/min).

We also see that the Tg results of DMA are closer to the ones derived from Diletometry, where RTV-S691 Tg = -110 °C and DOWSIL 93-500 Tg = -103 °C, than the ones derived from DSC. This is due to the fact that both techniques are based on mechanical principles and are performed with the same heating rate.

4.2. Standoff bonding results

As mentioned previously, the first step in the standoff bonding was selecting the surface treatment. Graph 18 shows the results of the pre-screening test using both 2216 and Solithane, between CFRP/Aluminum honeycomb and standoffs, and pulled in shear.

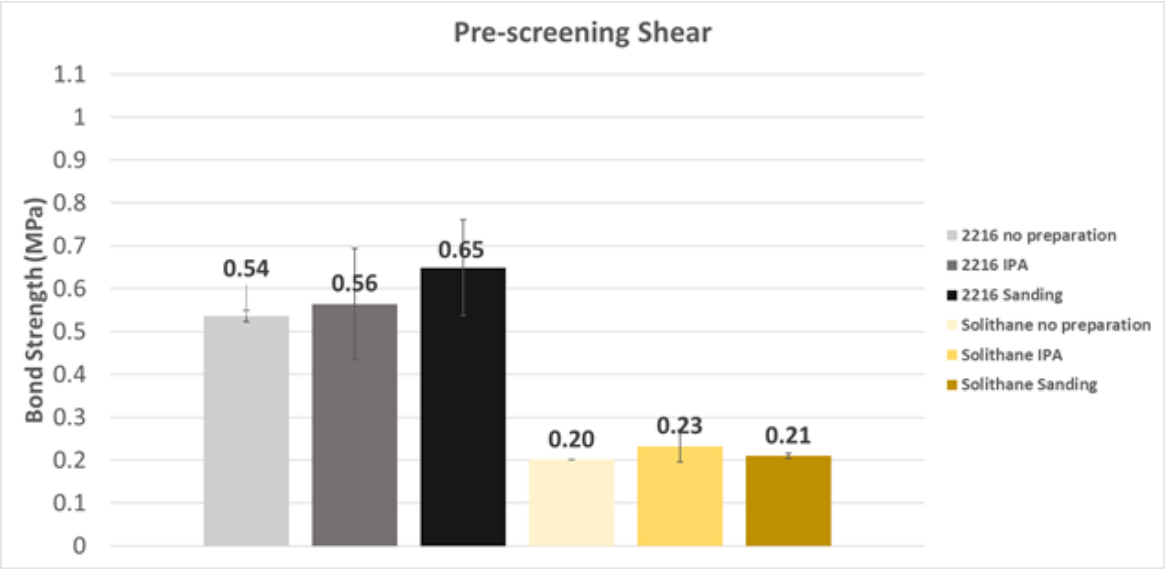

Graph 18. Bonding strength in pre-screening surface treatment shear samples

Sanding was considered to be the best surface treatment, as it showed 17% higher bond strength as compared to the lowest value in the case of the epoxy. This trend was not confirmed in the case of the polyurethane adhesive, but in that case the differences are less obvious.

After the pre-screening, the CFRP was sanded and IPA-cleaned, and then the rest of the samples were bonded and tested in pristine and thermal vacuum cycling configurations.

The graphs below show the bonding strength of pristine shear, pristine tension, thermally cycled shear and thermally cycled tension tests.

Graph 19 and Graph 20 display the results of shear testing, with pristine and thermal cycled samples respectively. It can be noted that thermal cycling benefits the bonding strength of all epoxy based adhesives, while not having a clear trend regarding the polyurethane based adhesive. In epoxy 2216, when pristine, the 500 μm bondline thickness is performing better than the rest thicknesses but after thermal cycling it gets outperformed by the 120 μm bondline thickness. For nano-enabled epoxy, when pristine, the 250 μm thickness is the option with the highest bonding strength but after thermal cycling it is the 500 μm. Finally, for Solithane 120 μm and 250 μm are performing

identically and 500 μm is performing the worst. After thermal cycling, 500μm outperforms the rest thicknesses, with 120 μm being the second best and 250μm being the worst.

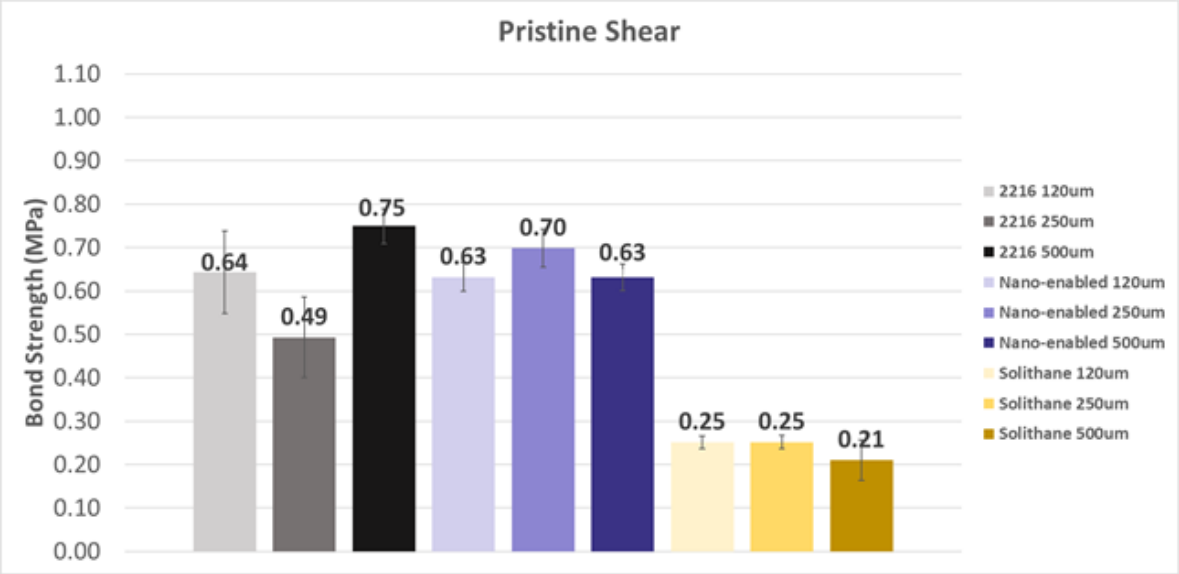

Graph 19. Bonding strength in pristine shear samples

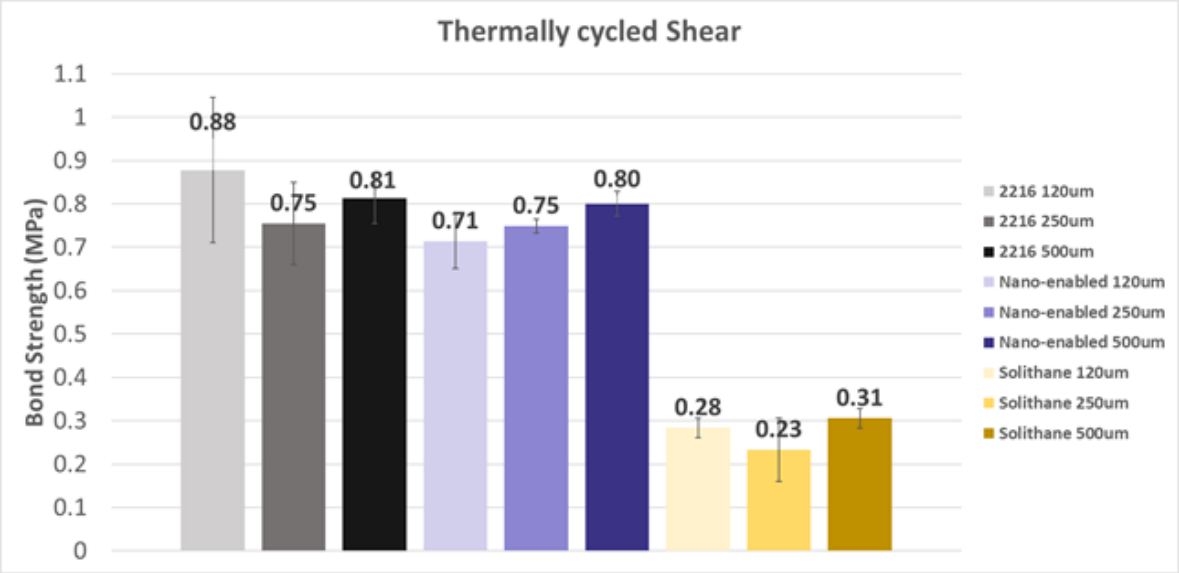

Graph 20. Bonding strength in thermally cycled shear samples

Graph 21 and Graph 22 show similar trends with Graph 19 and Graph 20. In tension, epoxy 2216 and nano-enabled epoxy have the same best thickness as in shear for both pristine and thermally cycled samples. Solithane is different as the identical

performing thicknesses are now the 250 μm and 500 μm, with the 250 μm being the best after thermal cycling, contrary to thermally cycled shear where it was worst.

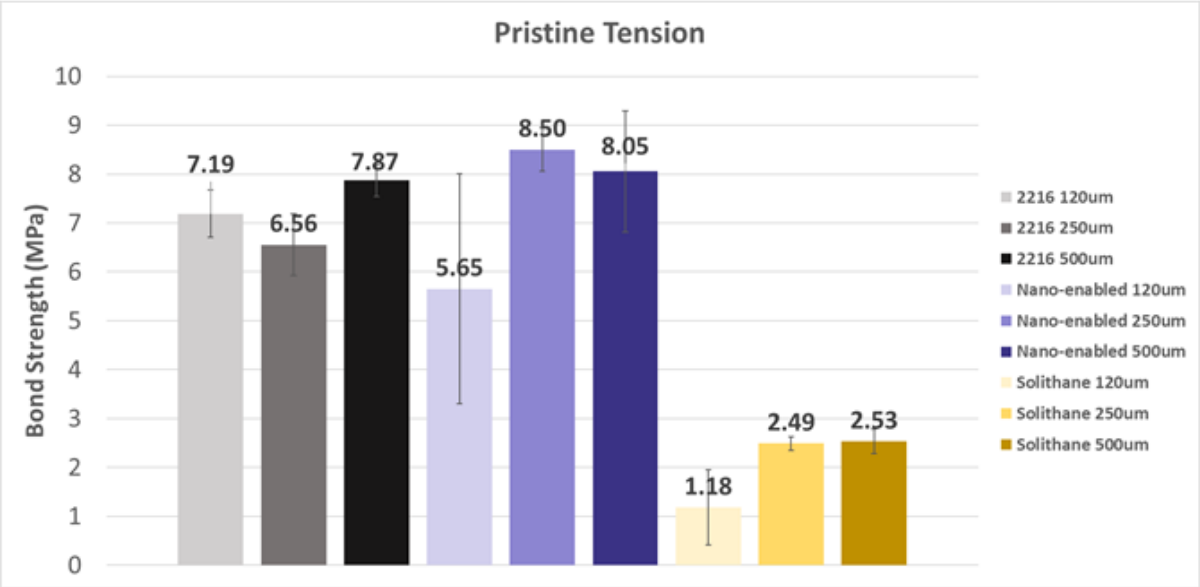

Graph 21. Bonding strength in pristine tension samples

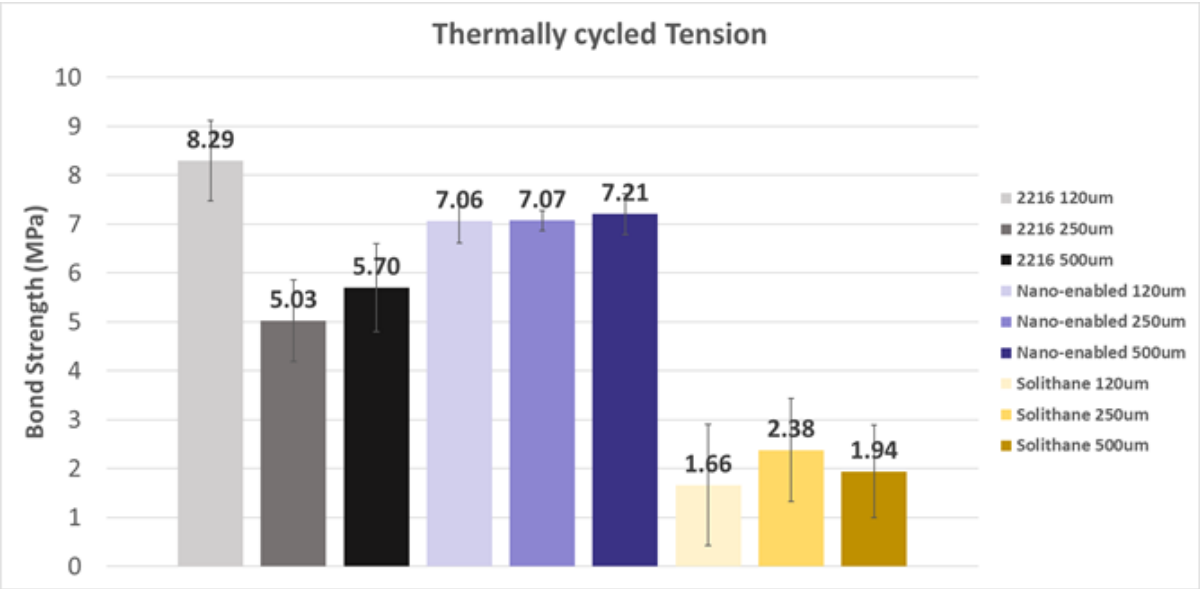

Graph 22. Bonding strength in thermally cycled tension samples

To sum up, regarding 2216 epoxy, if the sample will undergo thermal cycling, is clear that the best option is to go with the smallest bondline thickness. For the same conditions, the nano-enabled epoxy bonds stronger with the bigger bondline thickness. Finally, Solithane did not show a clear trend for both shear and tension modes.

5. SUMMARY AND WAY FORWARD

In this thesis, several materials were investigated in order to provide readily available data that can be used for material selection and product design in future missions.

Regarding standoff bonding, sanding the CFRP as a surface treatment, and cleaning afterwards with isopropyl alcohol, provided an 17% increase in the bond strength for epoxies. Polyurethane was not affected significantly by the surface preparations, as the data values were in the error limits. Epoxy adhesives, as expected, showed a higher bond strength than polyurethane. In particular, 2216 epoxy (Gray) result in at least 96% higher bond strength than Solithane 113. The nano-enabled adhesive showed similar bonding strength as the 2216 epoxy (Gray). In pristine 2216 samples, 500 μm proved to be the best bondline thickness for shear and tension, while for thermally cycled in vacuum 2216 samples, 120 μm bondline thickness outperformed the rest thicknesses. Pristine shear and tension samples present similar trends in the effect of bondline thickness of the epoxies, with 250μm thickness being the worst for 2216, while the best for the nano-enabled epoxy. Especially in tension, as it can be seen in the Figure 41 the adhesive fracture joint mode was mostly cohesive for Solithane 113, non-cohesive for 2216 as the CFRP stayed bonded on to the adhesive, and a mix of those for the nano-enabled adhesive. In shear mode, as can be seen in Figure 42, adhesive fracture joint modes did not follow a clear trend. Solithane 113 was cohesive, nano-enabled epoxy had some standoff fractures and 2216 epoxy had only one standoff fracture. Lastly, the effect of thermal cycling under vacuum was apparent as in most cases there was an increase in the bonding strength for epoxies but not for polyurethane. In the Figure 42 where the Solithane113 samples were bonded, in the right top there was no sample bonded, and this explains why there is no trace of adhesive.

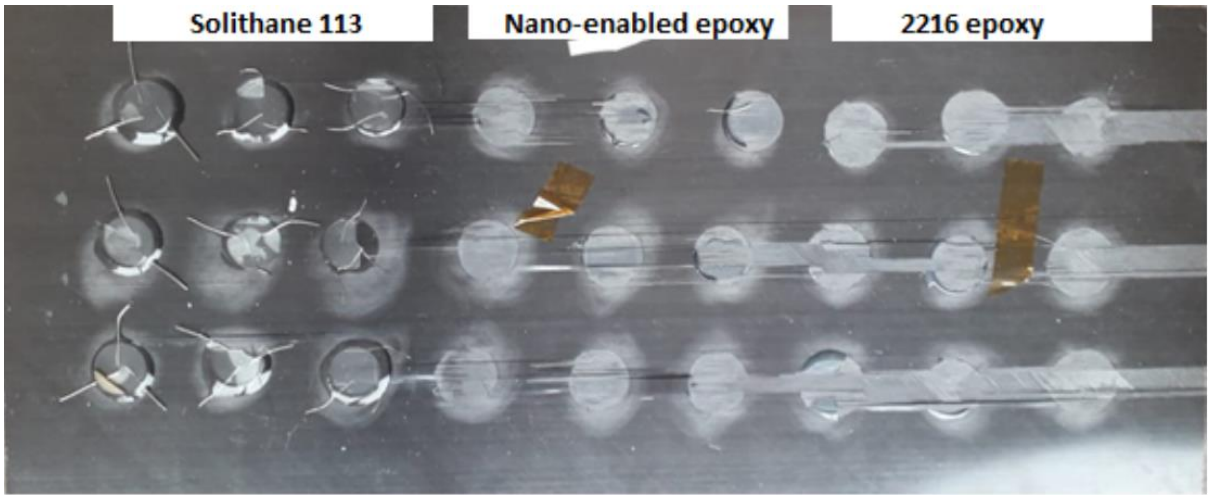

Figure 41. Tension CFRP/Alu after testing

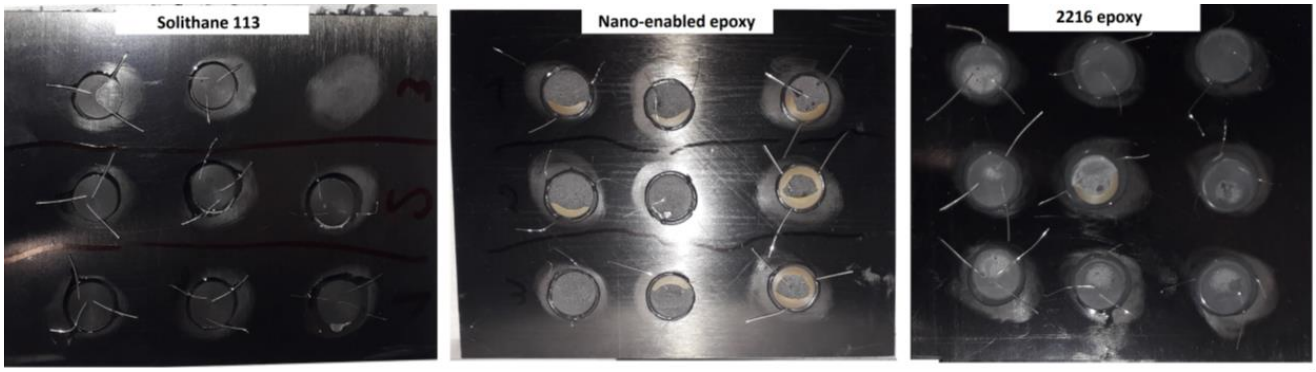

Figure 42. Shear CFRP/Alu after testing

The standoff bonding study could benefit from a further examination of more adhesive families and including a larger number of samples for a better statistical distribution of results. Conditioning of the samples could also be performed e.g., vibrations, humidity. Finally, a fracture observation using SEM would also provide valuable insights regarding the mode the adhesive fractured.

BIBLIOGRAPHY

1. High temperature challenge for Bepi Colombo [Internet]. [cited 2022 Mar 25]. Available from: https://www.esa.int/Science_Exploration/Space_Science/BepiColombo/High_temperature_challenge
2. JUICE factsheet [Internet]. [cited 2022 Mar 25]. Available from: https://www.esa.int/Science_Exploration/Space_Science/Juice_factsheet
3. Juice Challenges and expectations [Internet]. [cited 2022 Aug 20]. Available from: https://www.nae.edu/260902/The-JUICE-Mission-Challenges-and-Expectations
4. Jupiter in depth [Internet]. [cited 2022 Aug 20]. Available from: https://solarsystem.nasa.gov/planets/jupiter/in-depth/
5. S. J. Alberts, C. J. Dohene, W. L. Johnson. Testing Tensile and Shear Epoxy Strength at Cryogenic Temperatures. In: 2017 Cryogenic Engineering Conference. NASA; 2017.
6. S. Dagras JECTDL. Adhesives in Space Environment. In: Handbook of adhesion technology. 2018. p. 915–40.
7. Composite applications for space [Internet]. [cited 2022 Mar 12]. Available from: https://www.nasampe.org/page/CompositesApplicationsforSpace
8. Adhesive Systems for the Aerospace Industry [Internet]. [cited 2022 Jun 13]. Available from: https://www.masterbond.com/industries/adhesive-systems-aerospace-industry?matchtype=b&network=g&device=c&adposition=&keyword=adhesives%20for%20aerospace&gclid=Cj0KCQjwxveXBhDDARIsAI0Q0x2Pt_Ebb_eZr1fQIdd1Y2-rb7aehm_P1fsyjAiakpgoSLPJyy74sSoaArvREALw_wcB
9. Fred H. Yeatts. A comparative study of three epoxy resins in the industrial arts laboratory. [Texas]; 1974.
10. Thermoplastics and Thermosettings [Internet]. [cited 2022 Aug 20]. Available from: https://matmatch.com/learn/material/thermoplastics-vs-thermosetting-polymers
11. Polyurethane [Internet]. [cited 2022 Sep 20]. Available from: https://www.christinedemerchant.com/adhesive-glue-polyurethane.html
12. Silicone [Internet]. [cited 2022 Sep 20]. Available from: https://www.masterbond.com/techtips/why-use-silicone-adhesive
13. https://www.atriainnovation.com/graphene-characteristics-and-applications/.
14. Solithane ESA materials DB [Internet]. [cited 2022 Jun 18]. Available from: https://www.spacematdb.com/spacemat/datasearch.php?name=Solithane%20113/C%20113-300%20(100/73%20pbw)
15. Isotropic vs quasi-isotropic [Internet]. [cited 2022 Apr 2]. Available from: https://dragonplate.com/carbon-fiber-101-what-do-isotropic-quasi-isotropic-and-anisotropic-mean
16. https://dragonplate.com/quasi-isotropic-carbon-fiber-sheets.
17. M. He, W. Hu. A study on composite honeycomb sandwich panel structure. Mater Des. 2008;29(2):709–13.
18. Torlon [Internet]. [cited 2022 Mar 18]. Available from: https://www.solvay.com/en/brands/torlon-pai

19. J. D. Menczel, R. B. Prime. Thermal Analysis of Polymers: Fundamentals and applications. Hoboken, NJ, USA: John Wiley & Sons, Inc.; 2009.
20. Xie R, Weisen AR, Lee Y, Aplan MA, Fenton AM, Masucci AE, et al. Glass transition temperature from the chemical structure of conjugated polymers. Nat Commun. 2020 Dec 14;11(1):893.
21. Becker H. Polymer microfluidic devices. Talanta. 2002 Feb 11;56(2):267–87.
22. TMA principles [Internet]. [cited 2022 Feb 15]. Available from: https://www.hitachi-hightech.com/global/products/science/tech/ana/thermal/descriptions/tma.html

APPENDIX A: 2216 Technical datasheet

Below there are the 3 pages from 2216 technical datasheet regarding mix ratio, properties, curing and surface preparation. More information can be found: https://multimedia.3m.com/mws/media/153955O/3mtm-scotch-weldtm-epoxy-adhesive-2216-b-a.pdf

3M

Scotch-Weld™ Epoxy Adhesive
2216 B/A

Technical Data **October 2018**

Product Description

3M™ Scotch-Weld™ Epoxy Adhesive 2216 B/A is a flexible, two-part, room temperature curing epoxy with high peel and shear strength, available in three versions. 2216 B/A Gray meets DOD-A-82720.

Typical Uncured Physical Properties

Note: The following technical information and data should be considered representative or typical only and should not be used for specification purposes.

Product	3M™ Scotch-Weld™ Epoxy Adhesive					
	2216 B/A Gray		2216 B/A Tan NS		2216 B/A Translucent	
	Base	Accelerator	Base	Accelerator	Base	Accelerator
Color:	White	Gray	White	Tan	Translucent	Amber
Base:	Modified Epoxy	Modified Amine	Modified Epoxy	Modified Amine	Modified Epoxy	Modified Amine
Net Wt.: (lb/gal)	11.1-11.6	10.5-11.0	11.1-11.6	10.5-11.0	9.4-9.8	8.0-8.5
Viscosity: (cps) (Approx.) Brookfield RVF #7 sp. @ 20 rpm	75,000 - 150,000	40,000 - 80,000	75,000 - 150,000	550,000 - 900,000	11,000 - 15,000	5,000 - 9,000
Mix Ratio: (by weight)	5 parts	7 parts	5 parts	7 parts	1 part	1 part
Mix Ratio: (by volume)	2 parts	3 parts	2 parts	3 parts	1 part	1 part
Work Life: 100 g Mass @ 75°F (24°C)	90 minutes	90 minutes	120 minutes	120 minutes	120 minutes	120 minutes

Features

- Excellent for bonding many metals, woods, plastics, rubbers, and masonry products.
- Base and Accelerator are contrasting colors.
- Good retention of strength after environmental aging.
- Resistant to extreme shock, vibration, and flexing.
- Excellent for cryogenic bonding applications.
- Excellent for potting parts subject to thermal cycling.
- The tan NS Adhesive is non-sag for greater bond-line control.
- The translucent can be injected.
- Meets DOD-A-82720.

3M™ Scotch-Weld™ Epoxy Adhesive
2216 B/A

Typical Cured Physical Properties

Product	3M™ Scotch-Weld™ Epoxy Adhesive		
	2216 Gray	2216 Tan NS	2216 Translucent
Color	Gray	Tan	Translucent
Shore D Hardness ASTM D 2240	50-65	65-70	35-50
Time to Handling Strength	8-12 hrs.	8-12 hrs.	12-16 hrs.

Typical Cured Electrical Properties

Product	3M™ Scotch-Weld™ Epoxy Adhesive	
	2216 Gray	2216 Translucent
Arc Resistance	130 seconds	
Dielectric Strength	408 volts/mil	630 volts/mil
Dielectric Constant@73°F (23°C)	5.51–Measured @ 1.00 KHz	6.3 @ 1 KHz
Dielectric Constant@140°F (60°C)	14.17–Measured @ 1.00 KHz	—
Dissipation Factor 73°F (23°C)	0.112 Measured @ 1.00 KHz	0.119 @ 1 KHz
Dissipation Factor 140°F (60°C)	0.422–Measured @ 1.00 KHz	—
Surface Resistivity@73°F (23°C)	5.5 x 10^{16} ohm–@ 500 volts DC	—
Volume Resistivity@73°F (23°C)	1.9 x 10^{12} ohm-cm–@ 500 volts DC	3.0 x 10^{12} ohm-cm @ 500 volts DC

Typical Cured Thermal Properties

Product	3M™ Scotch-Weld™ Epoxy Adhesive	
	2216 Gray	2216 Translucent
Thermal Conductivity	0.228 Btu-ft/ft^{2}h°F	0.114 Btu-ft/ft^{2}h°F
Coefficient of Thermal Expansion	102 x 10^{-6} in/in/°C between 0-40°C 134 x 10^{-6} in/in/°C between 40-80°C	81 x 10^{-6} in/in/°C between -50-0°C 207 x 10^{-6} in/in/°C between 60-150°C

Typical Cured Outgassing Properties

Outgassing Data
NASA 1124 Revision 4

	% TML	% CVCM	% Wtr
3M™ Scotch-Weld™ Epoxy Adhesive 2216 Gray	.77	.04	.23

Cured in air for 7 days @ 77°F (25°C).

Handling/Curing Information

Directions for Use

1. For high strength structural bonds, paint, oxide films, oils, dust, mold release agents and all other surface contaminants must be completely removed. However, the amount of surface preparation directly depends on the required bond strength and the environmental aging resistance desired by user. For suggested surface preparations of common substrates, see the following section on surface preparation.
2. These products consist of two parts. Mix thoroughly by weight or volume in the proportions specified on the product label and in the uncured properties section. Mix approximately 15 seconds after a uniform color is obtained.

3M™ Scotch-Weld™ Epoxy Adhesive
2216 B/A

Handling/Curing Information *(continued)*

3. For maximum bond strength, apply product evenly to both surfaces to be joined.
4. Application to the substrates should be made within 90 minutes. Larger quantities and/or higher temperatures will reduce this working time.
5. Join the adhesive coated surfaces and allow to cure at 60°F (16°C) or above until firm. Heat, up to 200°F (93°C), will speed curing.
6. The following times and temperatures will result in a full cure:

Product	3M™ Scotch-Weld™ Epoxy Adhesive		
	2216 Gray	2216 Tan NS	2216 Translucent
Cure Temperature	Time	Time	Time
75°F (24°C)	7 days	7 days	30 days
150°F (66°C)	120 minutes	120 minutes	240 minutes
200°F (93°C)	30 minutes	30 minutes	60 minutes

7. Keep parts from moving until handling strength is reached. Contact pressure is necessary. Maximum shear strength is obtained with a 3-5 mil bond line. Maximum peel strength is obtained with a 17-25 mil bond line.
8. Excess uncured adhesive can be cleaned up with ketone type solvents.* Adhesive Coverage: A 0.005 in. thick bondline will typically yield a coverage of 320 sq. ft/gallon

Application and Equipment Suggestions

These products may be applied by spatula, trowel or flow equipment.

Two-part mixing/proportioning/dispensing equipment is available for intermittent or production line use. These systems are ideal because of their variable shot size and flow rate characteristics and are adaptable to many applications.

Surface Preparation

For high strength structural bonds, paint, oxide films, oils, dust, mold release agents and all other surface contaminants must be completely removed. However, the amount of surface preparation directly depends on the required bond strength and the environmental aging resistance desired by user.

The following cleaning methods are suggested for common surfaces.

Steel or Aluminum (Mechanical Abrasion)

1. Wipe free of dust with oil-free solvent such as acetone or alcohol solvents.*
2. Sandblast or abrade using clean fine grit abrasives (180 grit or finer).
3. Wipe again with solvents to remove loose particles.
4. If a primer is used, it should be applied within 4 hours after surface preparation.

*When using solvents, extinguish all ignition sources, including pilot lights, and follow the manufacturer's precautions and directions for use. Use solvents in accordance with local regulations.

APPENDIX B: Solithane 113 Technical Datasheet

Below the Solithane 113 technical datasheet page regarding curing. More information can be found:

https://www.boeingdistribution.com/product/SOLITHANE+C-113/SOLITHANE+C-113-300/S0LITHANE-C-113-1GL

SOLITHANE 113
BONDING

CURING

Cure Systems

As indicated in *Table I*, the physical properties of the cured compound depend upon the type and amount of curing agent used, either alone or in combination with other curatives. An increase in the amount of C113-300 curing agent:

- Lowers initial mix viscosity of system
- Increases pot life
- Lowers durometer hardness
- Lowers stress-strain properties
- Increases low-temperature properties

An increase in the amount of TIPA:

- Decreases pot life, cure time
- Increases durometer hardness
- Increases stress-strain properties*

*When used in blends with C113-300 curing agent.

Alternate cure systems by polyfunctional curing agents containing active hydrogens are also possible, (but not discussed in this bulletin). However, the use of the above cure system minimizes the number of curatives necessary to formulate different applications.

The rate of cure for three formulations from *Table IV*, expressed as the change in viscosity at 15 minute intervals at 140°F (80°C) is illustrated in *Figure IV*.

POST CURE

Optimum properties are generally reached after 7 days at 80°F (27°C) (R.T.). SOLITHANE 113 resin compounds are relatively unaffected by additional heating at temperatures up to 250°F (121°C). However, signs of instability become evident in some formulations after three weeks exposure to 300°F (149°C). The effect on the physical properties of cured SOLITHANE 113 compounds exposed to various temperatures is shown in *Table III*.

BONDING

SOLITHANE 113 resin compounds adhere to most substrates without the use of a primer. Some substrates can be simply treated with a solvent wipe or light abrading with sandpaper. However, bonding surfaces should be clean and free of oily films.

APPENDIX C: TGA graphs

CFRPs

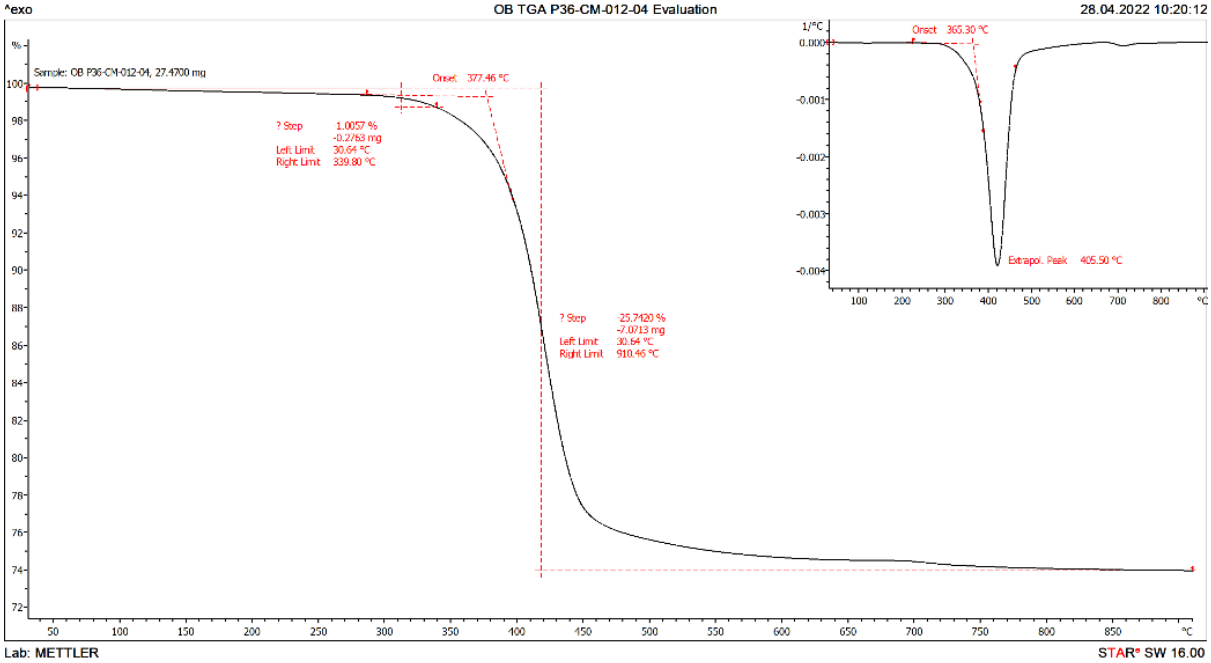

Graph 23. Normalized TGA results of P36-CM-012-04. First derivative shown on top right corner

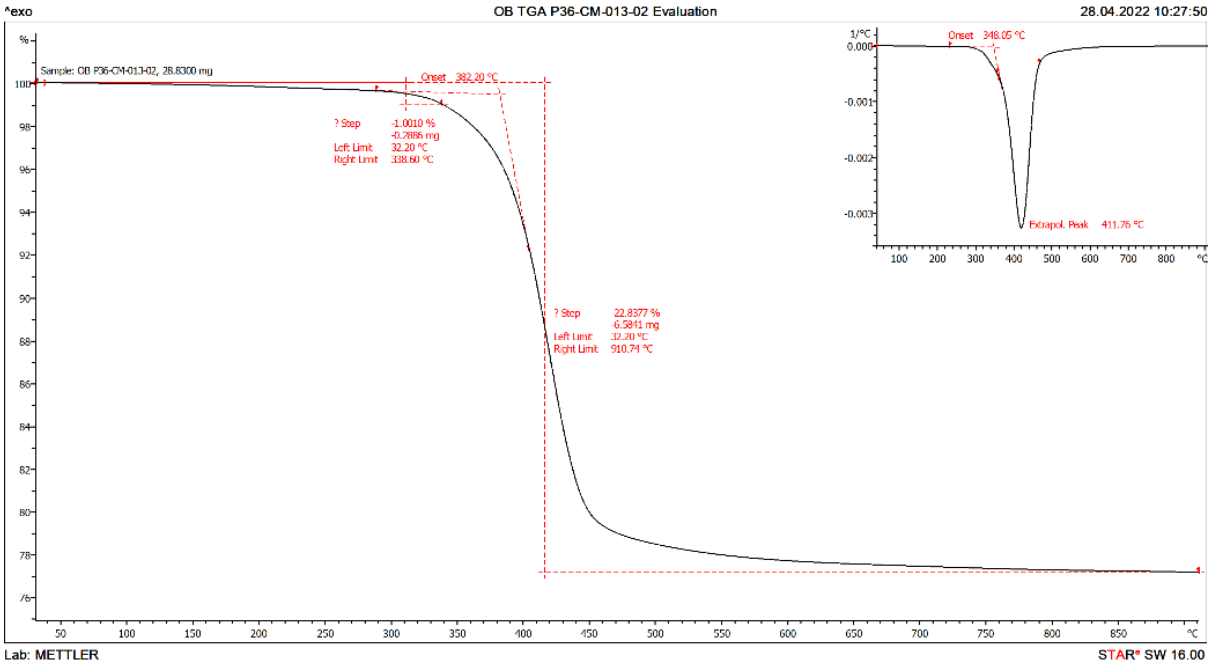

Graph 24. Normalized TGA results of P36-CM-013-.2. First derivative shown on top right corner

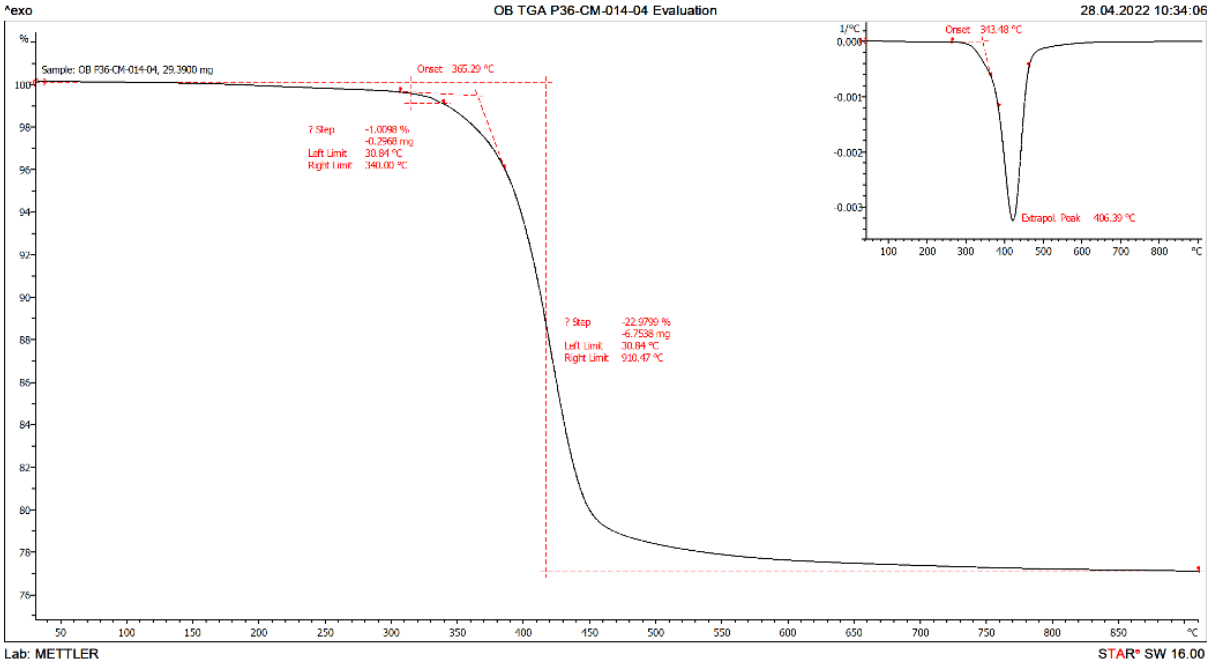

Graph 25. Normalized TGA results of P36-CM-014-04. First derivative shown on top right corner

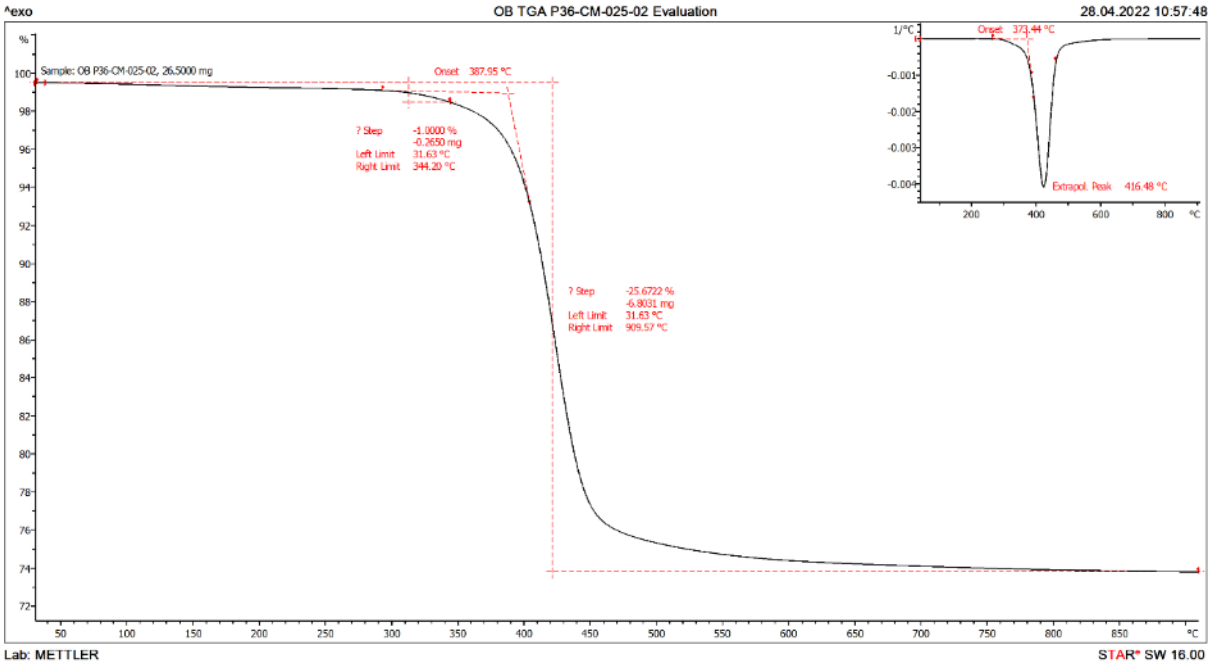

Graph 26. Normalized TGA results of P36-CM-025-02. First derivative shown on top right corner

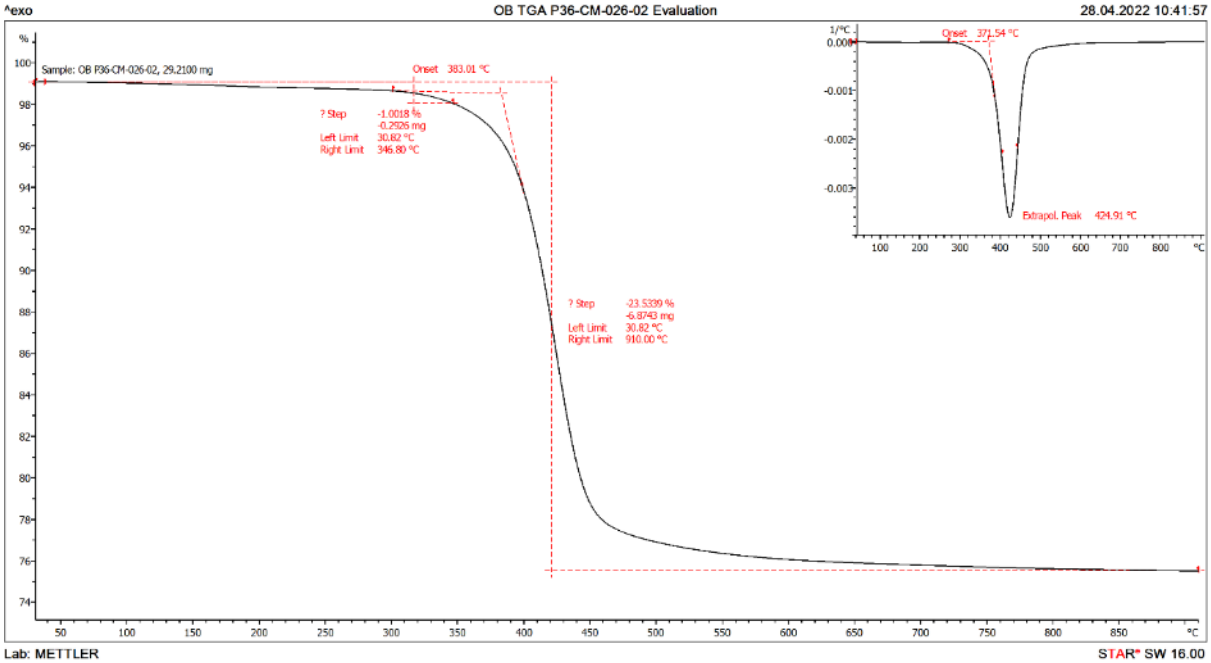

Graph 27. Normalized TGA results of P36-CM-026-02. First derivative shown on top right corner

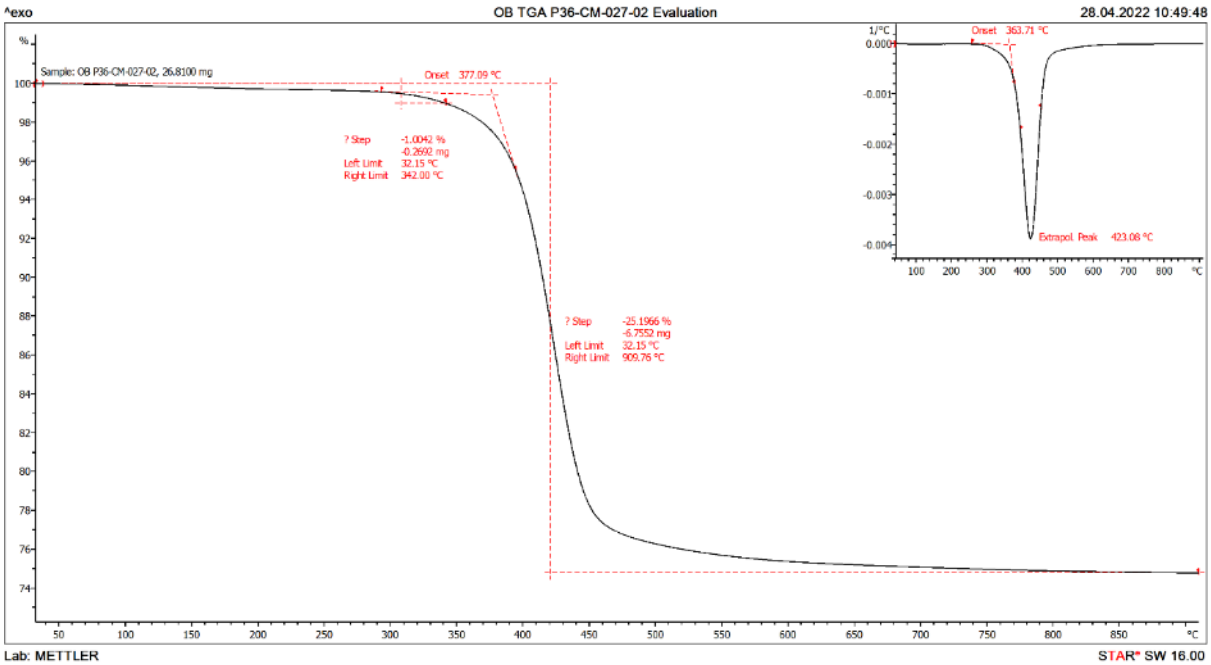

Graph 28. Normalized TGA results of P36-CM-027-02. First derivative shown on top right corner

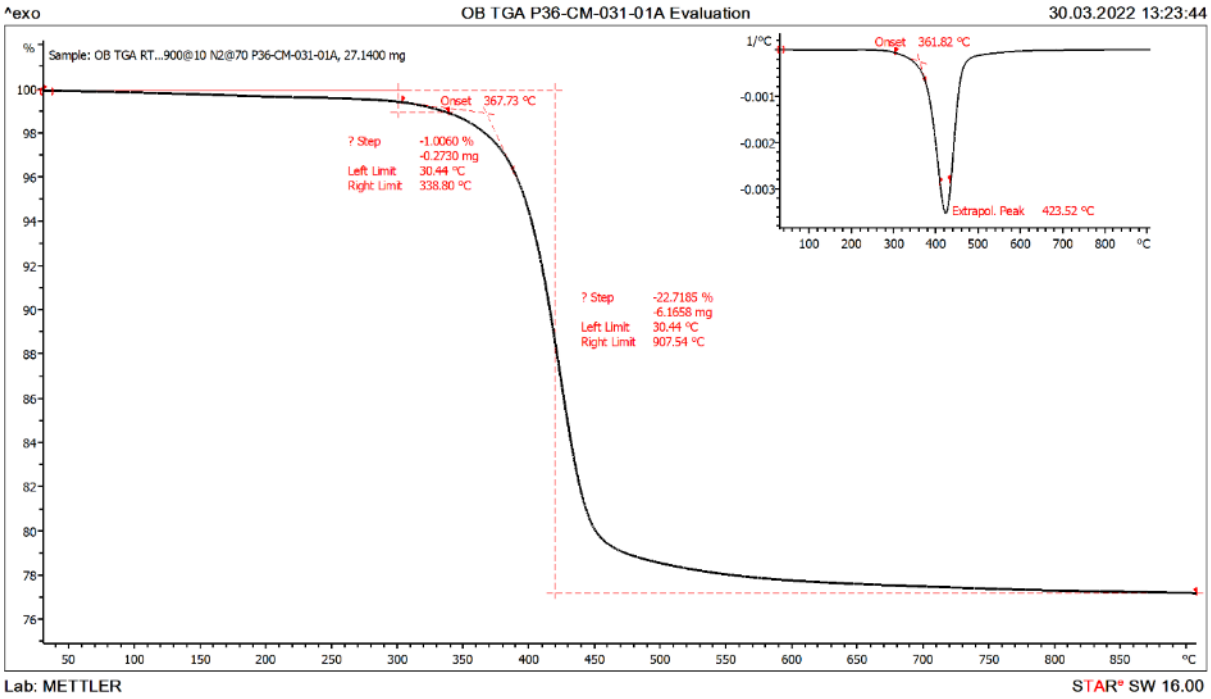

Graph 29. Normalized TGA results of P36-CM-031-01A. First derivative shown on top right corner

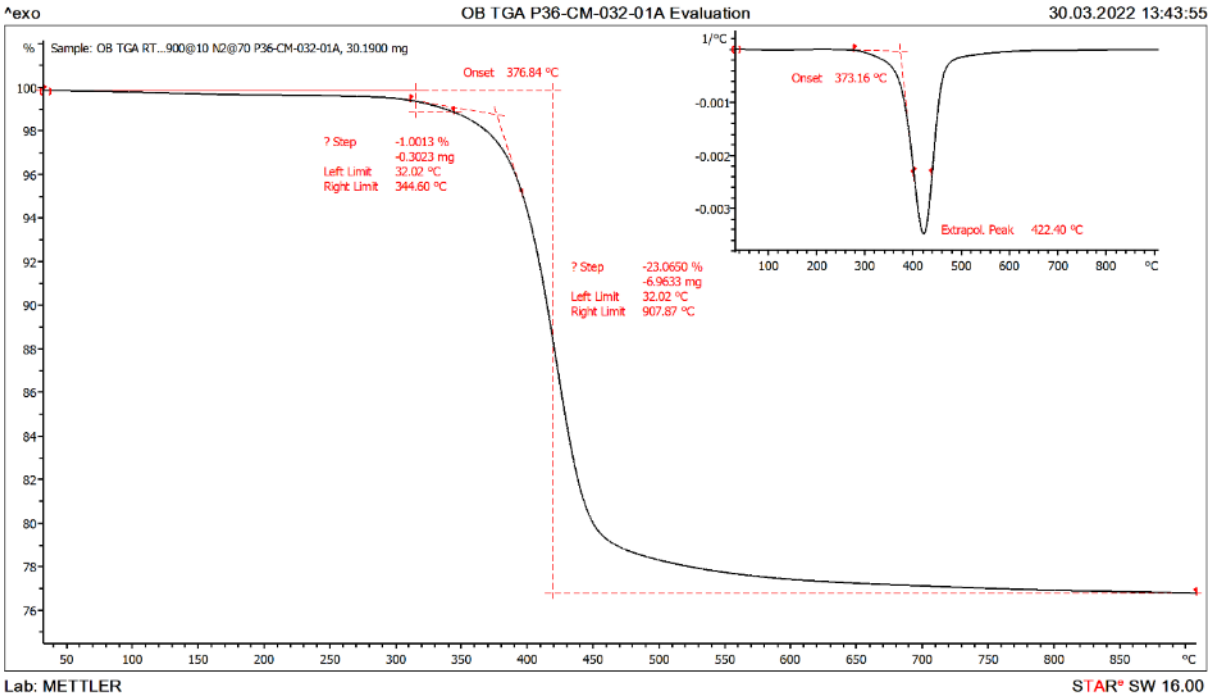

Graph 30. Normalized TGA results of P36-CM-032-01A. First derivative shown on top right corner

Film adhesives

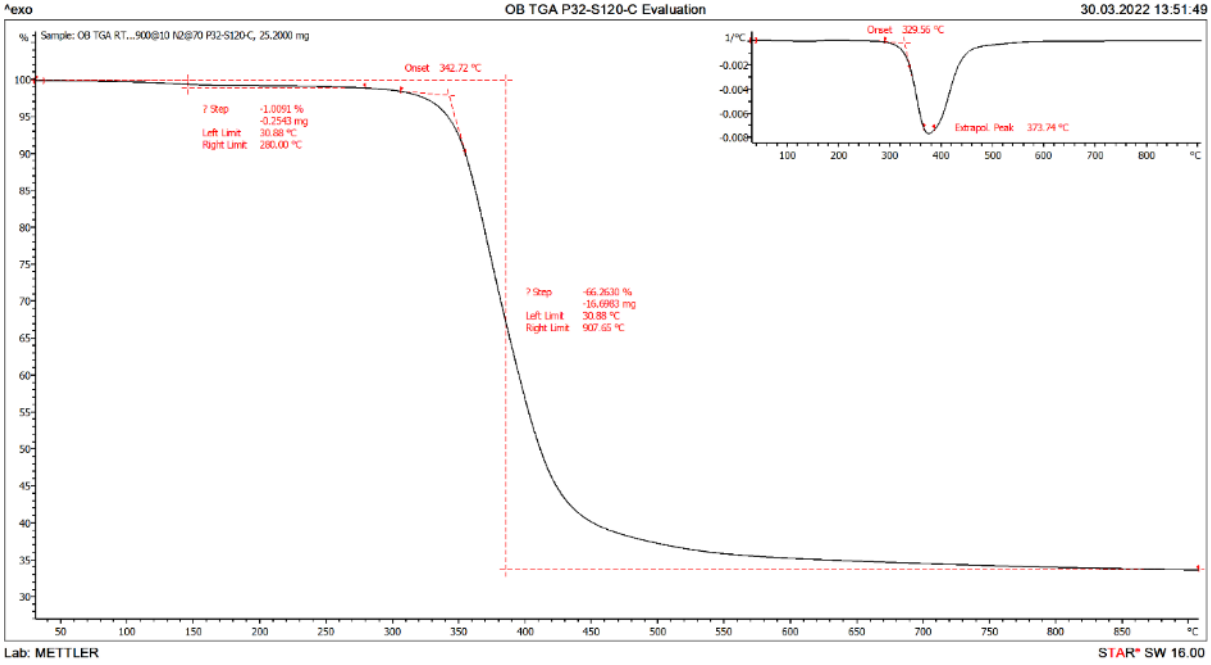

Graph 31. Normalized TGA results of P32-S120-C. First derivative shown on top right corner

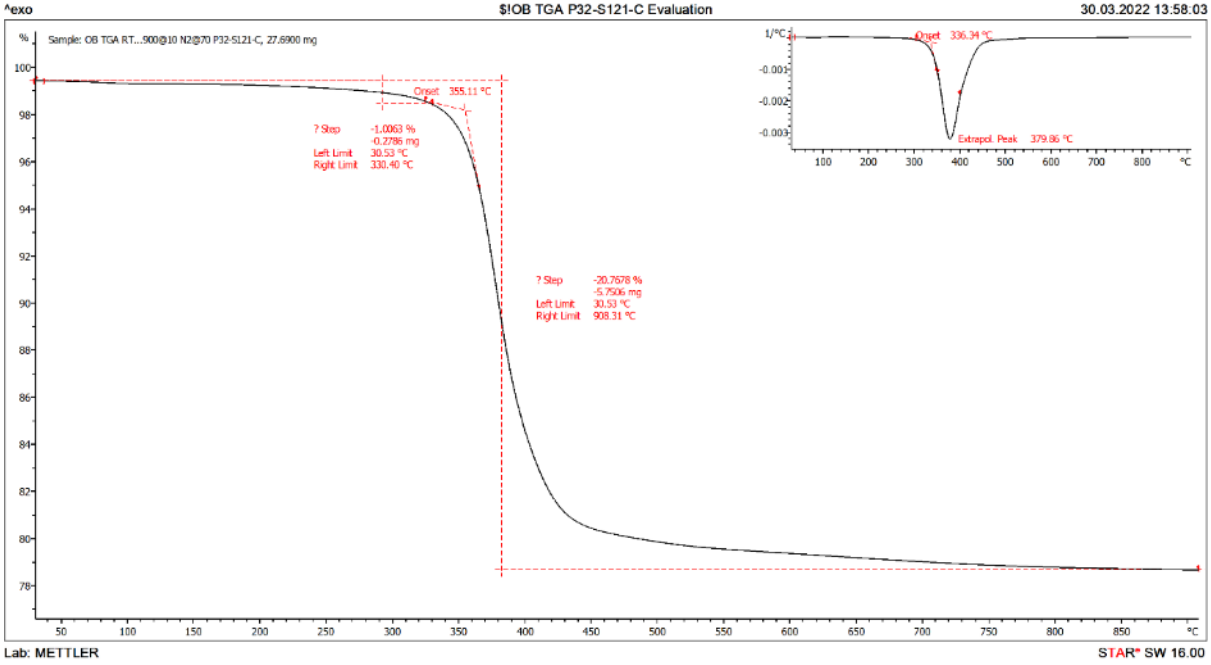

Graph 32. Normalized TGA results of P32-S121-C. First derivative shown on top right corner

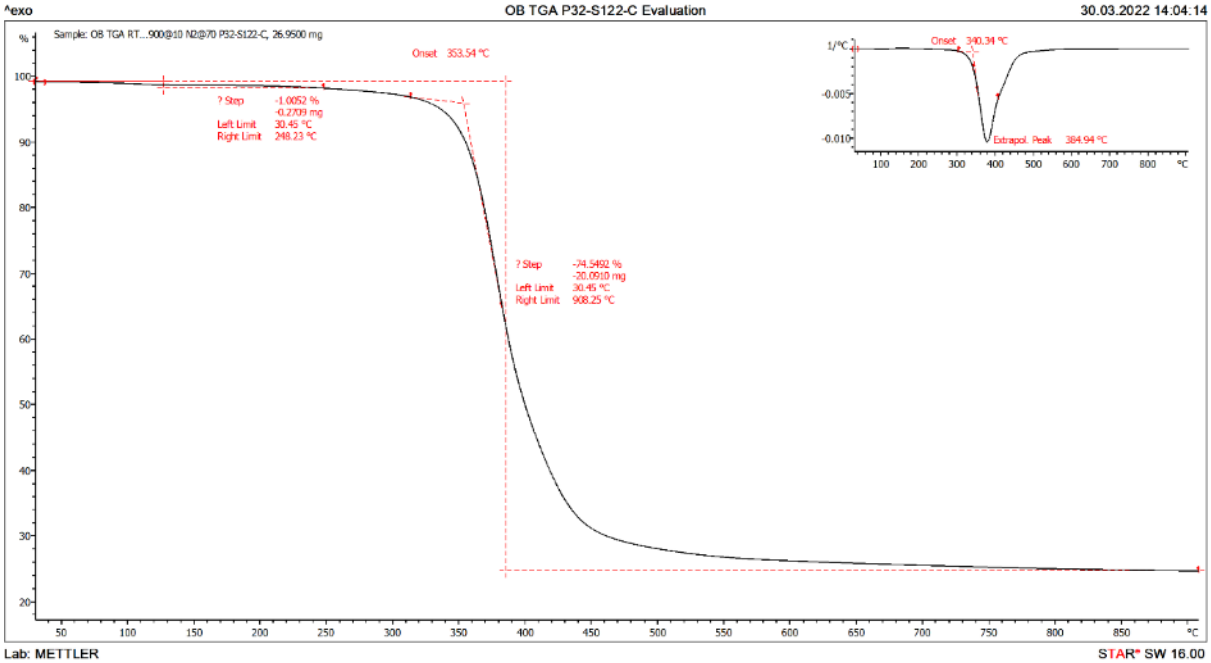

Graph 33. Normalized TGA results of P32-S122-C. First derivative shown on top right corner

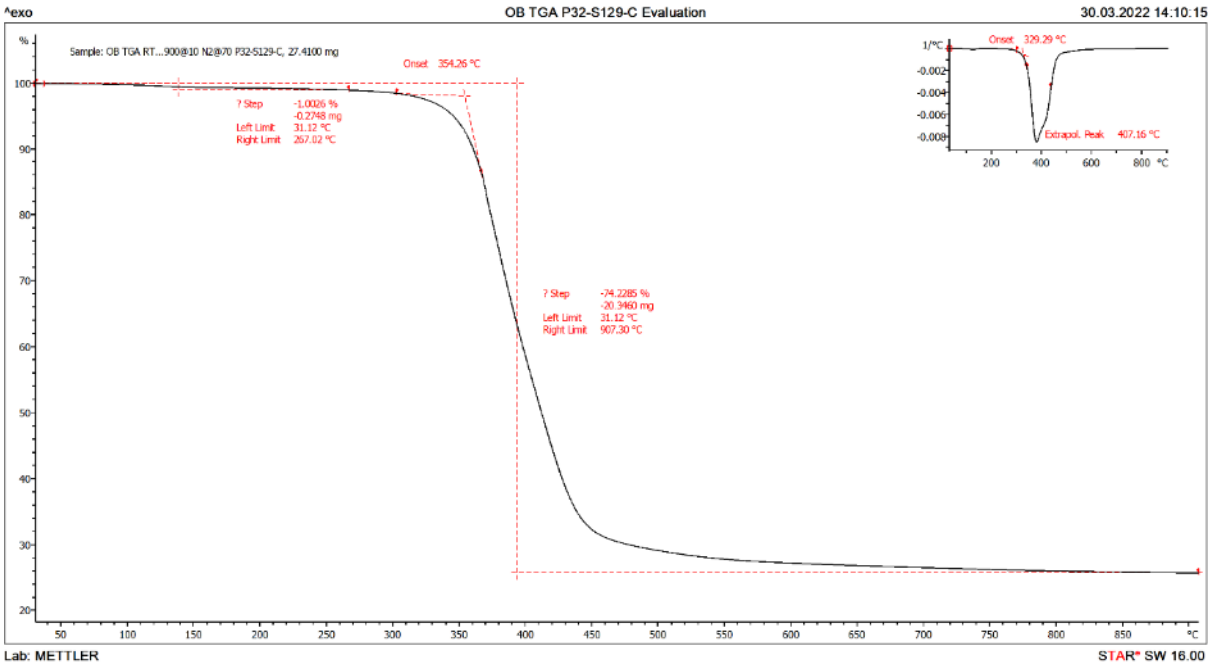

Graph 34. Normalized TGA results of P32-S129-C. First derivative shown on top right corner

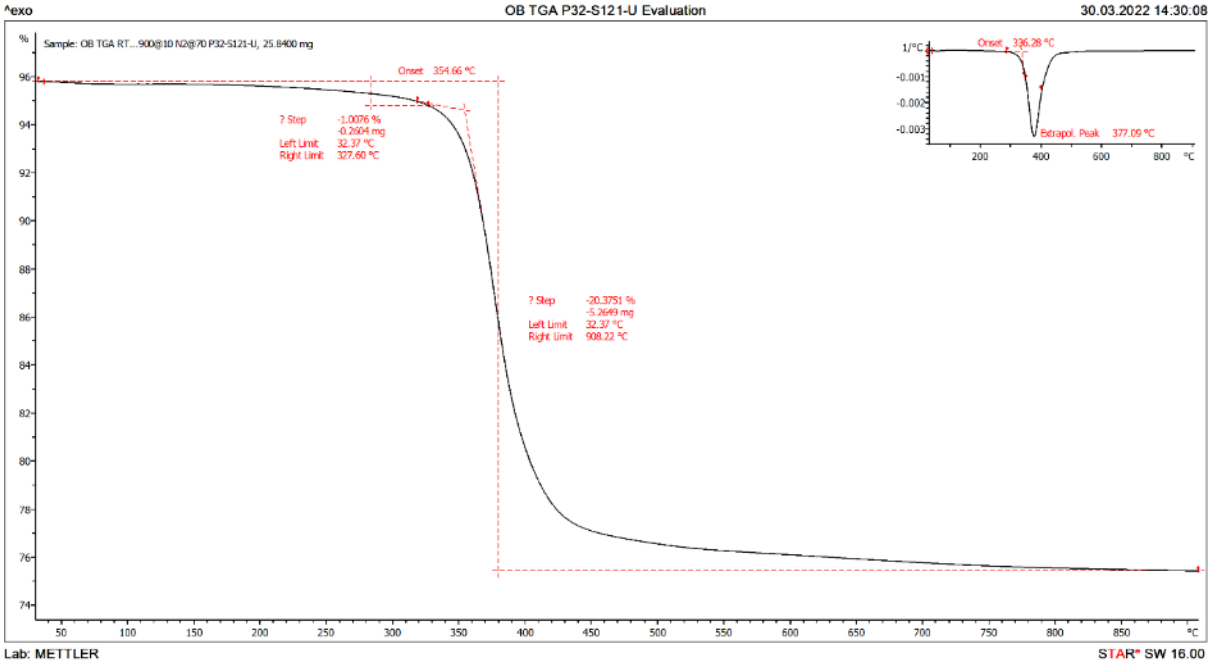

Graph 35. Normalized TGA results of P32-S121-U. First derivative shown on top right corner

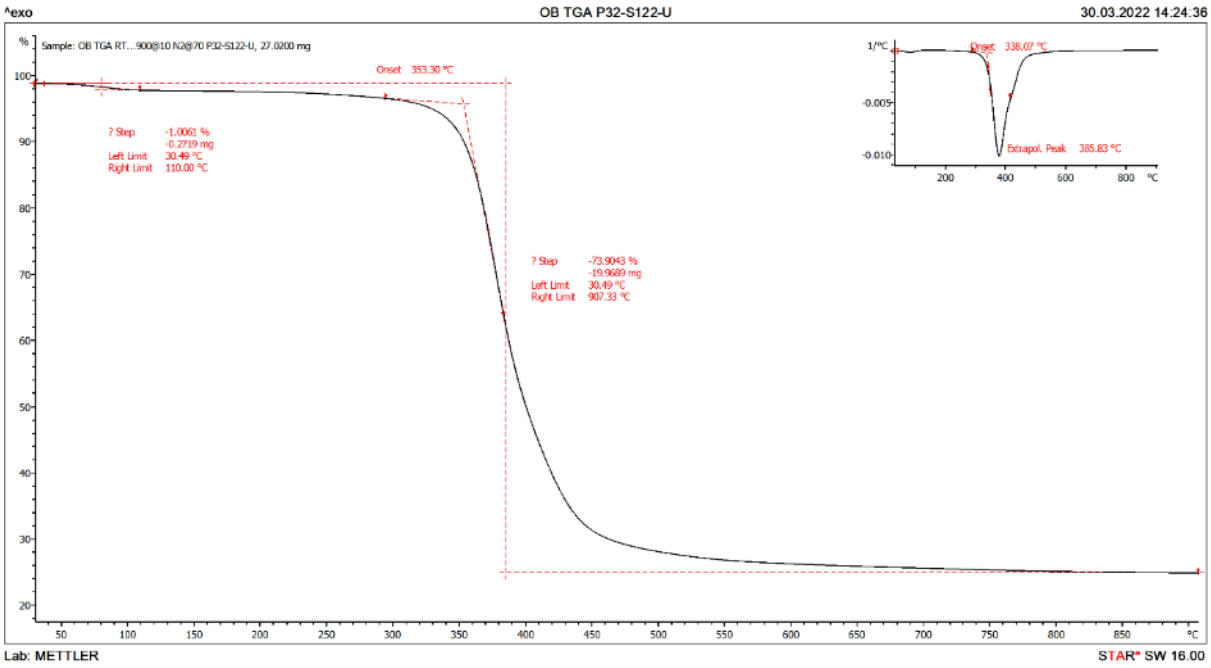

Graph 36. Normalized TGA results of P32-S122-U. First derivative shown on top right corner

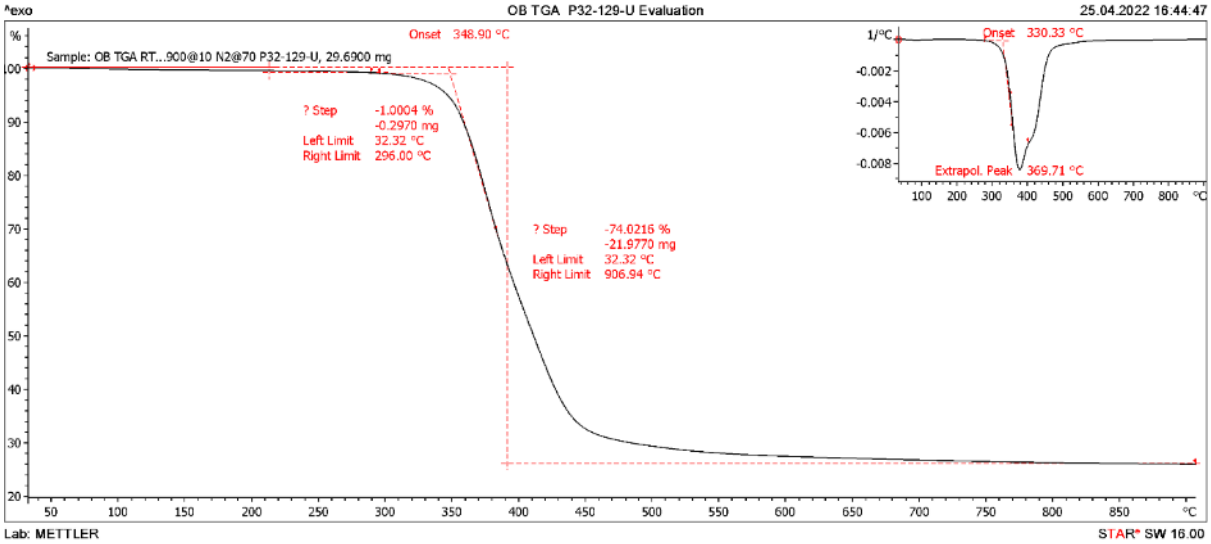

Graph 37. Normalized TGA results of P32-S129-U. First derivative shown on top right corner

Other adhesives

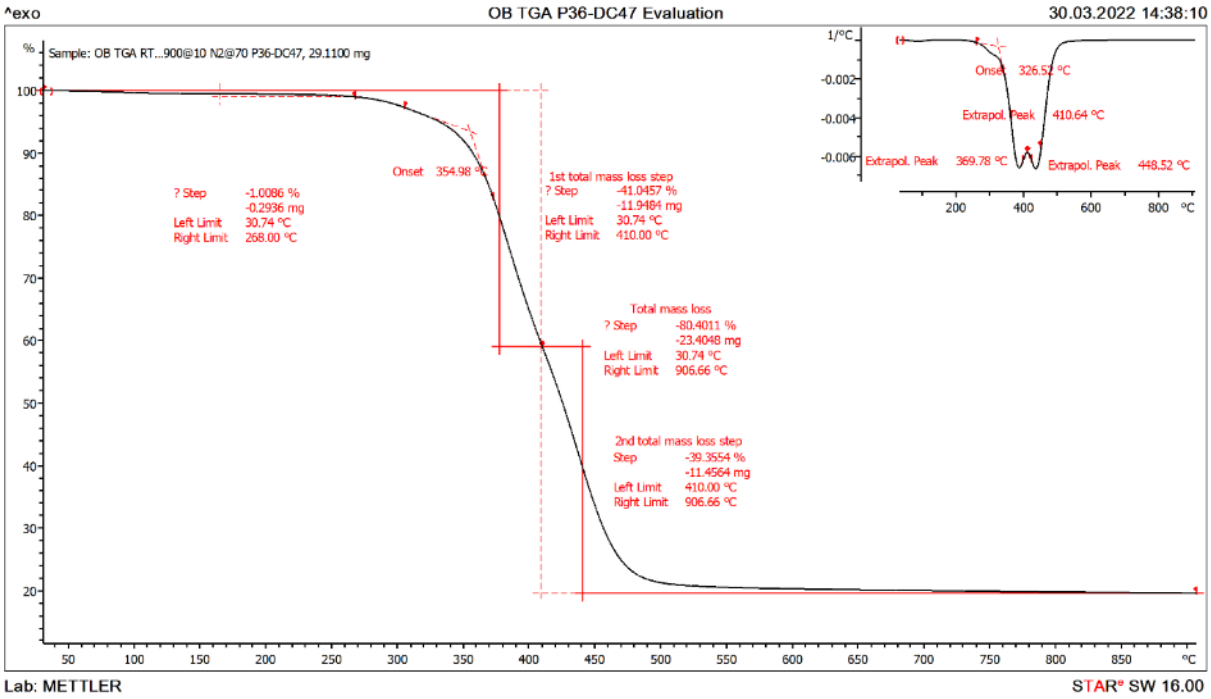

Graph 38. Normalized TGA results of P36-DC47. First derivative shown on top right corner

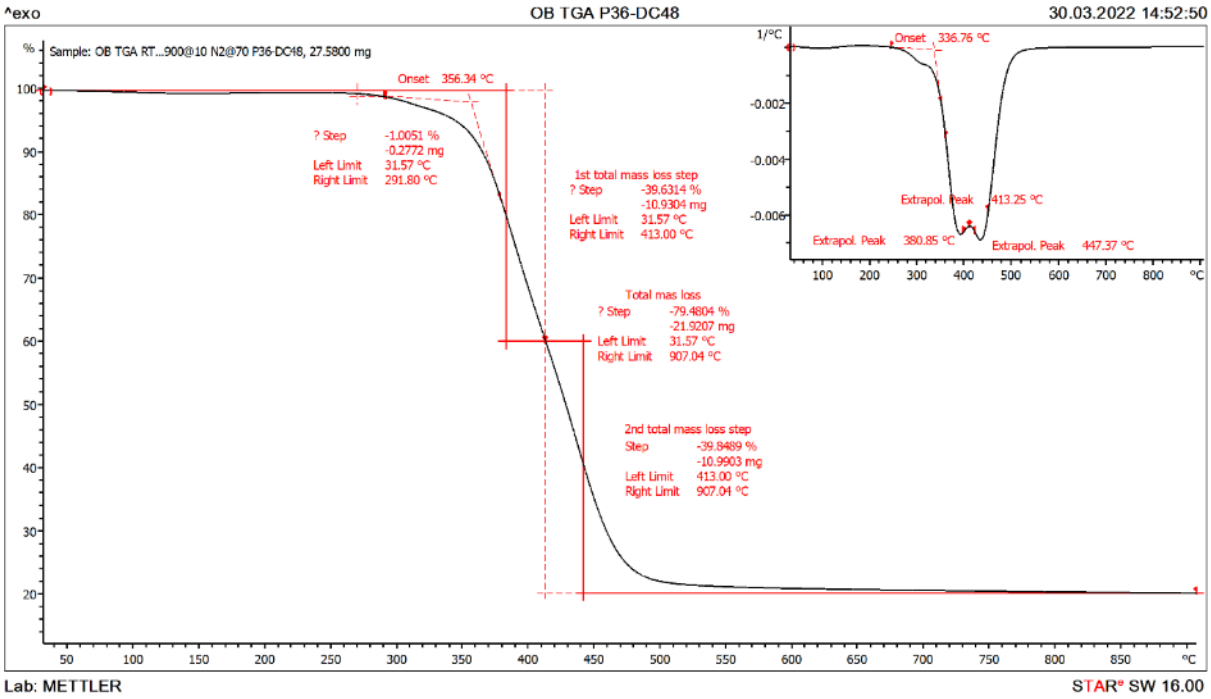

Graph 39. Normalized TGA results of P36-DC48. First derivative shown on top right corner

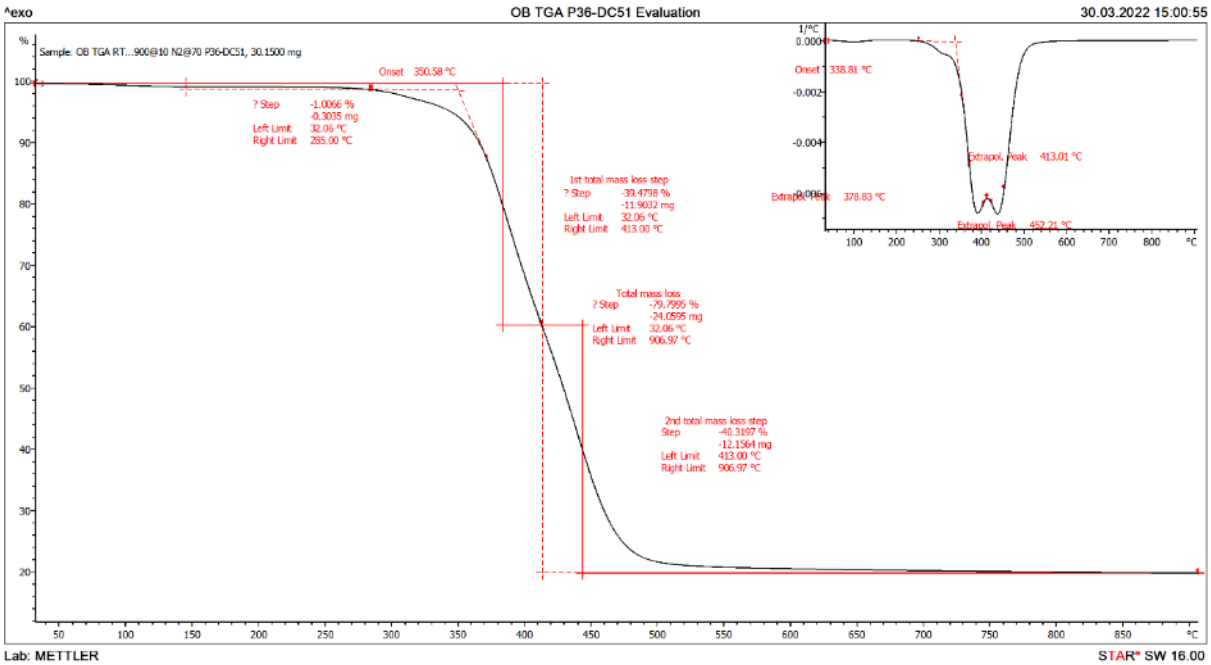

Graph 40. Normalized TGA results of P36-DC51. First derivative shown on top right corner

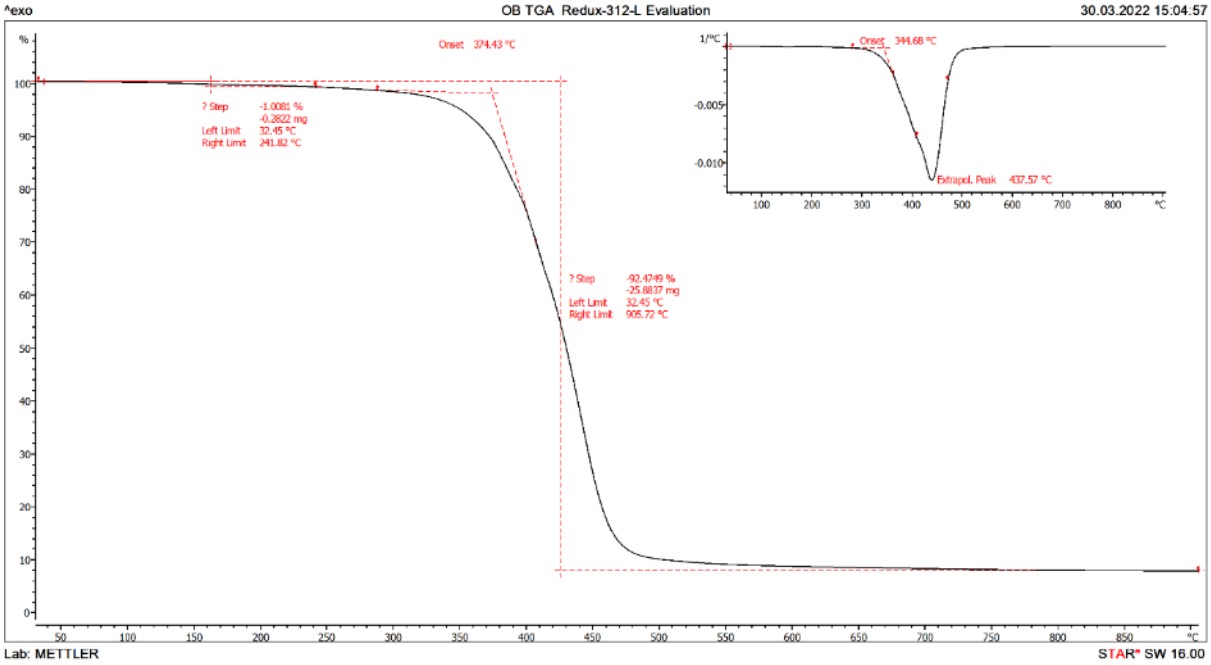

Graph 41. Normalized TGA results of P36-Redux312L. First derivative shown on top right corner

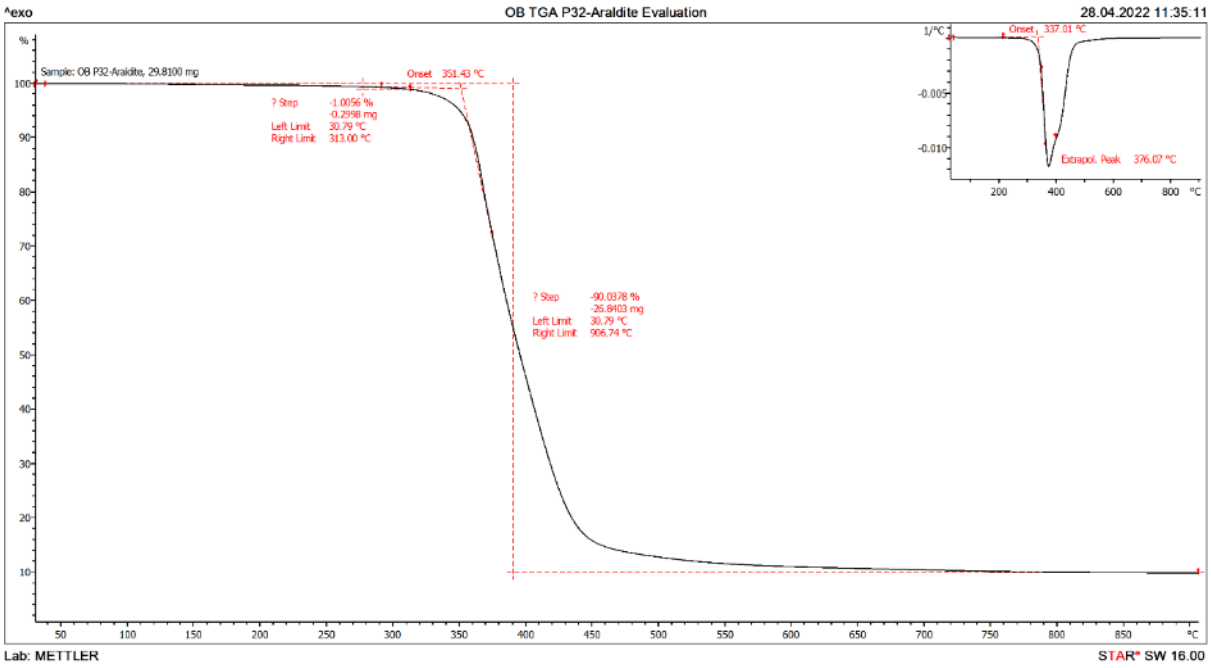

Graph 42. Normalized TGA results of P32-Araldite. First derivative shown on top right corner

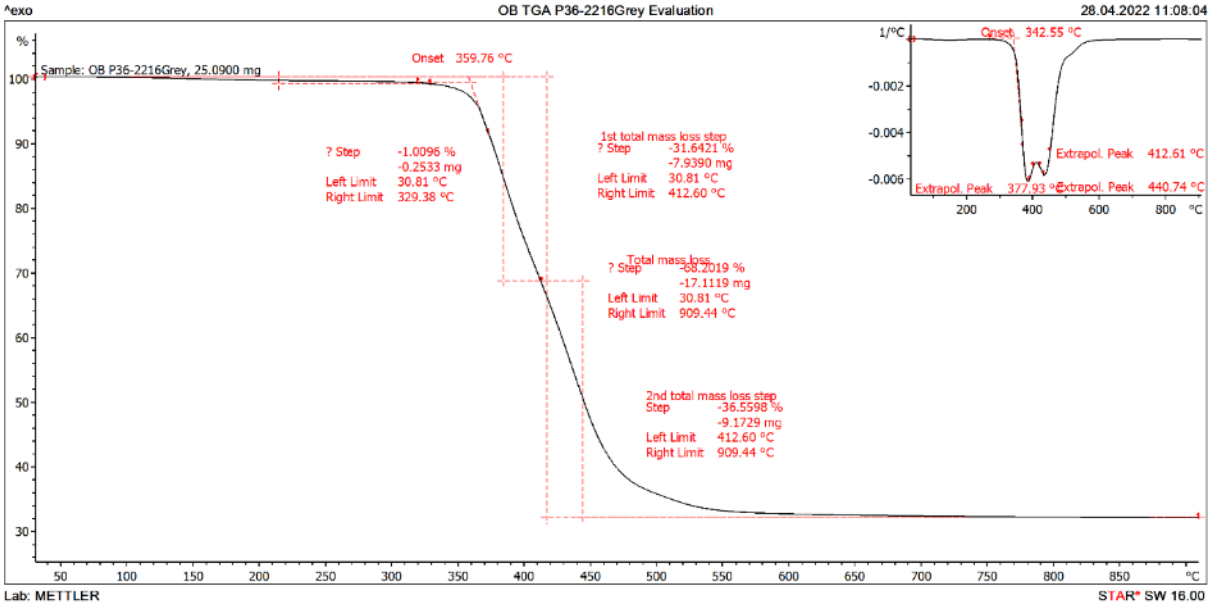

Graph 43. Normalized TGA results of P36-2216Grey. First derivative shown on top right corner

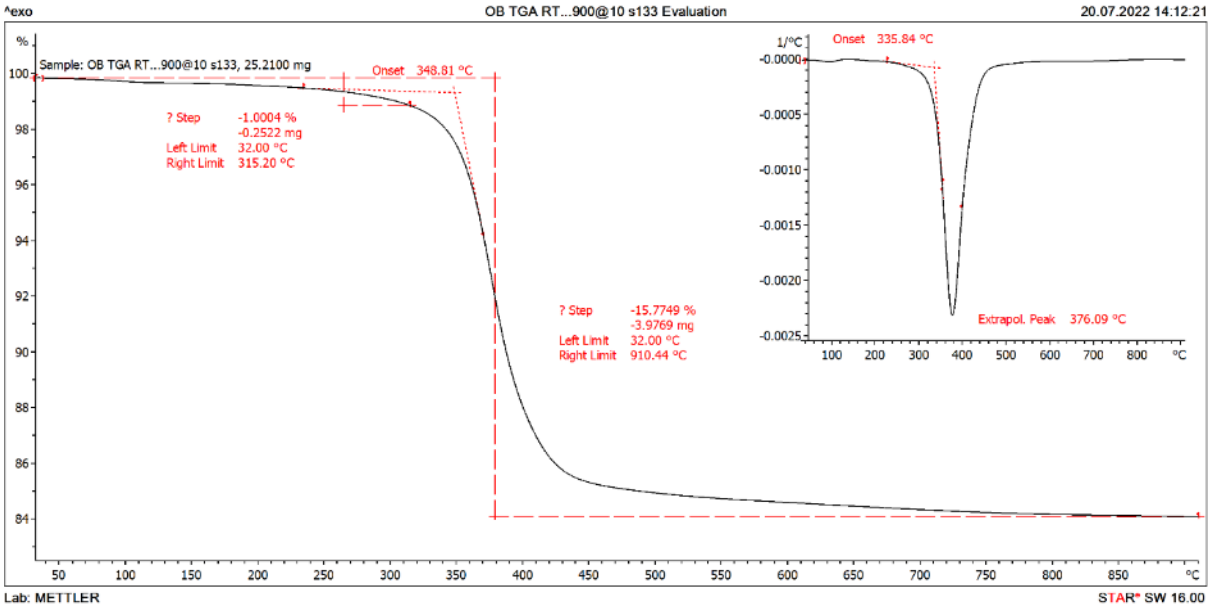

Graph 44. Normalized TGA results of P32-S133-ML. First derivative shown on top right corner

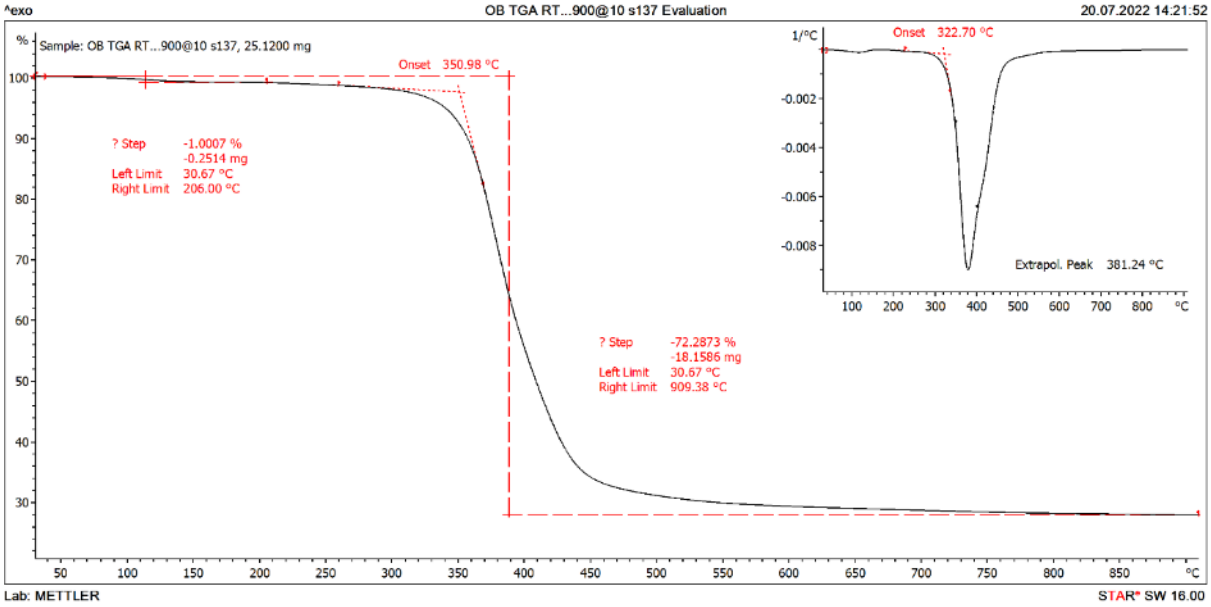

Graph 45. Normalized TGA results of P32-S137-ML. First derivative shown on top right corner

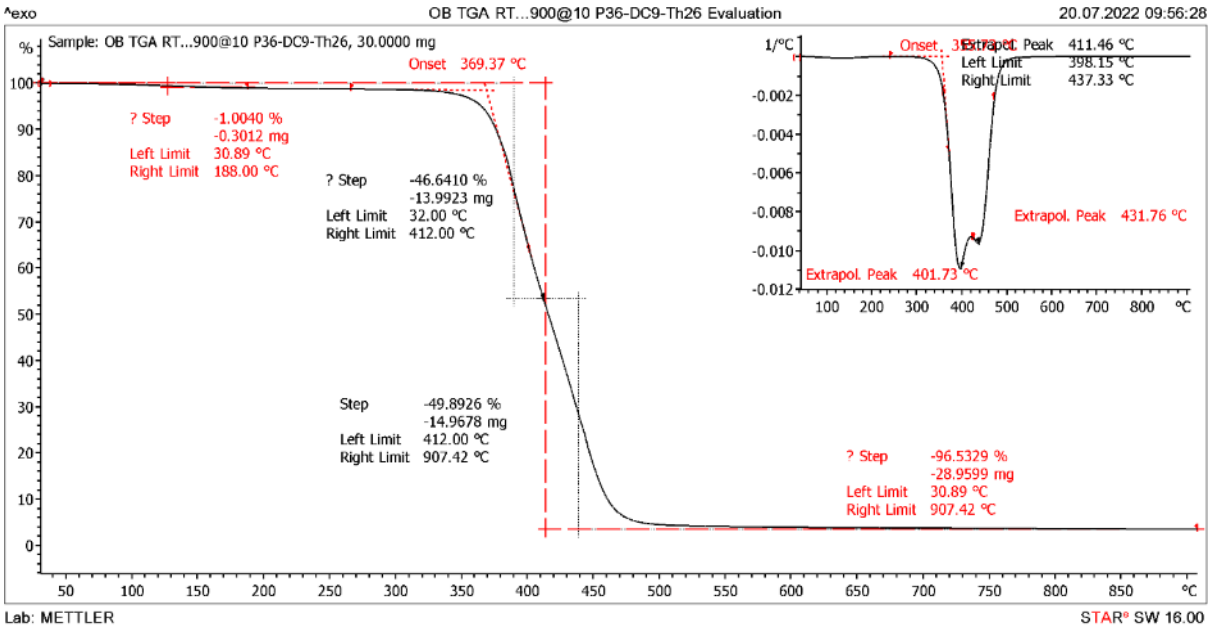

Graph 46. Normalized TGA results of P36-DC-9-Th26. First derivative shown on top right corner

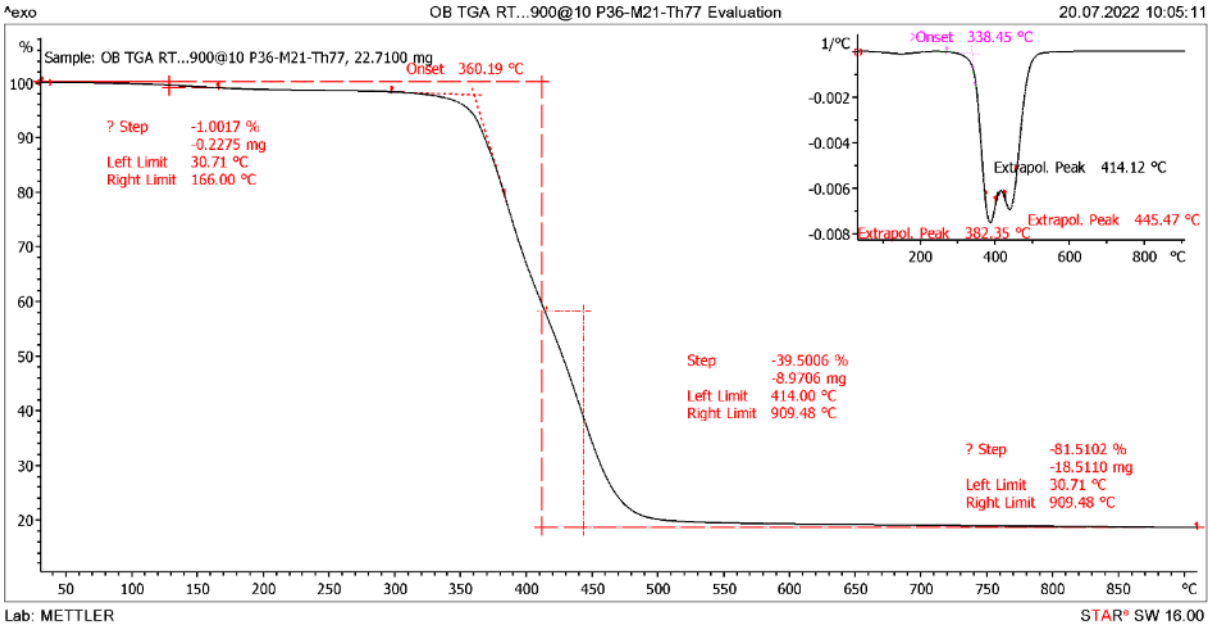

Graph 47. Normalized TGA results of P36-M21-Th77. First derivative shown on top right corner

APPENDIX D: DSC Graphs

CFRPs

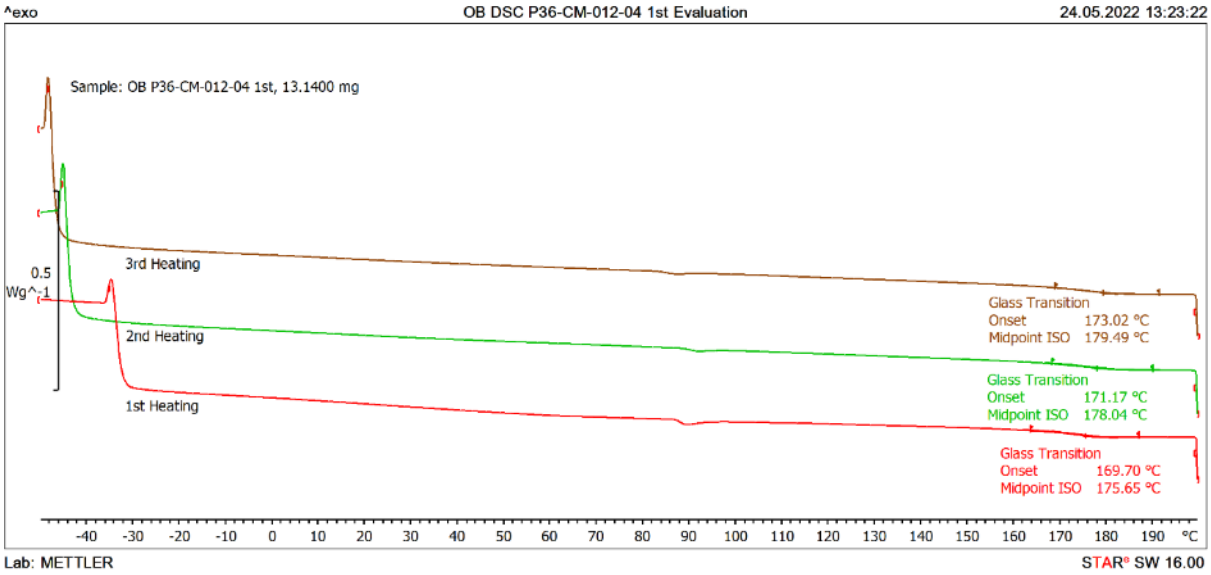

Graph 48. Normalized DSC results of P36-CM-012-04 S1. Calculated Tg values shown in 2st, 2nd and 3rd curves

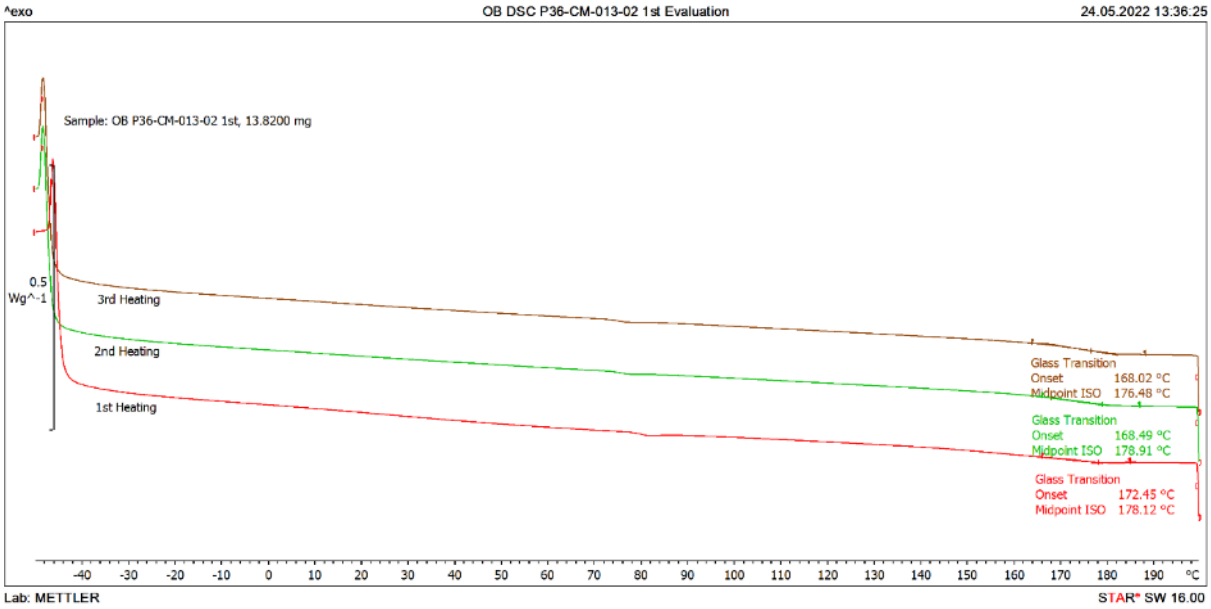

Graph 49. Normalized DSC results of P36-CM-013-02 S1. Calculated Tg values shown in 2st, 2nd and 3rd curves

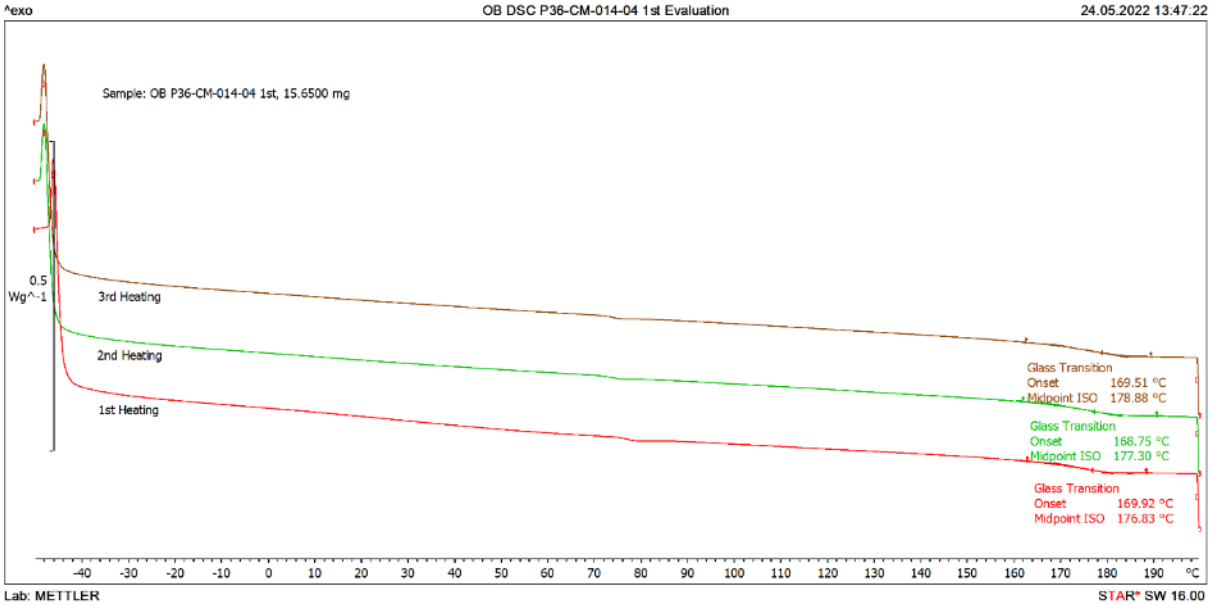

Graph 50. Normalized DSC results of P36-CM-014-04 S1. Calculated Tg values shown in 2st, 2nd and 3rd curves

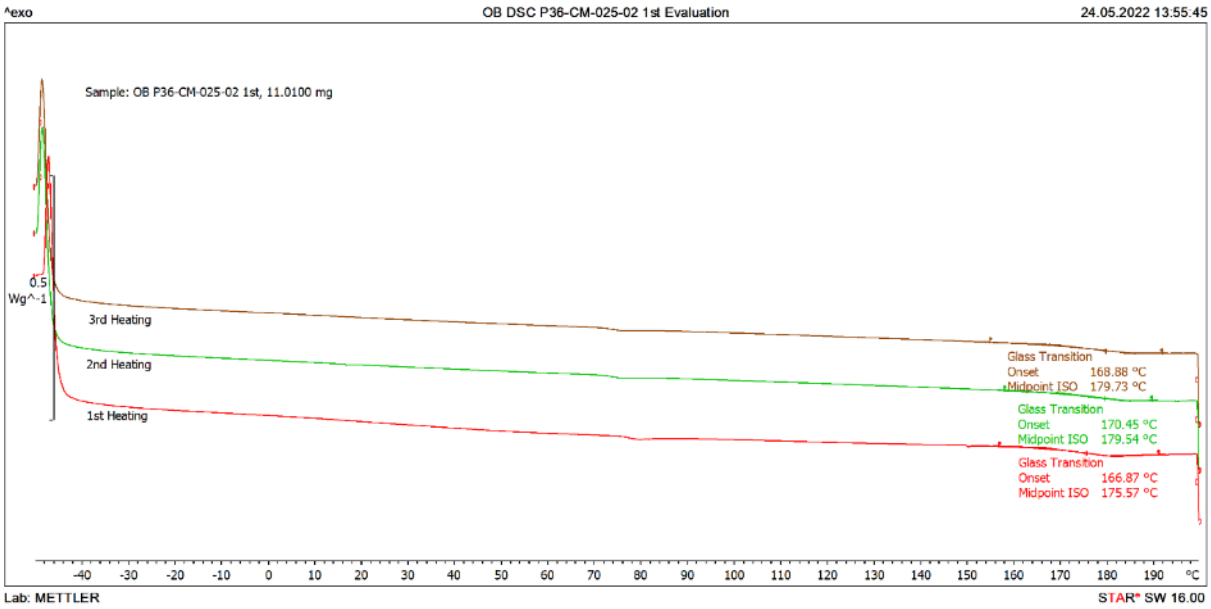

Graph 51. Normalized DSC results of P36-CM-025-02 S1. Calculated Tg values shown in 2st, 2nd and 3rd curves

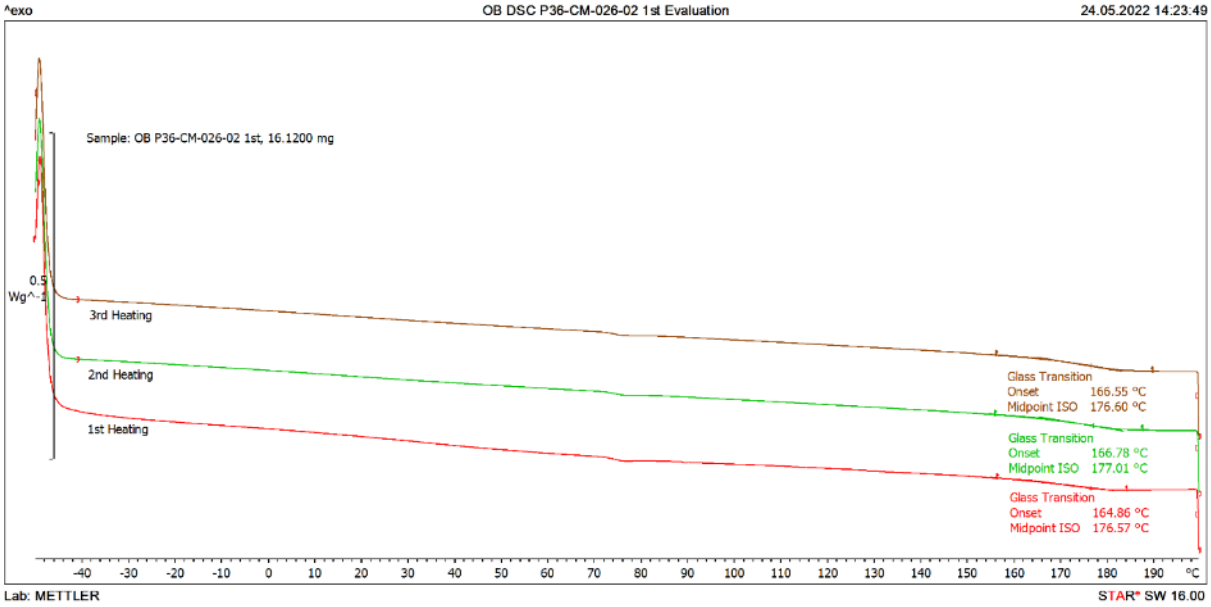

Graph 52. Normalized DSC results of P36-CM-026-02 S1. Calculated Tg values shown in 2st, 2nd and 3rd curves

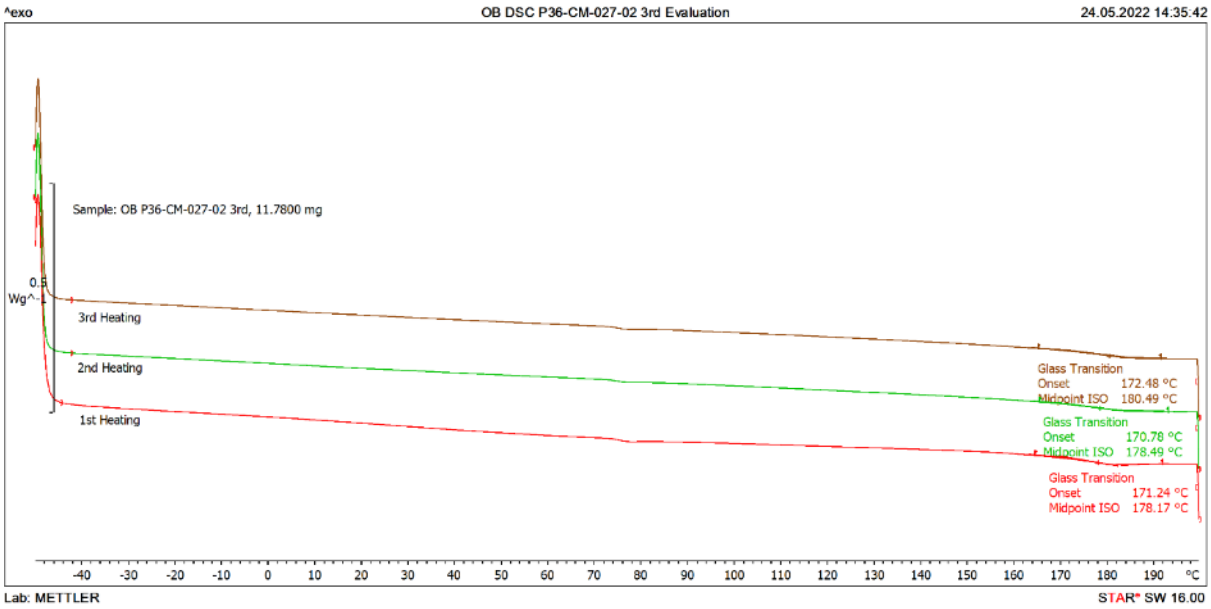

Graph 53. Normalized DSC results of P36-CM-027-02. Calculated Tg values shown in 2st, 2nd and 3rd curves

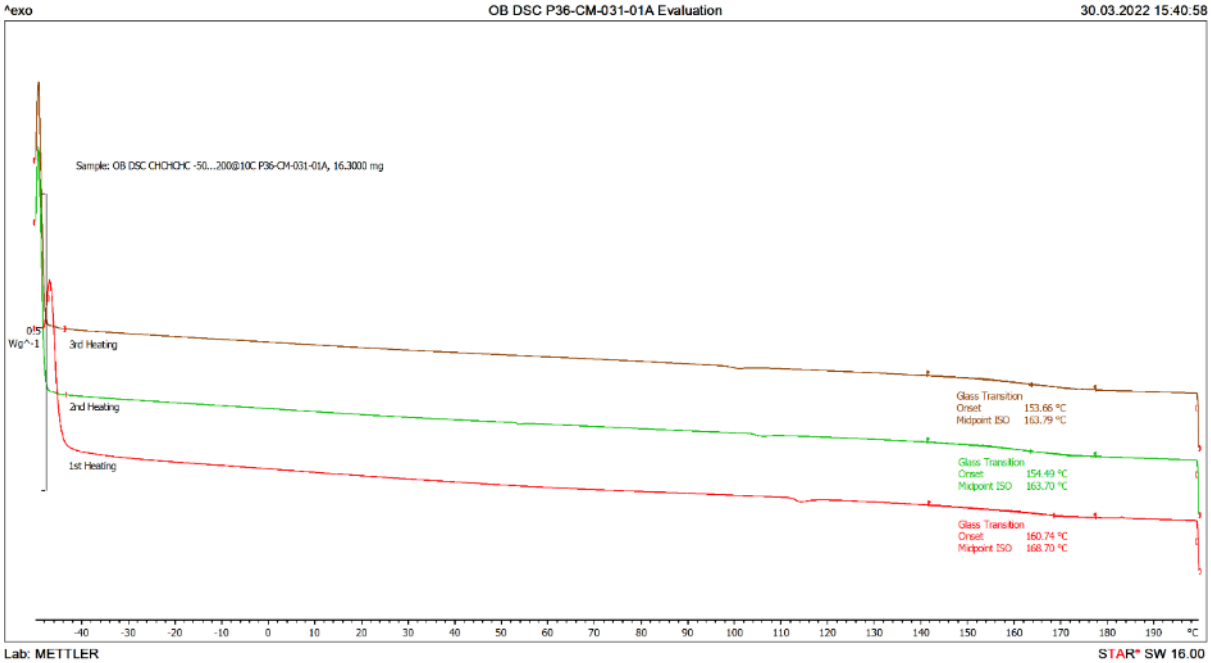

Graph 54. Normalized DSC results of P36-CM-031-01A S1. Calculated Tg values shown in 2st, 2nd and 3rd curves

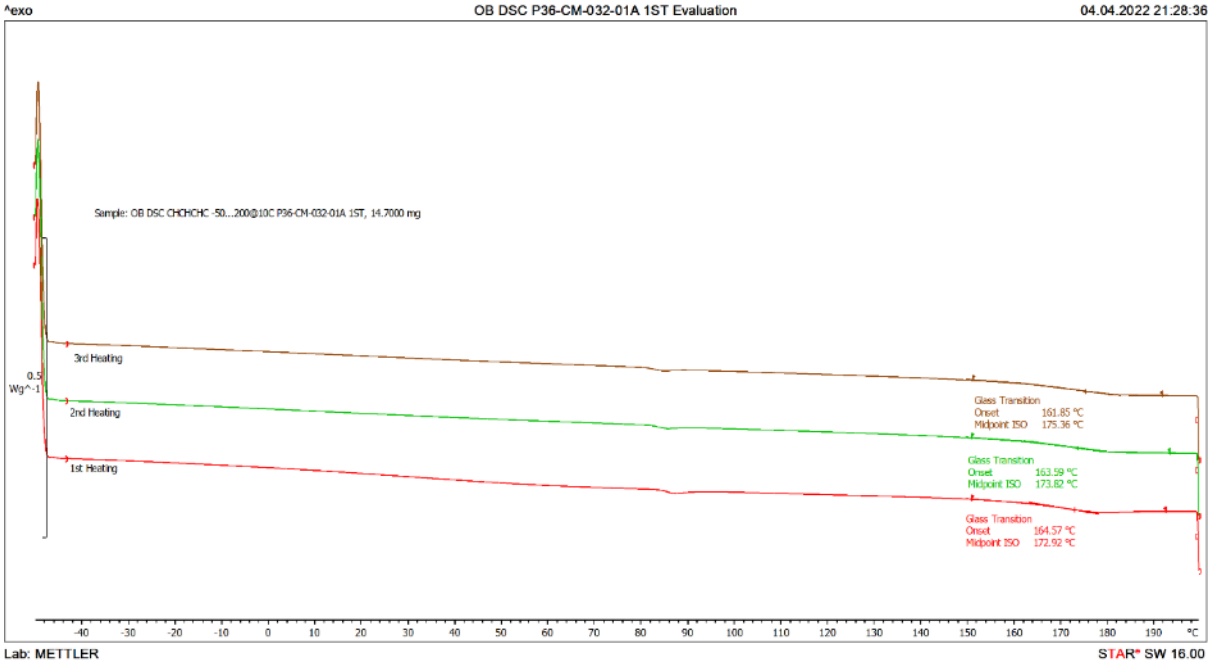

Graph 55. Normalized DSC results of P36-CM-032-01A S1. Calculated Tg values shown in 2st, 2nd and 3rd curves

Film adhesives

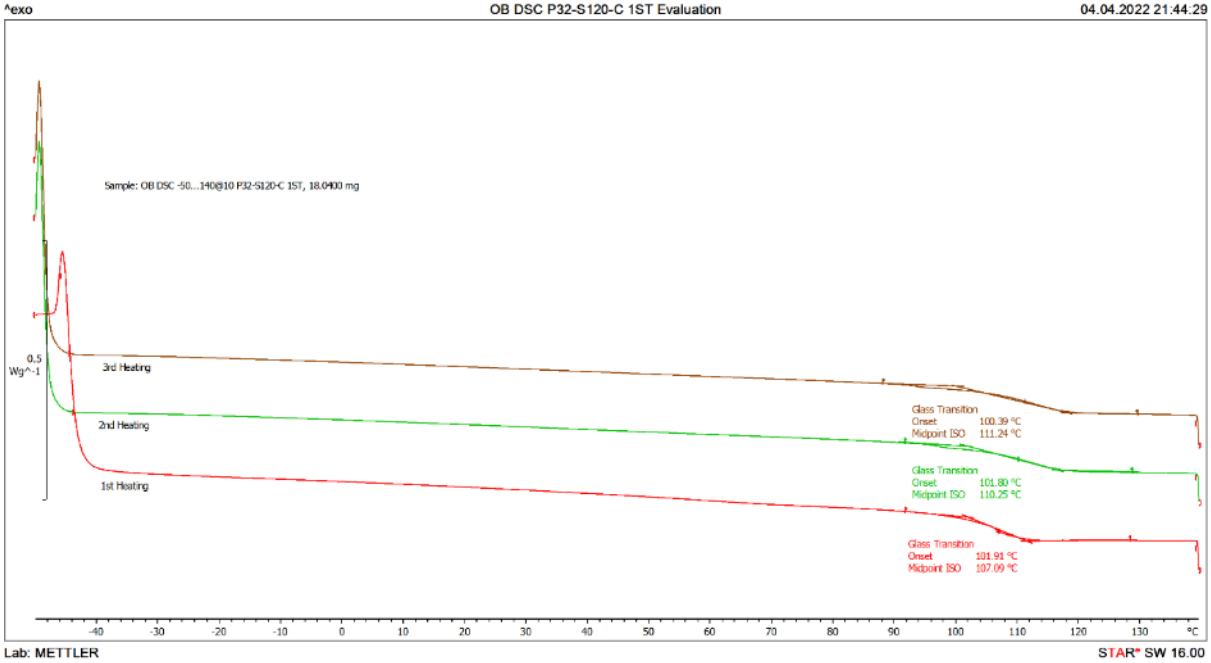

Graph 56. Normalized DSC results of P32-S120-C S1 . Calculated Tg values shown in 2st, 2nd and 3rd curves

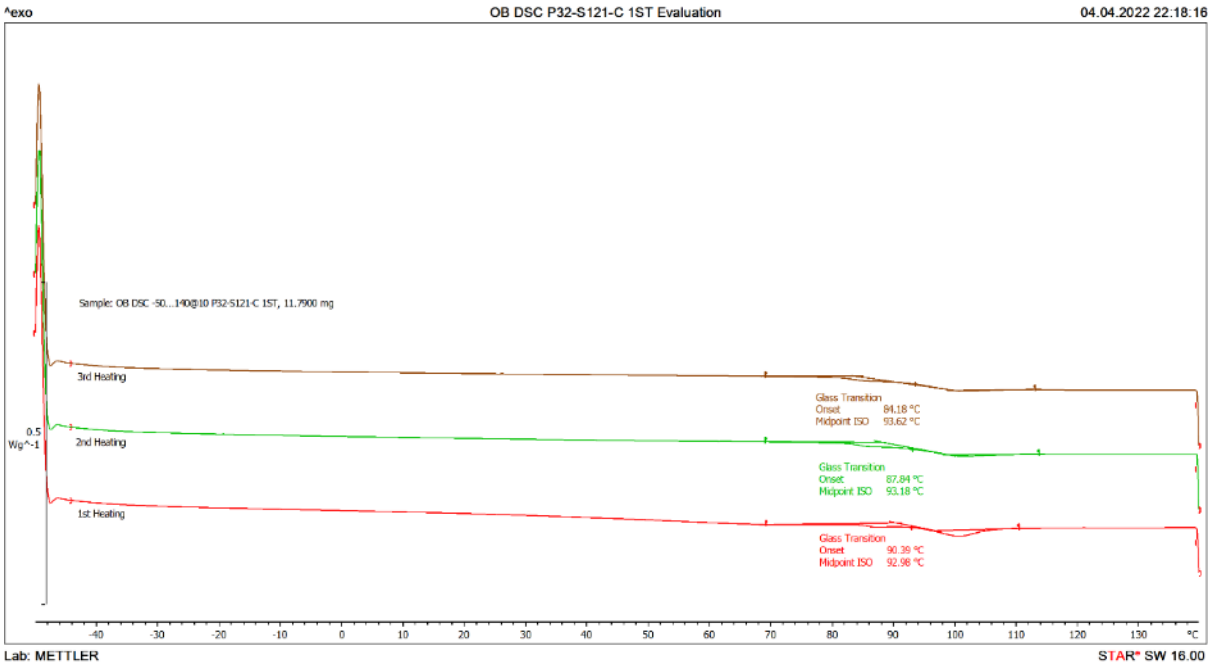

Graph 57. Normalized DSC results of P32-S121-C S1. Calculated Tg values shown in 2st, 2nd and 3rd curves

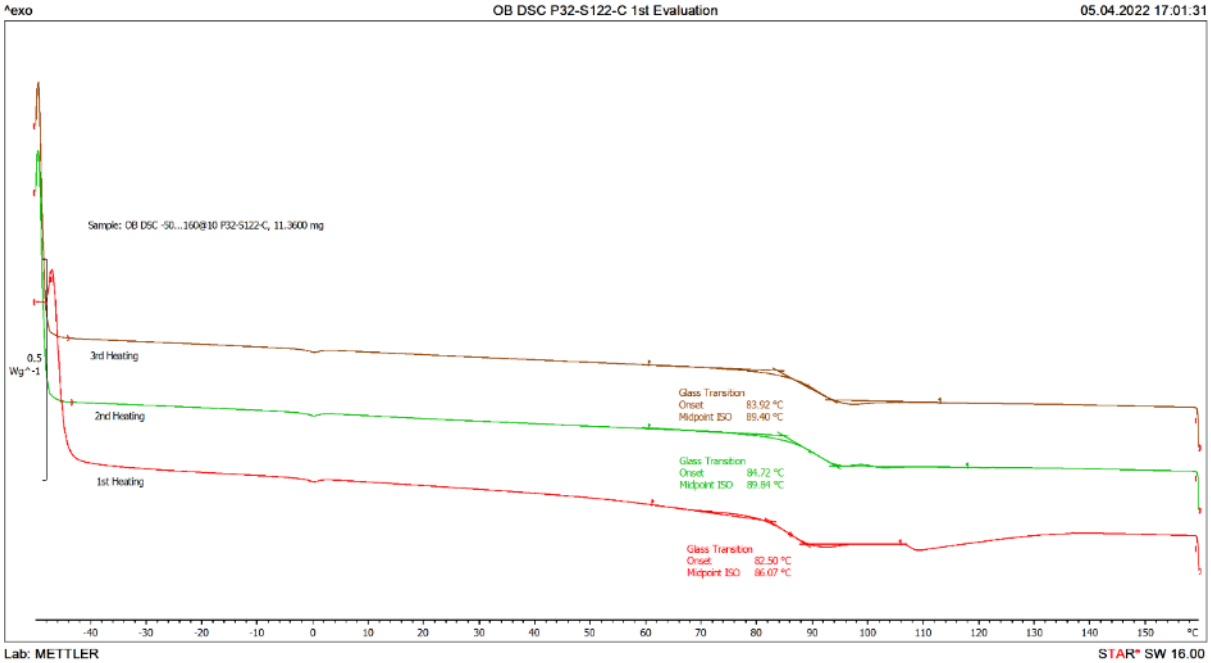

Graph 58. Normalized DSC results of P32-S122-C S1. Calculated Tg values shown in 2st, 2nd and 3rd curves

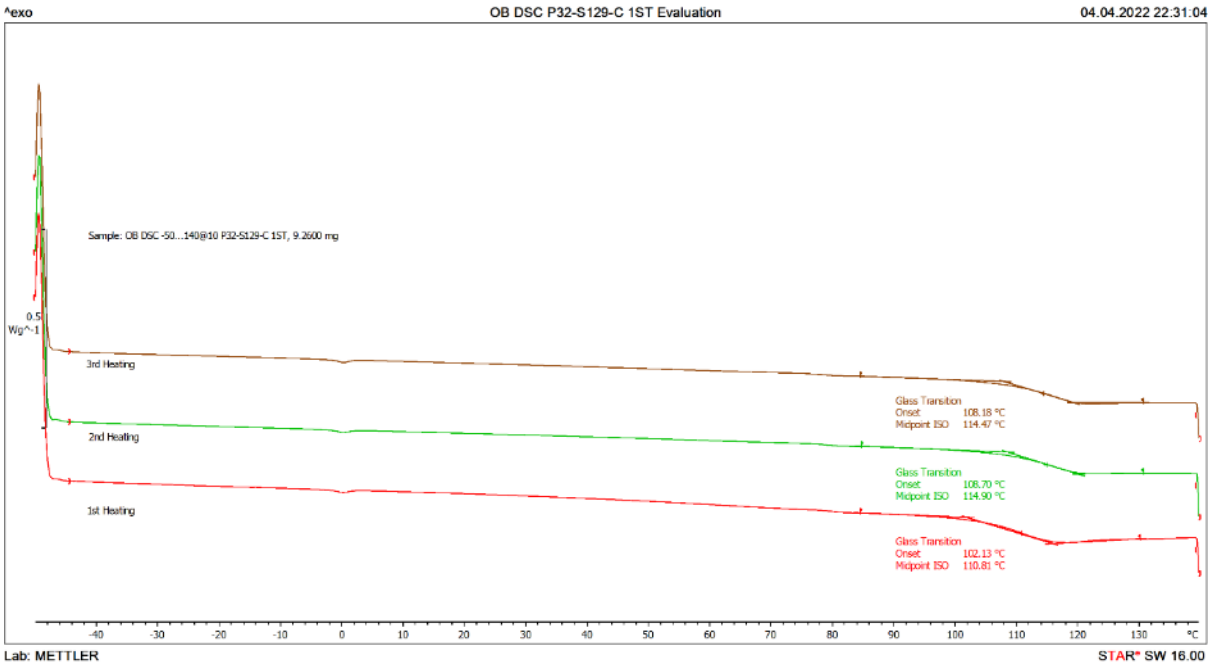

Graph 59. Normalized DSC results of P32-S129-C S1. Calculated Tg values shown in 2st, 2nd and 3rd curves

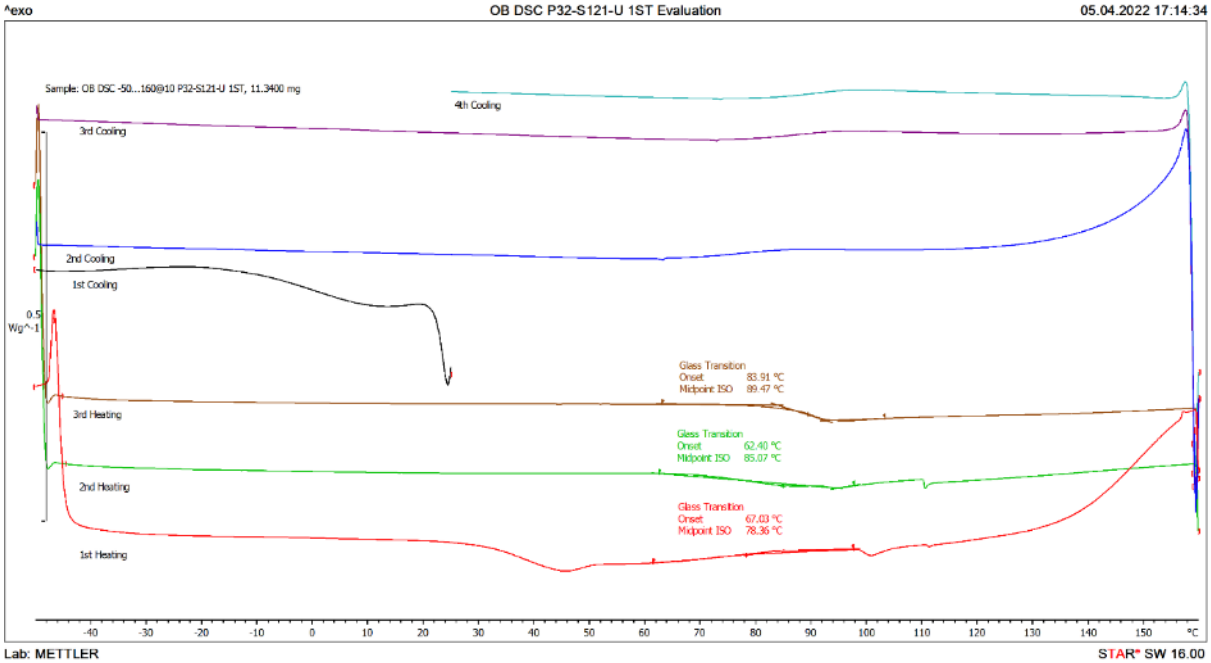

Graph 60. Normalized DSC results of P32-S121-U S1. Calculated Tg values shown in 2st, 2nd and 3rd hestinh curves

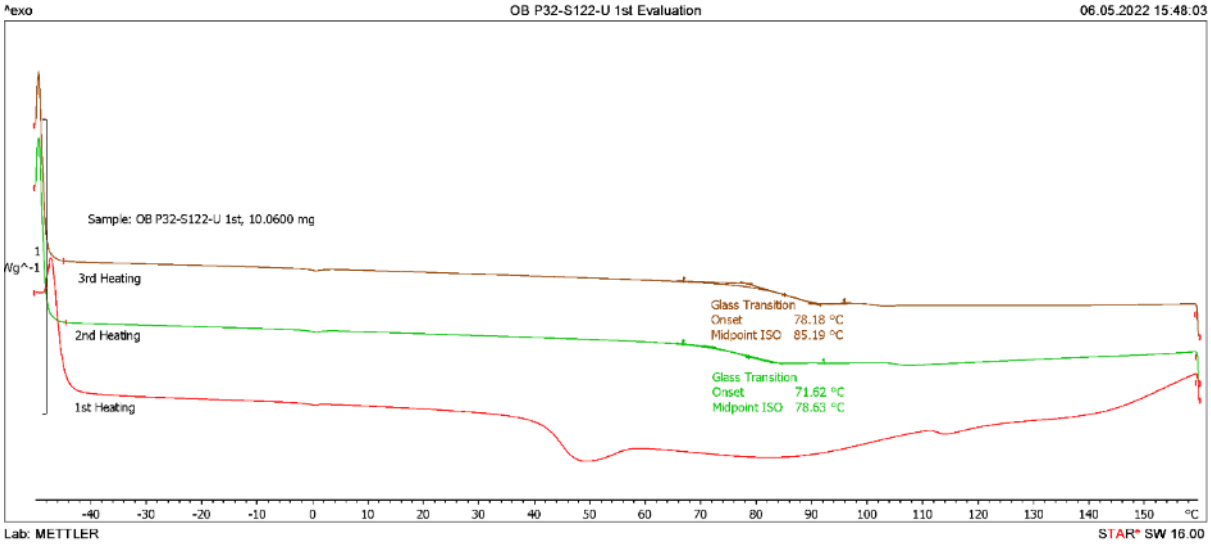

Graph 61. Normalized DSC results of P32-S122-U. Calculated Tg values shown in 2st, 2nd and 3rd curves

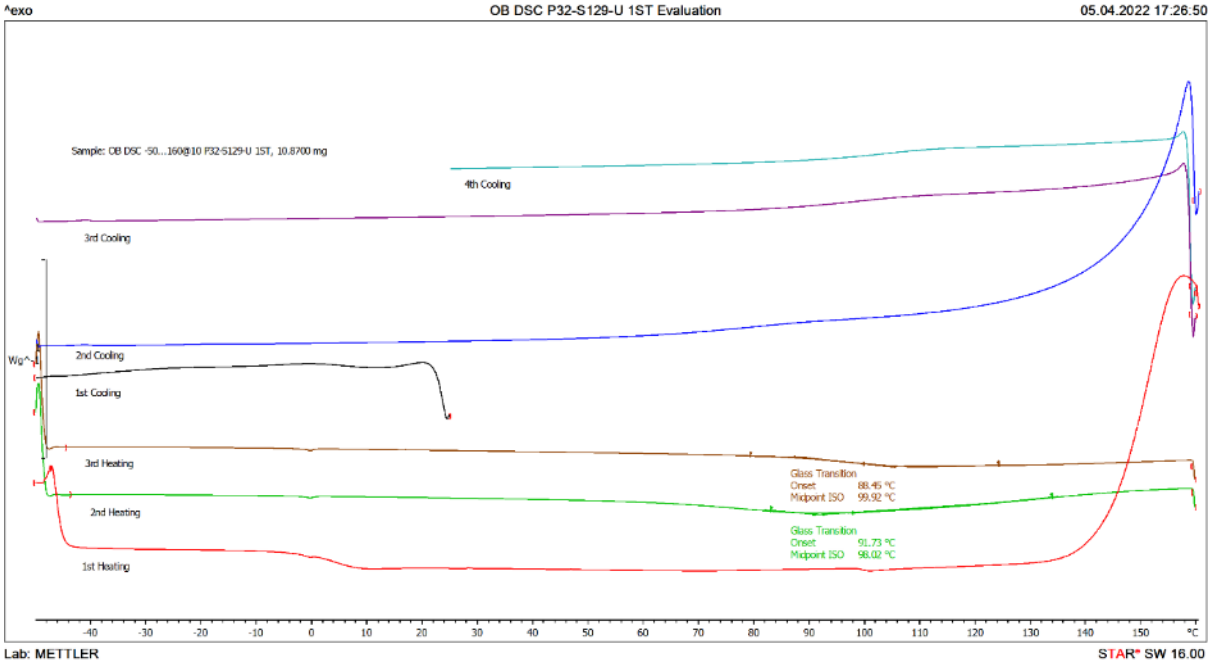

Graph 62. Normalized DSC results of P32-S129-U S1. Calculated Tg values shown in 2st, 2nd and 3rd curves

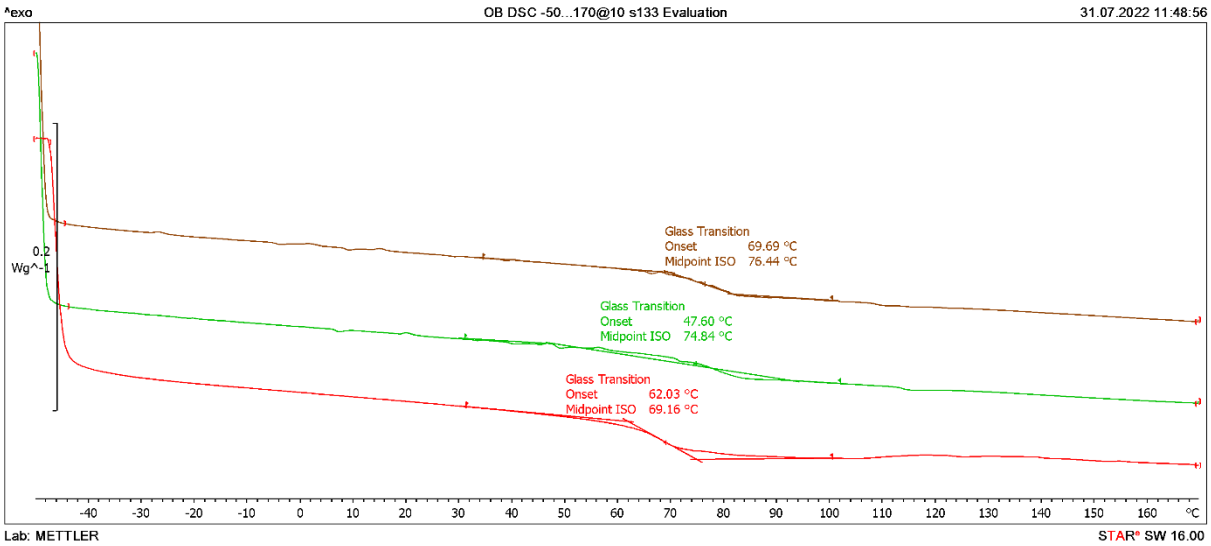

Graph 63. Normalized DSC results of s133. Calculated Tg values shown in 2st, 2nd and 3rd curves

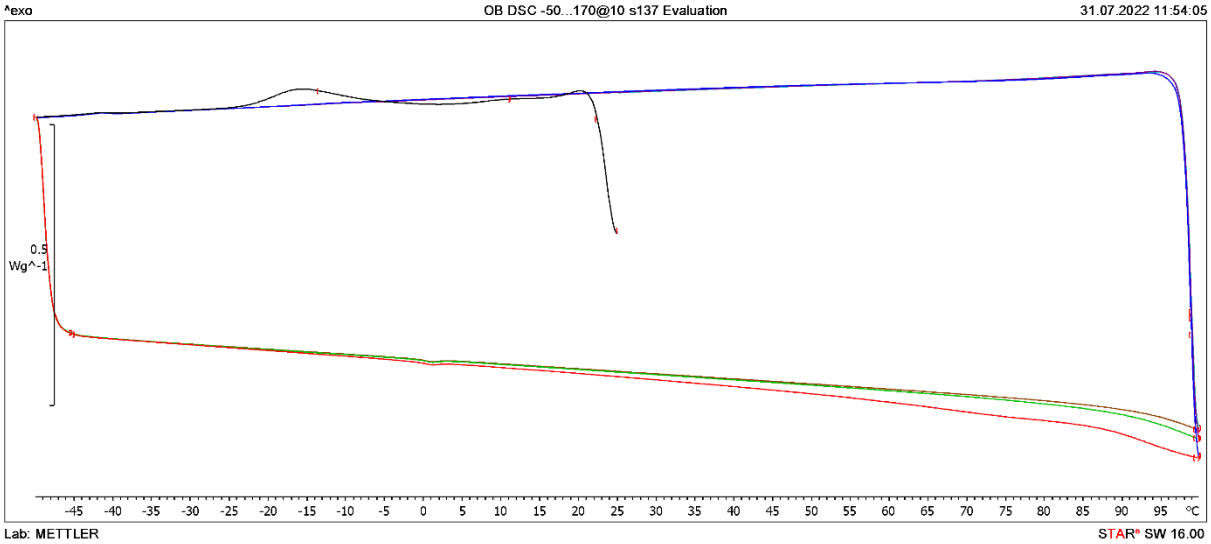

Graph 64. Normalized DSC results of s137. Calculated Tg values shown in 2st, 2nd and 3rd curves

Other adhesives

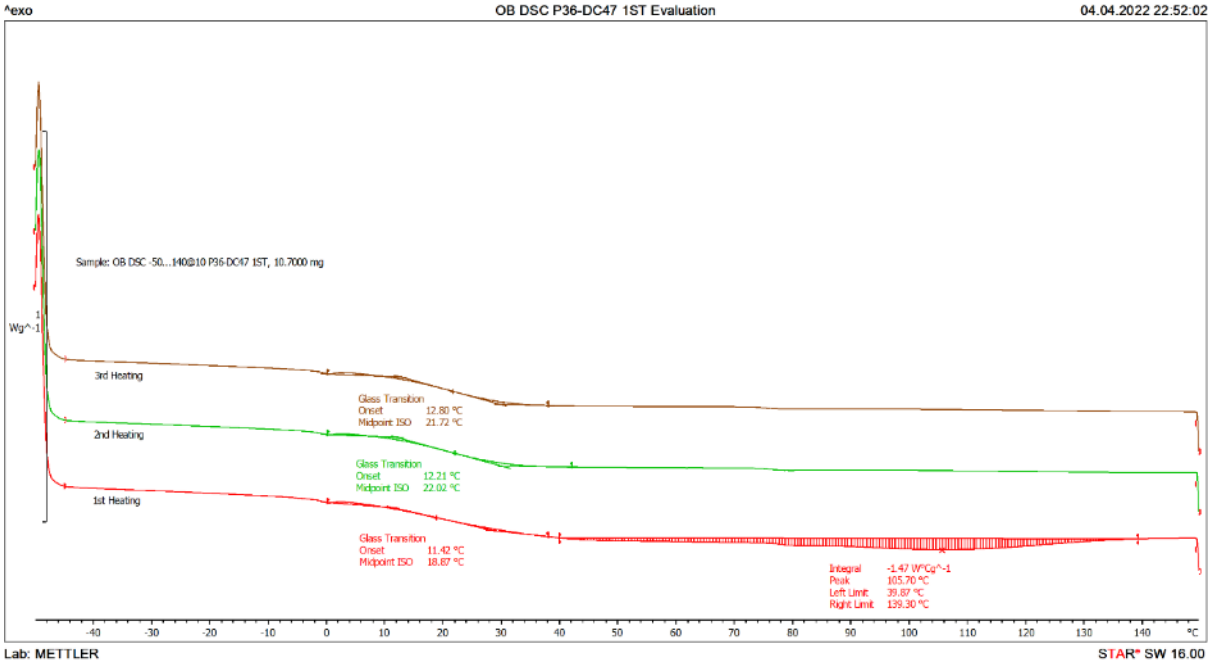

Graph 65. Normalized DSC results of P36-DC47 S1. Calculated Tg values shown in 2st, 2nd and 3rd curves

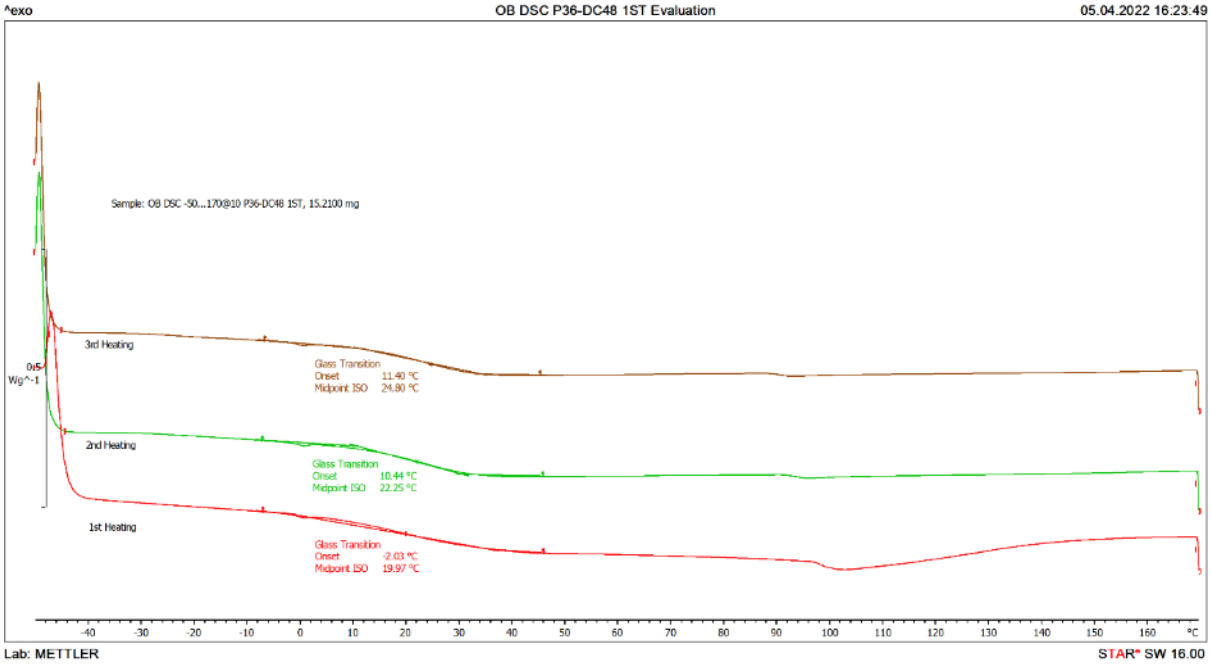

Graph 66. Normalized DSC results of P36-DC48. Calculated Tg values shown in 2st, 2nd and 3rd curves

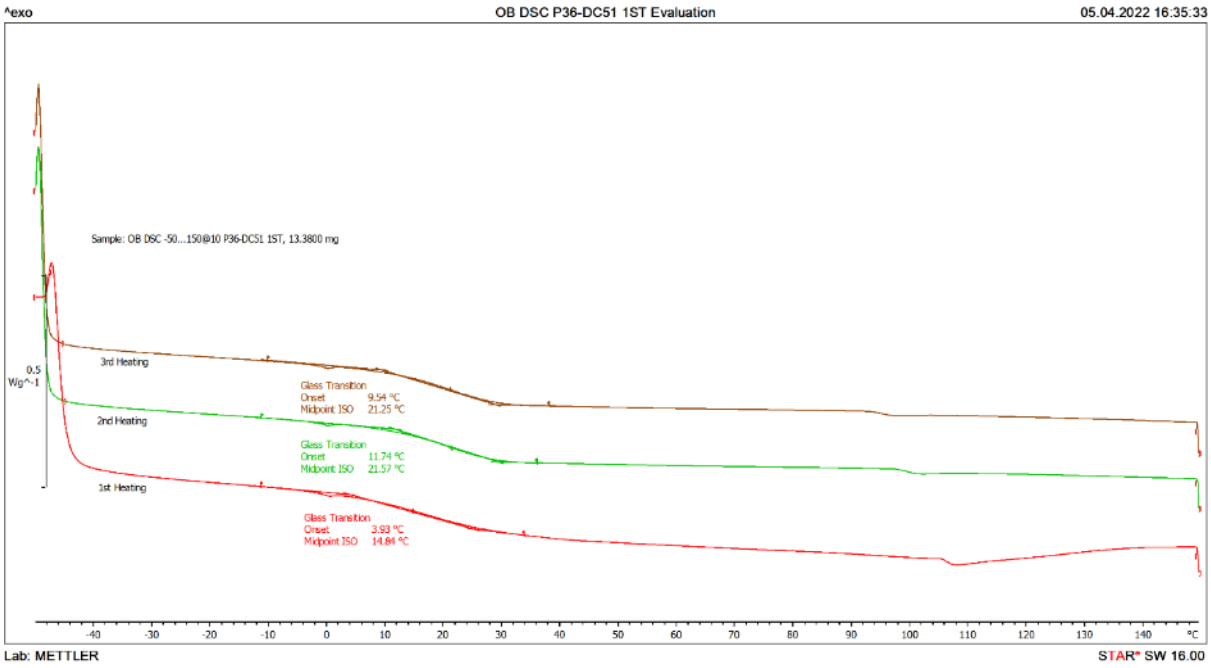

Graph 67. Normalized DSC results of P36-DC51 S1. Calculated Tg values shown in 2st, 2nd and 3rd curves

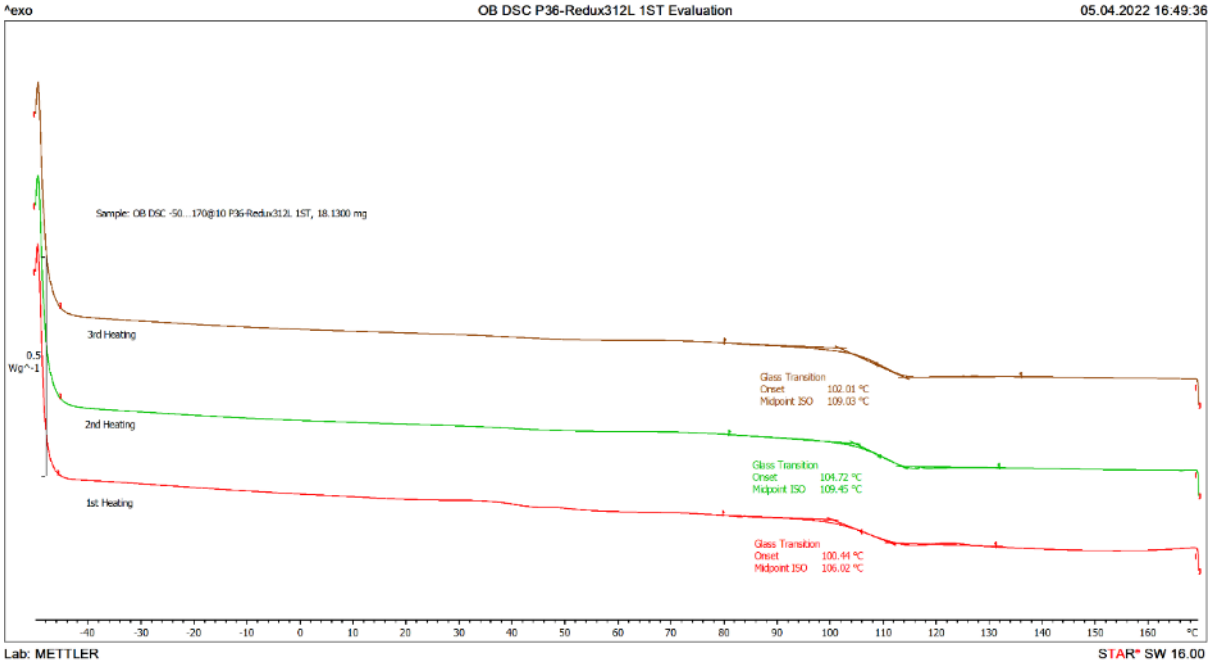

Graph 68. Normalized DSC results of P36-Redux312L. Calculated Tg values shown in 2st, 2nd and 3rd curves

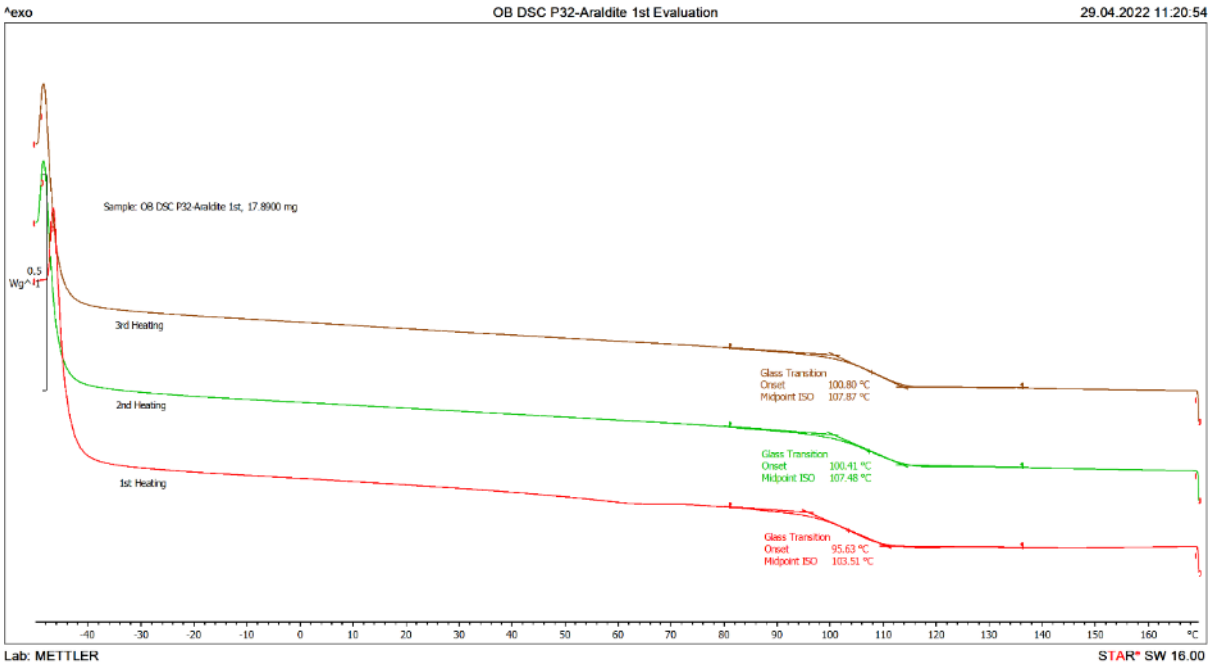

Graph 69. Normalized DSC results of P32-Araldite S1. Calculated Tg values shown in 2st, 2nd and 3rd curves

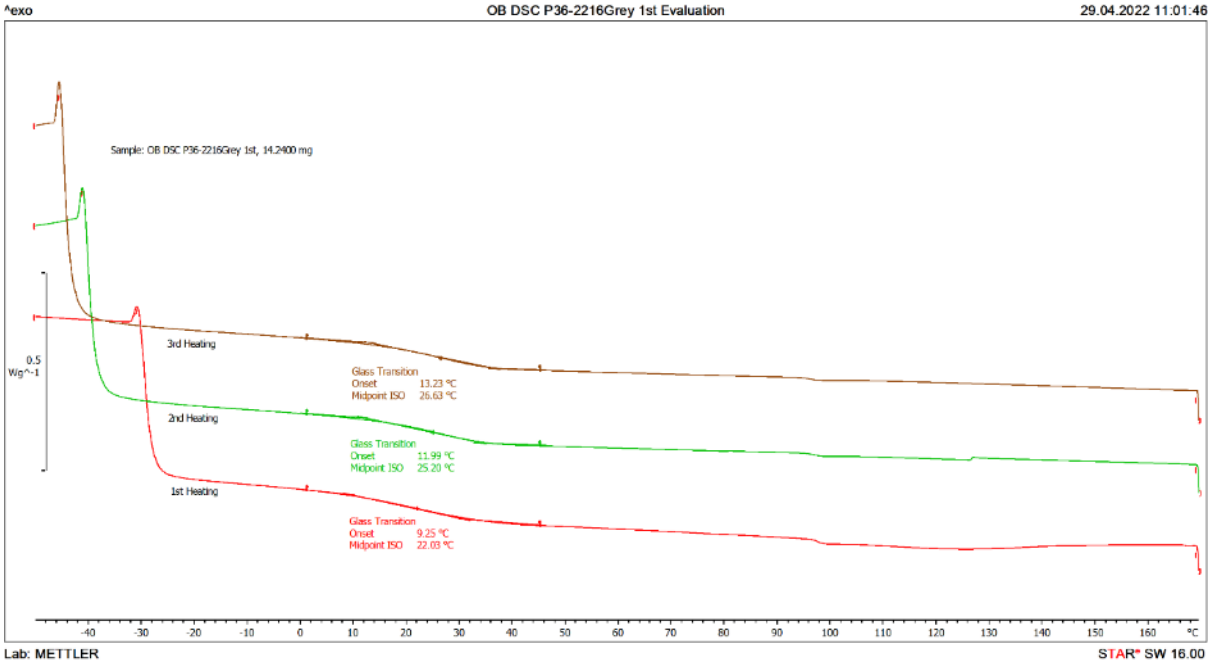

Graph 70. Normalized DSC results of 2216Grey S1. Calculated Tg values shown in 2st, 2nd and 3rd curves

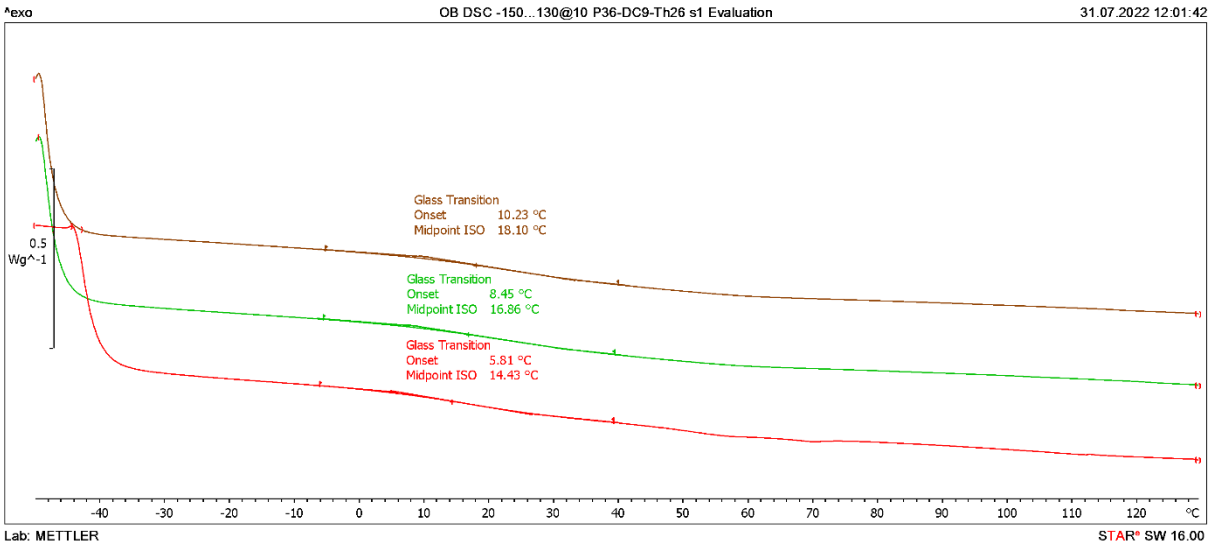

Graph 71. Normalized DSC results of P36-DC9-Th26 S1. Calculated Tg values shown in 2st, 2nd and 3rd curves

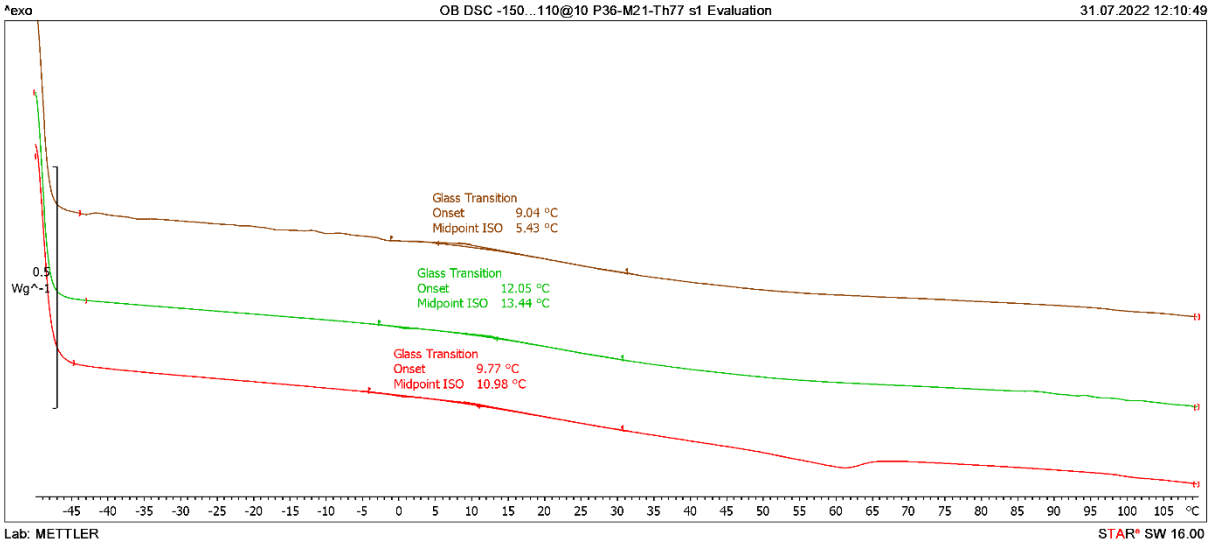

Graph 72. Normalized DSC results of P36-M21-Th77 S1. Calculated Tg values shown in 2st, 2nd and 3rd curves

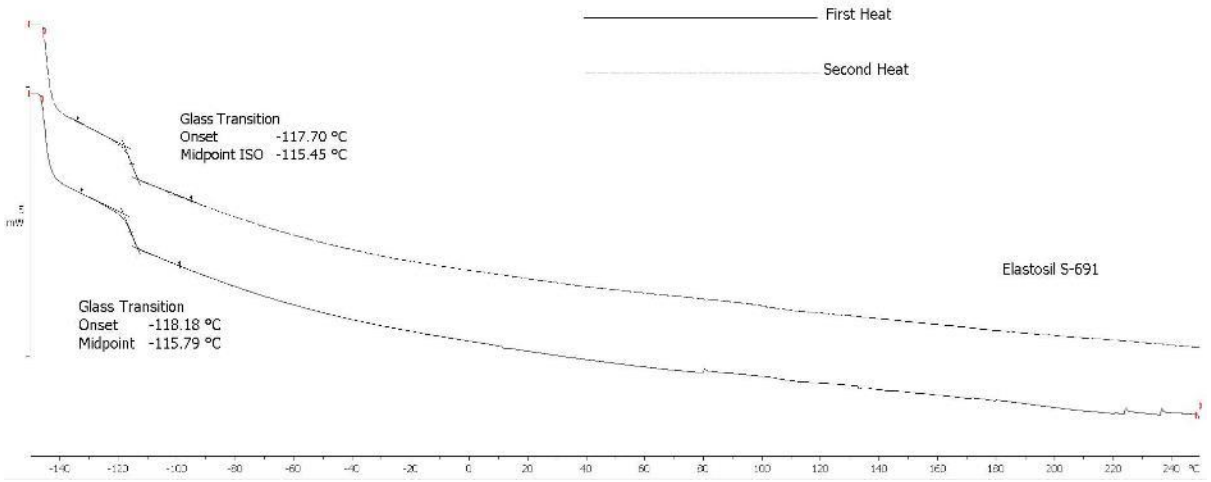

Graph 73. Normalized DSC results of RTV-S691. Calculated Tg values shown in 2st, 2nd and 3rd curves

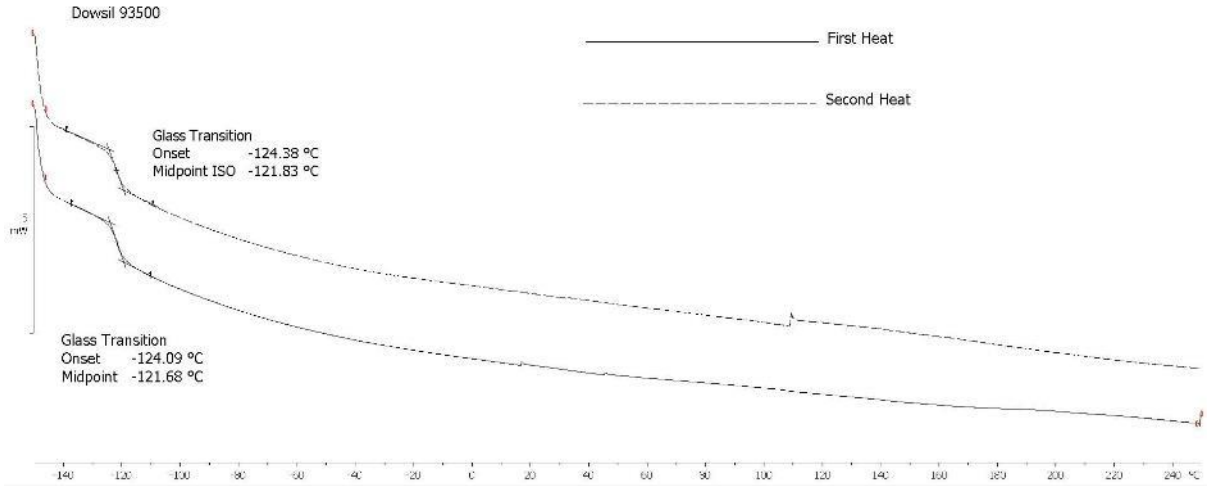

Graph 74. Normalized DSC results of DOWSIL 93-500. Calculated Tg values shown in 2st, 2nd and 3rd curves

APPENDIX E: TMA Graphs

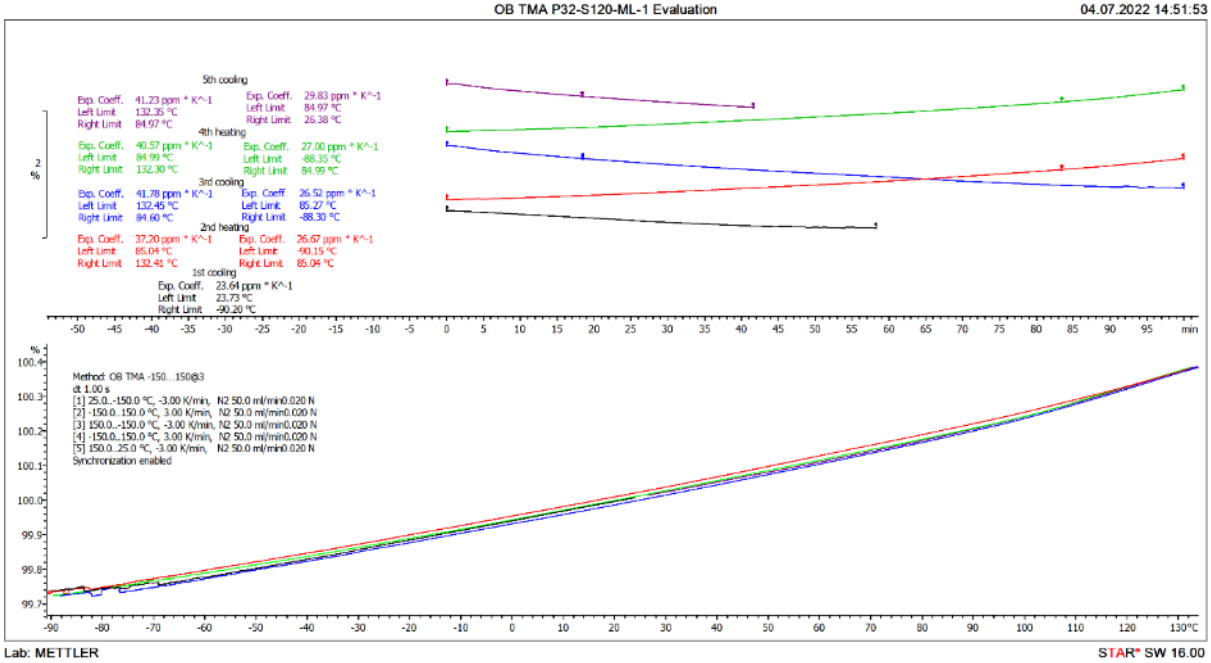

Graph 75. Normalized TMA results of P32-S120-ML. Top: curves vs. time. Bottom: curves vs temperature (same colors)

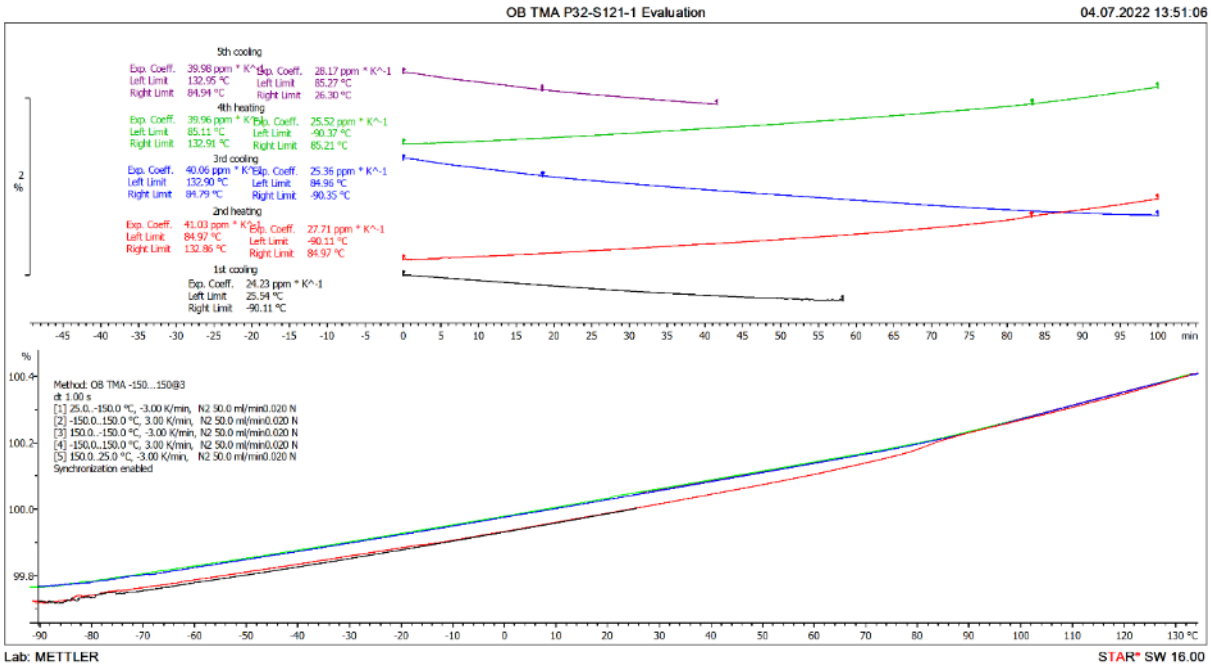

Graph 76. Normalized TMA results of P32-S121-ML. Top: curves vs. time. Bottom: curves vs temperature (same colors)

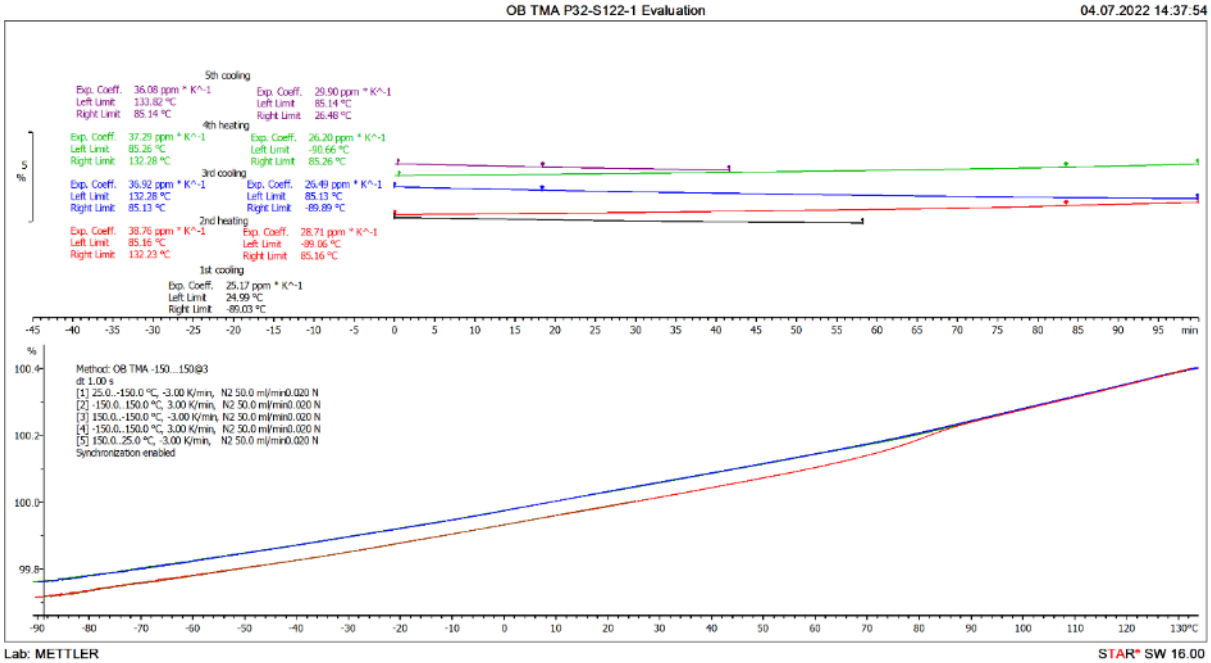

Graph 77. Normalized TMA results of P32-S122-ML. Top: curves vs. time. Bottom: curves vs temperature (same colors)

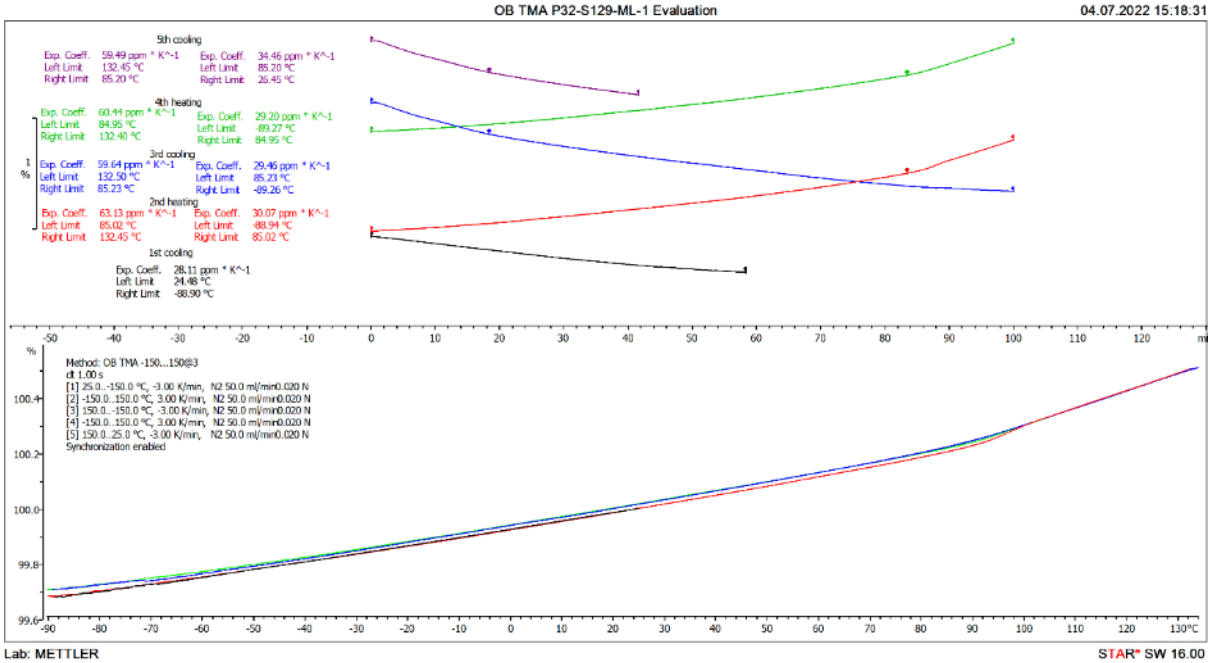

Graph 78. Normalized TMA results of P32-S129-ML. Top: curves vs. time. Bottom: curves vs temperature (same colors)

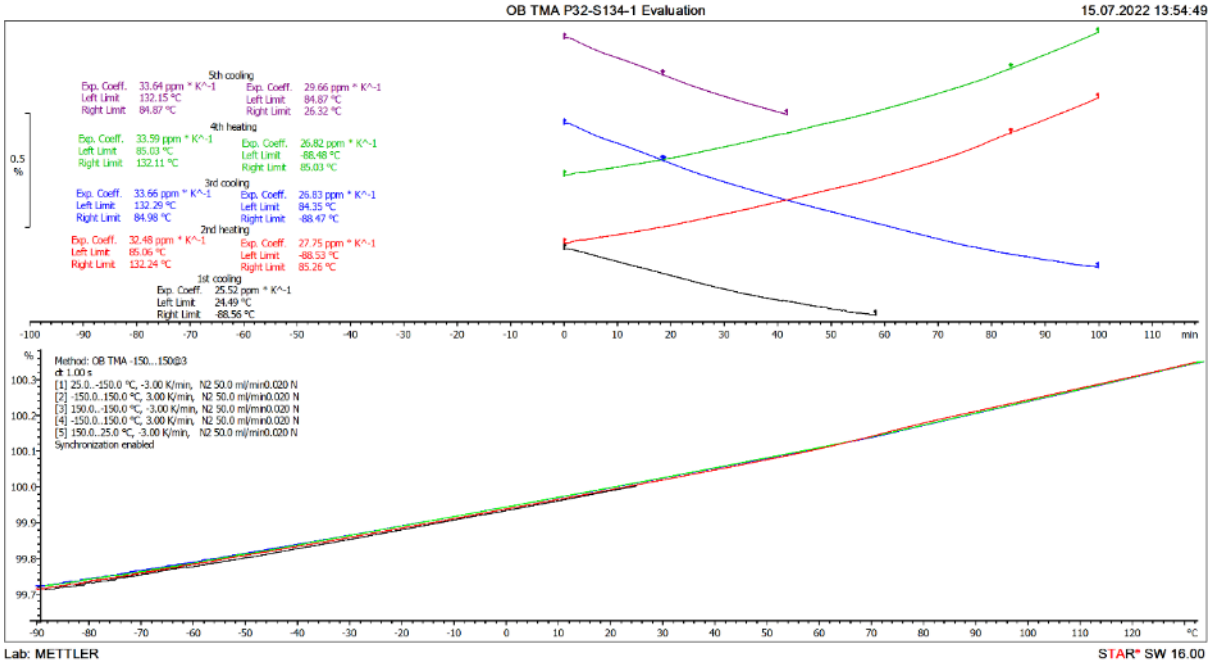

Graph 79. Normalized TMA results of P32-S134-ML. Top: curves vs. time. Bottom: curves vs temperature (same colors)

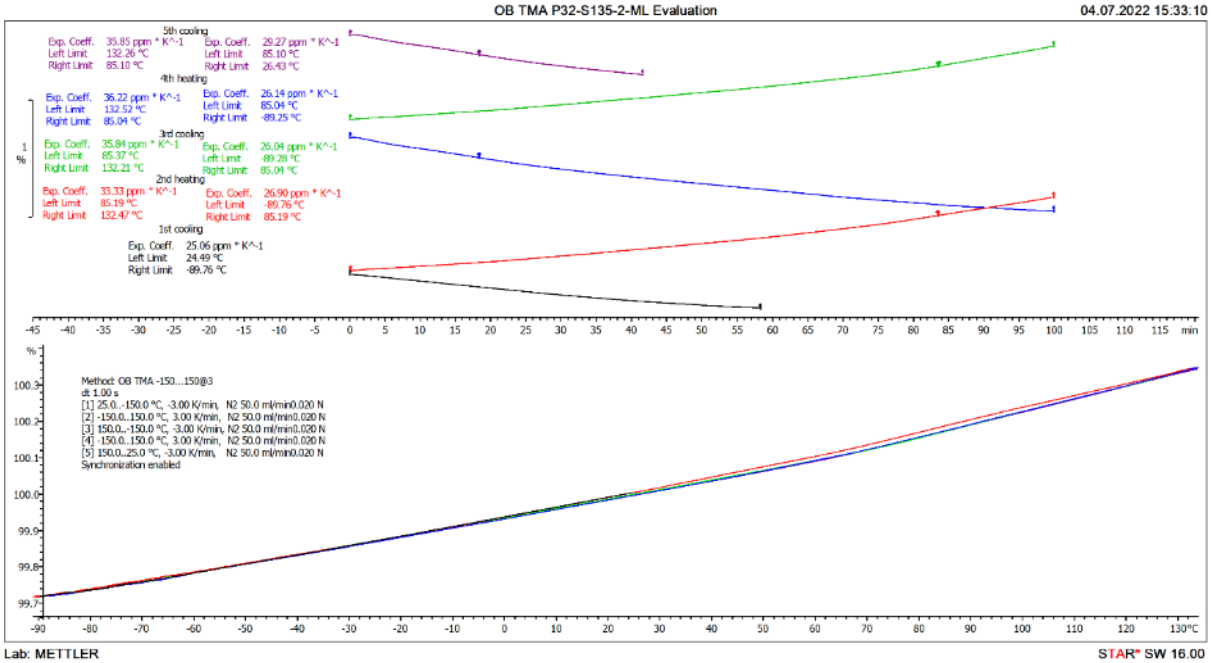

Graph 80. Normalized TMA results of P32-S135-ML. Top: curves vs. time. Bottom: curves vs temperature (same colors)

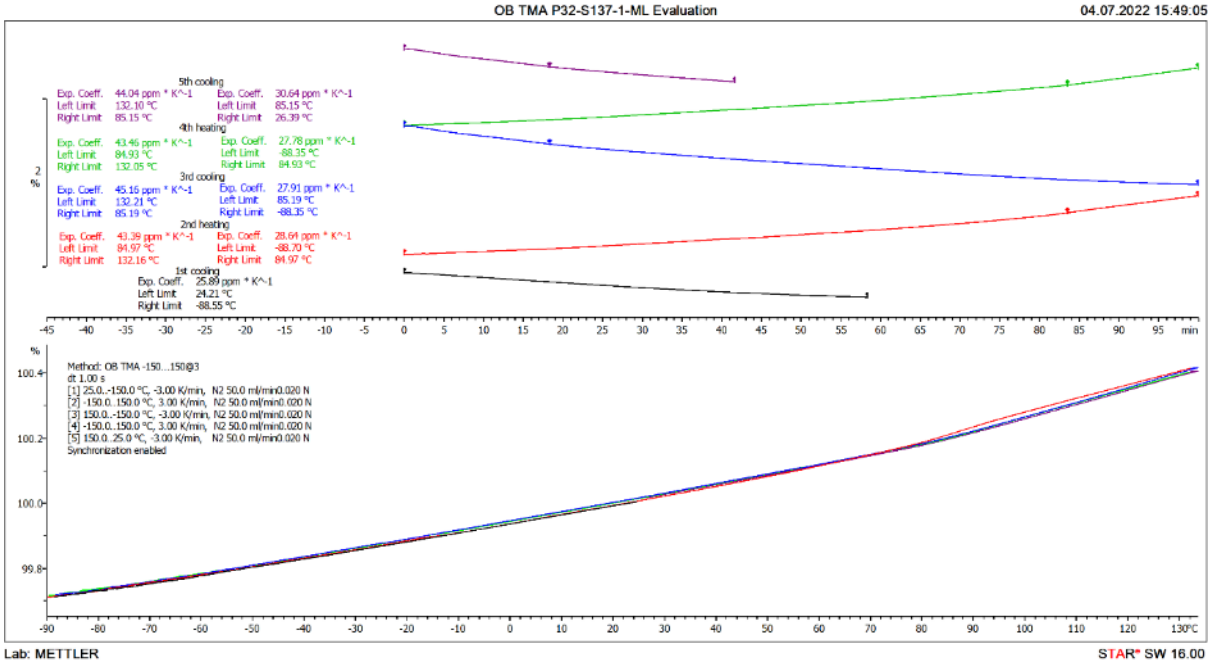

Graph 81. Normalized TMA results of P32-S137-ML. Top: curves vs. time. Bottom: curves vs temperature (same colors)

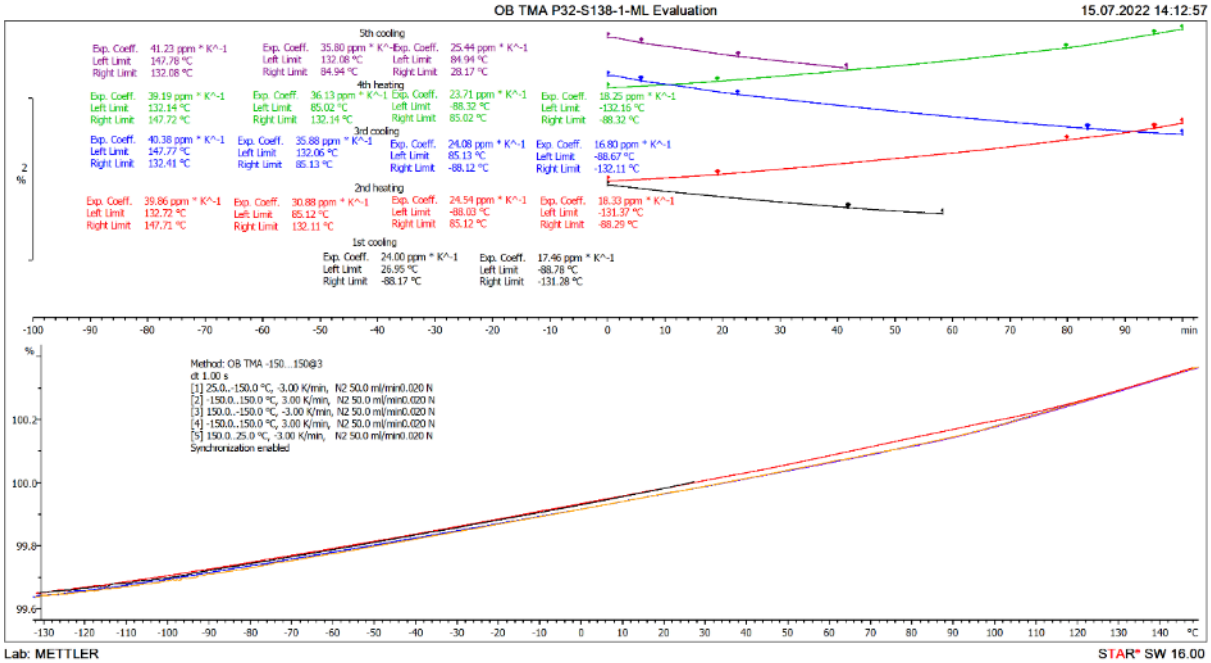

Graph 82. Normalized TMA results of P32-S138-ML. Top: curves vs. time. Bottom: curves vs temperature (same colors)

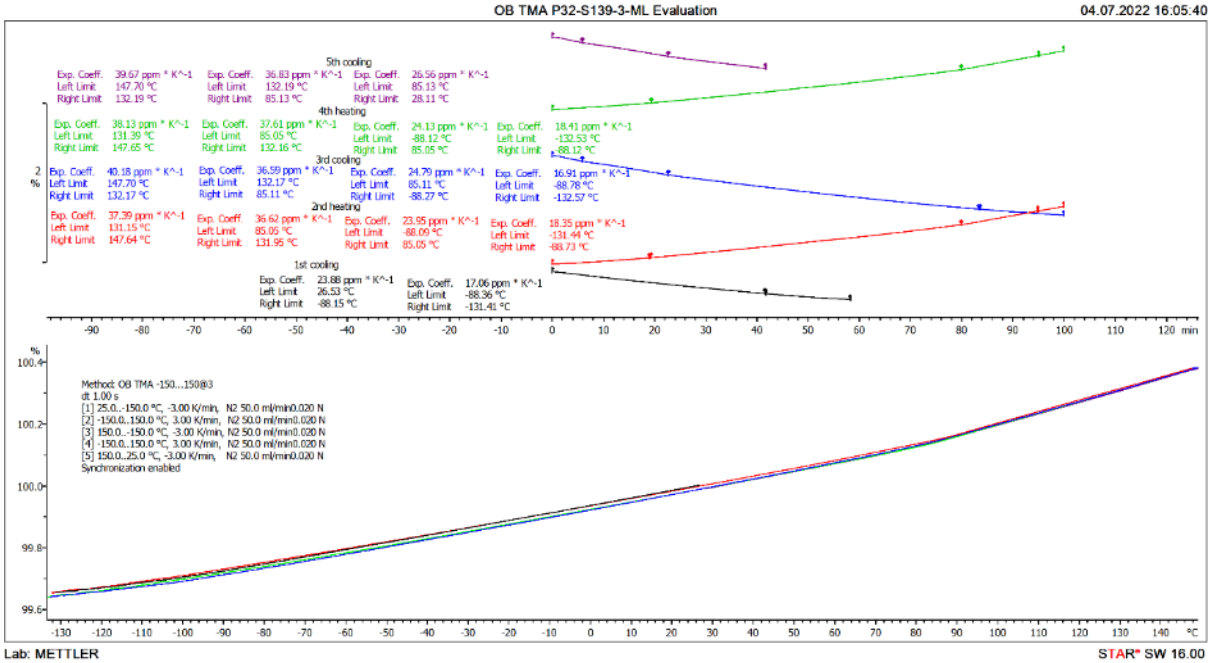

Graph 83. Normalized TMA results of P32-S139-ML. Top: curves vs. time. Bottom: curves vs temperature (same colors)

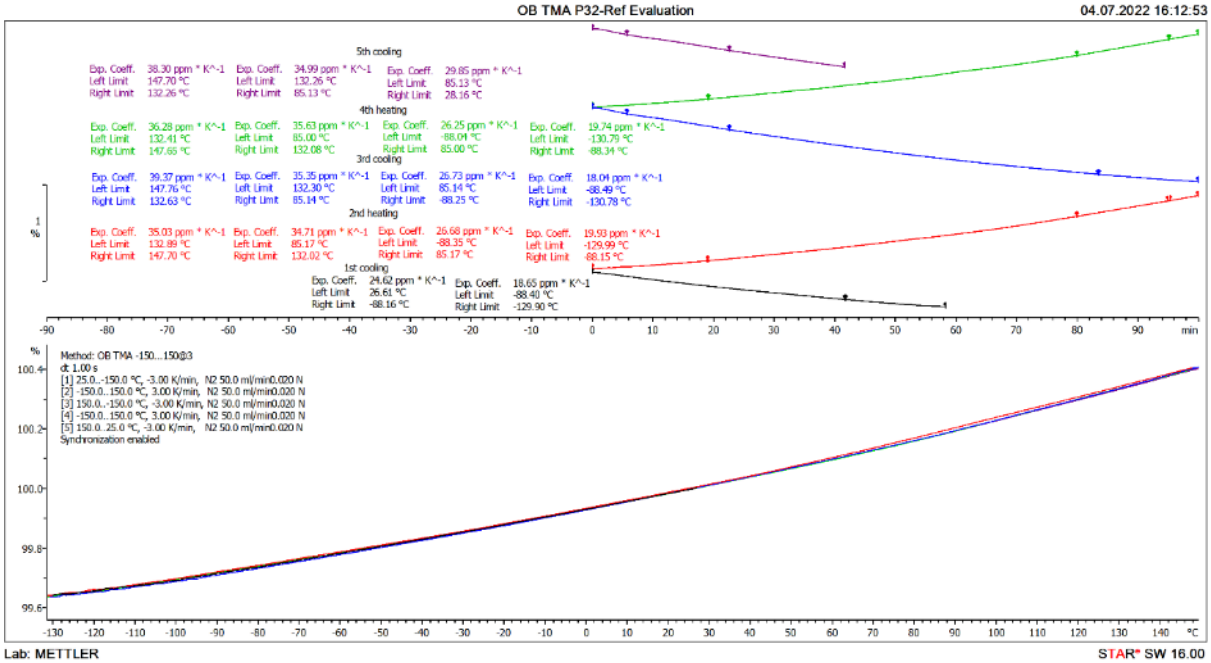

Graph 84. Normalized TMA results of P32-Ref. Top: curves vs. time. Bottom: curves vs temperature (same colors)

APPENDIX F: DMA Graphs

2qewr

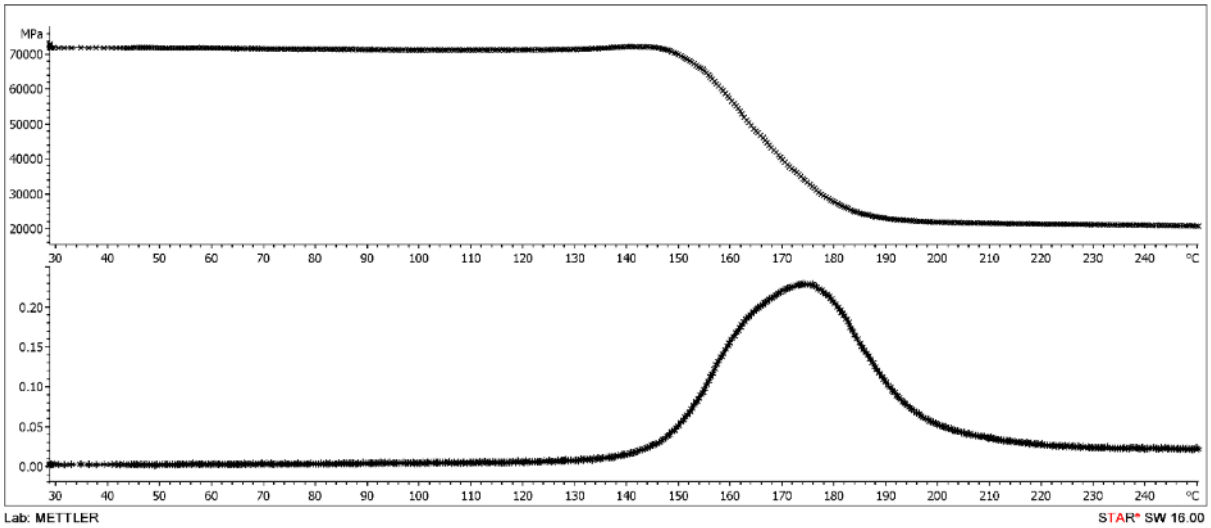

Graph 85. DMA results of P36-CM-012-04. Top: Storage modulus (M') vs temperature. Bottom: Tan delta vs temperature

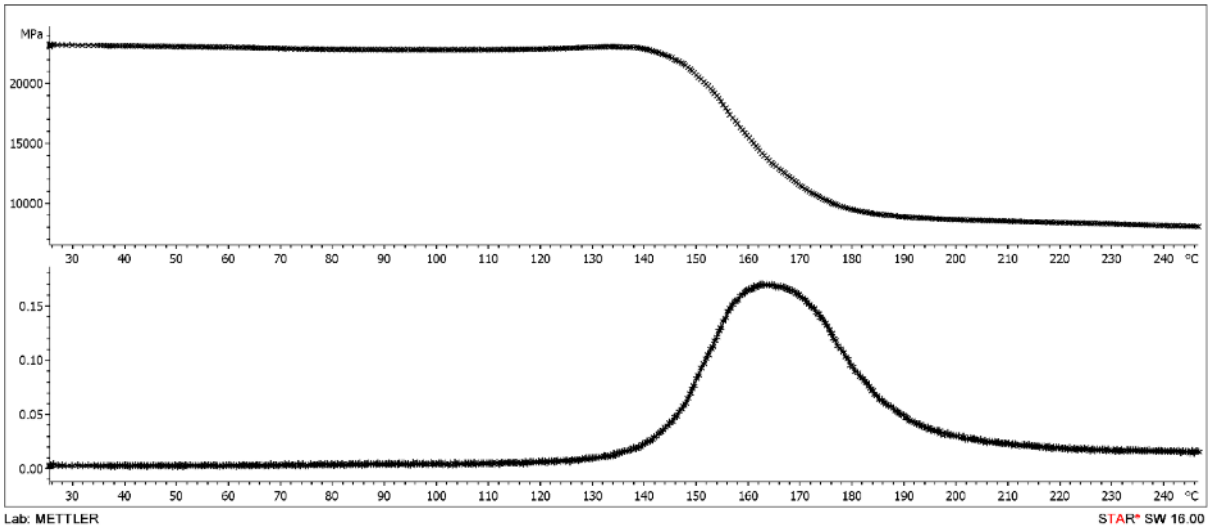

Graph 86. DMA results of P36-CM-013-02. Top: Storage modulus (M') vs temperature. Bottom: Tan delta vs temperature

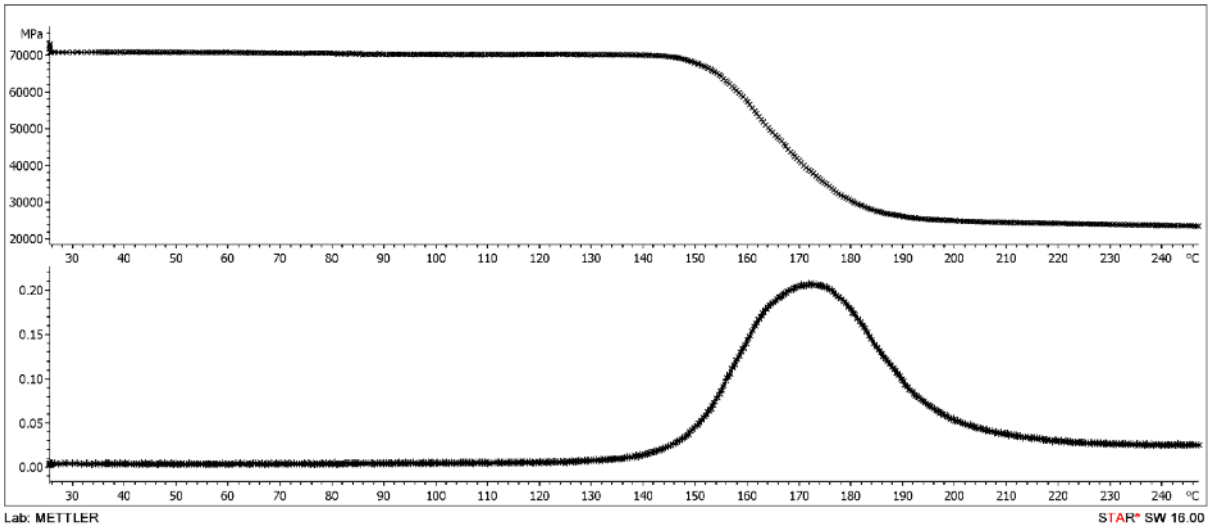

Graph 87. DMA results of P36-CM-014-04. Top: Storage modulus (M') vs temperature. Bottom: Tan delta vs temperature

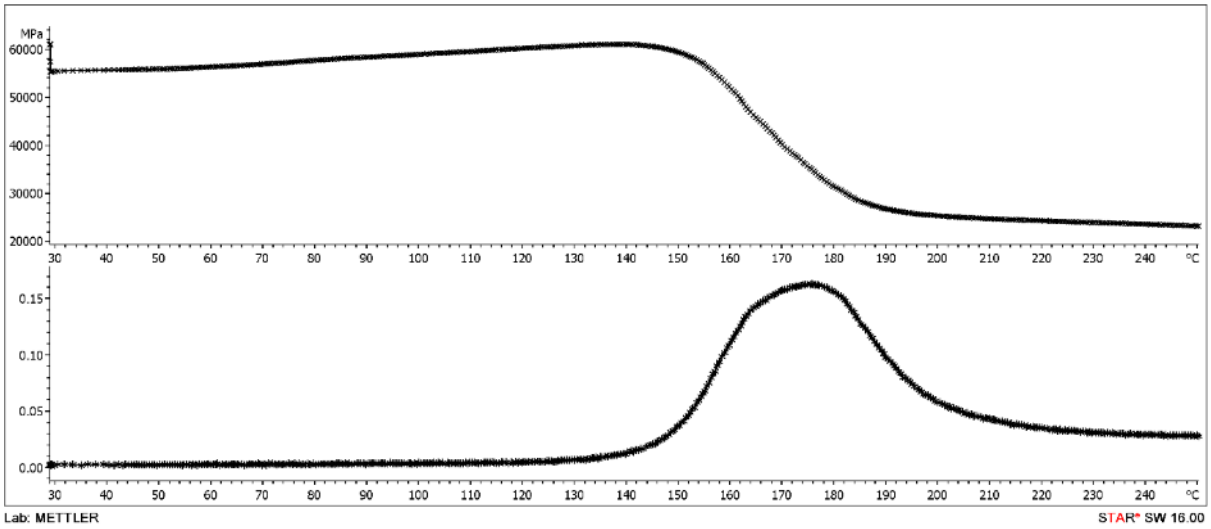

Graph 88. DMA results of P36-CM-025-02. Top: Storage modulus (M') vs temperature. Bottom: Tan delta vs temperature

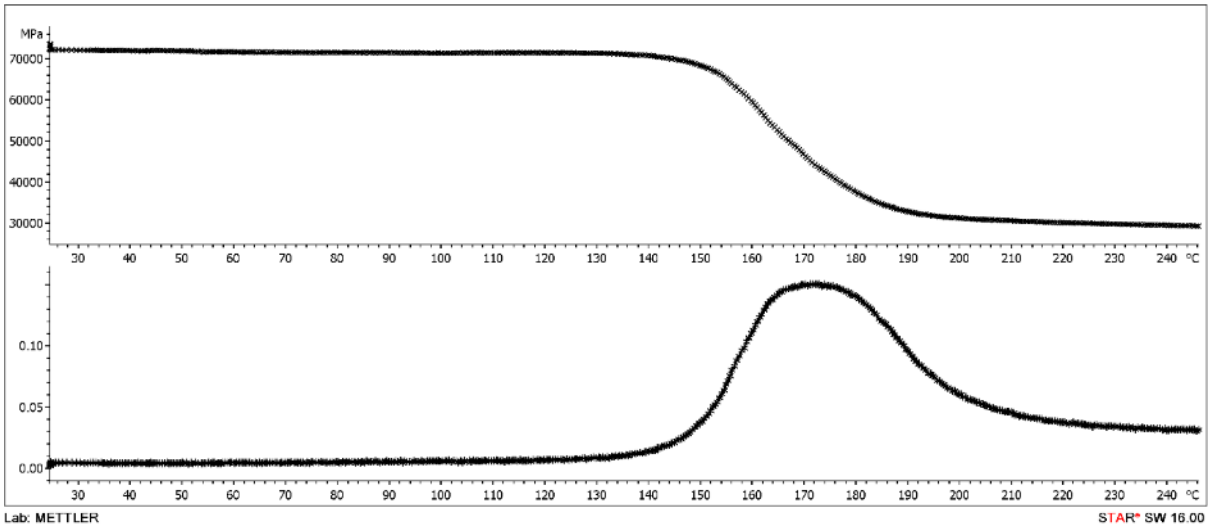

Graph 89. DMA results of P36-CM-026-02. Top: Storage modulus (M') vs temperature. Bottom: Tan delta vs temperature

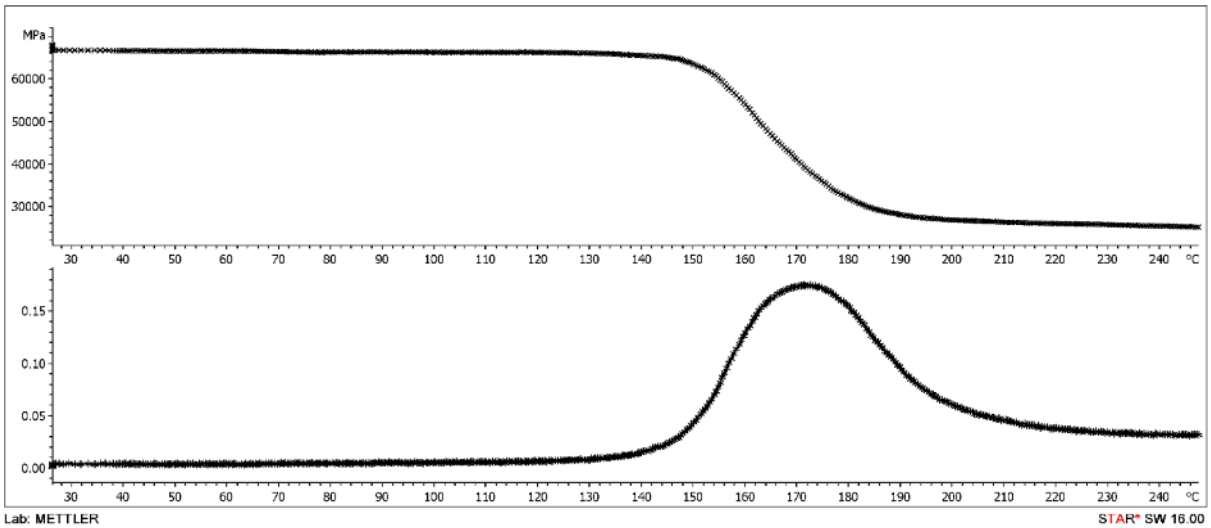

Graph 90. DMA results of P36-CM-027-02. Top: Storage modulus (M') vs temperature. Bottom: Tan delta vs temperature

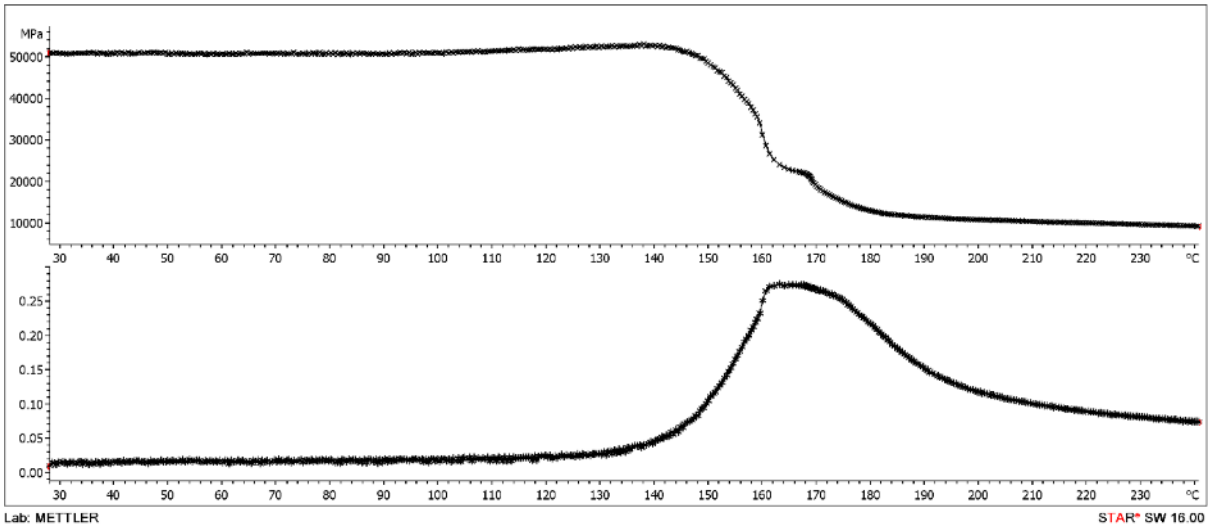

Graph 91. DMA results of P36-CM-031-01A. Top: Storage modulus (M') vs temperature. Bottom: Tan delta vs temperature

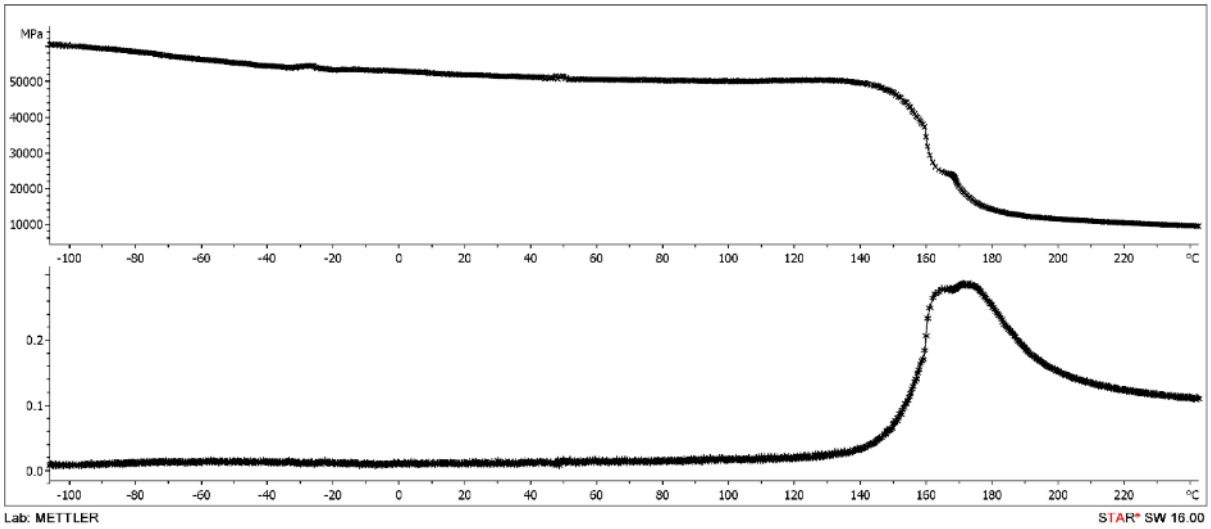

Graph 92. DMA results of P36-CM-032-01A. Top: Storage modulus (M') vs temperature. Bottom: Tan delta vs temperature